Propylene Polymerization Using 4th Generation Ziegler-Natta Catalysts: Polymerization Kinetics and Polymer Microstructural Investigation

by

Ahmad Alshaiban

A thesis

presented to the University of Waterloo

in fulfillment of the

thesis requirement for the degree of

Doctor of Philosophy

in

Chemical Engineering

Waterloo, Ontario, Canada, 2011

AUTHOR'S DECLARATION

I hereby declare that I am the sole author of this thesis. This is a true copy of the thesis, including any required final revisions, as accepted by my examiners.

I understand that my thesis may be made electronically available to the public.

ABSTRACT

A systematic study of propylene polymerization using a 4th generation Ziegler-Natta catalyst is presented in this thesis. The apparent kinetic rate constants for propylene polymerization were estimated in the presence and absence of hydrogen and/or donor. The estimated activation energies for activation, propagation, and deactivation were found to be close to values previously reported in the literature for similar catalysts.

The polypropylene samples were characterized using high-temperature gel permeation chromatography (GPC), carbon-13 nuclear magnetic resonance (^{13}C NMR), and crystallization elution fractionation (CEF). The effect of hydrogen and external electron donor on polypropylene microstructure was investigated at two polymerization temperatures. In addition to the expected electron donor positive effect on tacticity, hydrogen was also found to increase polypropylene tacticity. The effect of changing these polymerization conditions on molecular weight and polydispersity was also investigated. Finally, CEF profiles show how the distribution of polypropylene crystallizability changes by adding hydrogen and electron donor to the reactor.

The concentrations of hydrogen and external donor were also varied to study their effect of polymerization kinetics and polymer microstructure. The estimated activation energies were close to those found in the first part of this investigation in the presence and/or absence of donor and hydrogen. A polypropylene microstructural study showed a positive effect of hydrogen concentration on *mmmm* pentad at low donor concentration, likely due to an increase in stereoselectivity of the aspecific sites by hydrogen. However, increasing donor concentration over a given threshold seems to transform the aspecific sitess into stereospecific sites that are no longer significantly affected by hydrogen. These experimental results were compared to a previously developed Monte Carlo model and found to agree with the trends predicted by simulation.

Finally, the effect of diisopropyldimethoxysilane (P), n-propyltrimethoxysilane (N), paraethoxyethylbenzoate (PEEB), and dicyclopentyldimethoxysilane (D) external donors on catalyst activity and stereoselectivity was investigated. P and D donors were

more stereoselective than N and PEEB donors; however, D donor had the best activity among all donors investigated. Therefore, D donor was mixed with PEEB to combine its high activity with the self-extinguishing properties of PEEB. The D/PEEB 90/10 (mol/mol) mixture generated a catalyst with good stereoselectivity but poor activity. When the ratio was increased to 95/5 and 98/2, the resulting catalyst had high activity and good stereoselectivity. Interestingly, the D/PEEB combination with just a small fraction of PEEB has a positive effect on the catalysts activation term which may decrease polymerization costs with this system.

ACKNOWLEDGMENTS

My great gratitude is to Allah the only god, the Almighty who guided me in every step of this work with his infinite graciousness and bounties.

For this work, I am deeply thankful to my supervisor Professor Joao Soares. Honestly, this achievement would never have been accomplished without his support, constant encouragement, and valuable advice throughout this entire academic journey.

I would also like to express my appreciation and thanks to my supervisory committee members: Professor Robin A. Hutchinson, Professor Jean Duhamel, Professor Xianshe Feng, and Professor Zhongwei Chen.

I would also like to take this opportunity to thank my lab-mate and the co-op students for their assistance throughout the period of this work.

I would also acknowledge the financial support from Saudi Basic Industries Corporation (SABIC).

The heart words come at last! My deep thanks go to my most beloved ones in my life: my mother Fatemah Alyahya, my father Abdullah Alyahya, my wife Reem Alfehaid, and daughters Elia and Fatemah for their love, prayers, support, encouragement, and their invaluable help and motivation. The period of this academic journey in Canada could not be enjoyable, warm, nor full of love without you Reem, Elia, and Fatemah. I would like also to extend my deep appreciations to my brothers Yahya, Hassan, and Ibrahim; my sisters Salwa, Norah, and Haylah; my uncles Abdulrahman Alfehid and Gawaher Almefleh and all of their families for their love and continuous prayers.

DEDICATION

To

My Mother, Fatemah Alyahya

My Father, Abdullah Alyahya

My Beloved Wife, Reem Alfehid

TABLE OF CONTENTS

LIST OF TABLES

LIST OF FIGURES

NOMENCLATURE

Al	Alkylaluminum
B^j_r	Polymer segment with chain length r at state j = I or II
C_d	Deactivated catalyst site
C_j	Inactive catalyst site at state j = I or II
C_j	Inactive catalyst site at state j = I or II
[C]	Catalyst concentration ($mol \cdot L^{-1}$)
$D^j_{r,i}$	Dead chain with chain length r and i stereoblocks terminated at state j = I or II
Do	Electron donor
[D]	Electron donor concentration ($mol \cdot L^{-1}$)
H	Hydrogen
[H_2]	Hydrogen concentration ($mol \cdot L^{-1}$)
I	Catalyst poison
$k_{p,j}$	Rate constant for monomer propagation at state j = I or II ($L \cdot mol^{-1} s^{-1}$)
k^+_{Do}	Forward rate constant for transformation by donor ($L \cdot mol^{-1} s^{-1}$)
k^-_{Do}	Backward rate constant for transformation by donor (s^{-1})
k_{a1}	Rate constant for activation (subscript "1" or "2" stands for the state I and II respectively) ($L \cdot mol^{-1} s^{-1}$)
$k_{Al \cdot I}$	Rate constant for the scavenging or passivation by alkylaluminum ($L \cdot mol^{-1} s^{-1}$)

k_{Al1}	Rate constant for transfer to alkylaluminum (subscript "1" or "2" stands for the state *I* and *II* respectively) (L·mol $^{-1}$s^{-1})
k_d	Rate constant for deactivation (s^{-1})
k_{dI}	Rate constant for deactivation by poison *I* (L·mol $^{-1}$s^{-1})
k_{H1}	Rate constant for transfer to hydrogen (subscript "1" or "2" stands for the state *I* and *II* respectively) (L·mol $^{-1}$s^{-1})
k_{i1}	Rate constant for initiation of the free active site P_0 (subscript "1" or "2" stands for the state *I* and *II* respectively) (L·mol $^{-1}$s^{-1})
k_{iH1}	Rate constant for the reinitiation of the metal hydride active site P_H (subscript "1" or "2" stands for the state *I* and *II* respectively) (L·mol $^{-1}$s^{-1})
k_{iR1}	Rate constant for the reinitiation of P_{Et} (subscript "1" or "2" stands for the state *I* and *II* respectively) (L·mol $^{-1}$s^{-1})
k_{M1}	Rate constant for transfer to monomer (subscript "1" or "2" stands for the state *I* and *II* respectively) (L·mol $^{-1}$s^{-1})
$k_{\beta 1}$	Rate constant for transfer by β-hydride elimination (subscript "1" or "2" stands for the state *I* and *II* respectively) (s^{-1})
$k_{p,j}^{n}$	propagation rate constant of site *n* and at state *j*.
$k_{d,j}^{n}$	deactivation rate constant of site *n* and at state *j*.
$K_{a,j}^{n}$	overall activation rate constant of site *n* and at state *j*.
L	Ligand
M	Monomer (propylene)
[M]	Monomer (propylene) concentration (mol·L^{-1})
M_n	Number average molecular weight (g/mol)

M_w	Weight average molecular weight (g/mol)
P_0	Monomer-free active site
P_{Et}	Active site coordinated with an ethyl group
P_H	Active site coordinated with hydrogen (metal hydride)
$P^j_{r,i}$	Living chain with chain length *r* and *i* stereoblocks at state *j* = *I* or *II*
P_r	Living chain with chain length *r*
R_p	Reaction rate of propagation (mol/min)
R_t	Reaction rate of chain transfer (mol/min)
t	Time (s)
Y^m	Moment (m = 0^{th} , 1^{st} , or 2^{nd}) of living chains terminated at state *j* = *I* or *II* and with *i* stereoblocks

Superscripts

I	(Super or subscript *I*) stands for stereospecific site type (isotactic)
II	(Super or subscript *II*) stands for non-stereospecific site type (atactic)
n	in MWD: number of active sites

Subscripts

r	Chain length
i	Number of stereoblocks in a chain

Acronyms

CHMDMS	cyclohexyl-methyl-dimethoxysilane

CCD	chemical composition distribution
CEF	crystallization elution fractionation
^{13}C NMR	carbon-13 nuclear magnetic resonance spectroscopy
CRYSTAF	crystallization analysis fractionation
DCPDMS	dicyclopentyl-dimethoxysilane (D-donor)
DIPDMS	diisopropyl-dimethoxysilane (P-donor)
DIBP	di-iso-butyl-phthalate
DNBP	di-n-butyl phathalate
DPDMS	diphenyl-dimethoxysilane
DSC	differential scanning calorimetry
EB	ethyl benzoate
FIPA	flow injection polymer analysis
GPC	gel permeation chromatography; known also as size exclusion chromatography (SEC)
IR	infrared
IV	intinsic viscosity
MWD	molecular weight distribution
NPTMS	n-propyltrimethoxysilane (N-donor)
PDI	Polydispersity index
PEEB	*p*-ethoxy-ethyl-benzoate
PTES	propyltriethoxysilane
TCB	1,2,4-trichlorobenzene
TCE	tetrachloroethane-1,2-d_2
TEAL	triethylaluminum (used as co-catalyst and impurity scavenger)
TFPMDMS	3,3,3-tri-fluro-propyl-(methyl)-dimethoxy-silane
TMS	tetramethylsilane

TREF	temperature rising elution fractionation
PREP	preparative fractionation
p-TREF	preparative temperature rising elution fractionation

Chapter 1

INTRODUCTION

Polypropylene has a variety of applications in our daily life, from packaging, toys, pipes, and tools, to some promising specialty applications in the electronic, airplane, and automotive industries. Polypropylene, as well as polyethylene, is increasingly replacing other materials because of their versatile properties, low cost, reduced environmental impact, and easy recycling. The world demand for polypropylene jumped from 6.4 million metric tons in 1983 to 38.6 metric tons in 2004, with a growing rate as high as 5.8% from 2004 to 2009 (*Alberta-Polypropylene Market Study,* CMAI , Sep. 2004). Recent analyses (*MarketPublisher.com*, Jan. 2010) predict that the world annual polypropylene production will increase from 52 metric tons in 2008 to 69.1 metric tons in 2013, and forecast an annual increase on polypropylene world demand by 3.7 % in the 2010-2013 timeframe.

Propylene is an asymmetric monomer; therefore, monomer insertions having different orientations during polymerization lead to distinct chain configurations. Microstructures with varying degrees of stereoregularity and regioregularity lead to polypropylene resins ranging from amorphous to highly crystalline materials at room temperature, albeit isotactic polypropylene, with a melting temperature in the range of 165-173 °C, is by far the most commercially relevant material.

Most polypropylene industrial manufacturing processes use heterogeneous Ziegler-Natta catalysts. A unique feature of these catalysts is the presence of more than one active site type, leading to the production of polyolefins with broad distributions of molecular weight (MWD), chemical composition (CCD) – in the case of propylene/ethylene copolymers – and non-uniform stereoregularity. These distributions influence strongly the mechanical and rheological properties of polypropylene, and are ultimately responsible for the performance and final applications of the product.

The nature of the different active site types on heterogeneous Ziegler-Natta catalysts is still not well understood. The inherent complexity of heterogeneous Ziegler-Natta catalysts, where mass and heat transfer limitations are combined with a rather complex chemistry of site activation in the presence of internal and external donors, plus other phenomena – such as comonomer rate enhancement, hydrogen effects, and poisoning – makes this a very challenging problem.

1.1. MOTIVATION AND RESEARCH OBJECTIVES

Process simulation is a powerful tool used by several polyolefin manufacturing companies. Process simulators, such as Polymer Plus (Aspen), are tools that give a general description of polymerization processes. However, more effort is required to develop models capable of describing polymer microstructure in details by considering more complex polymerization mechanism steps. This specific task must be done for each individual polymerization system under a given set of operating conditions (Chakravarti and Ray, 2001; Chakravarti *et al.*, 2001).

Saudi Basic Industries Corporation (SABIC), the sponsor of this research project, is the world's fourth largest producer of polyolefins, the third largest producer of polyethylene, and the fifth largest producer of polypropylene (*Alberta - Polypropylene Market Study* CMAI , Sep. 2004). This PhD thesis project developed a quantitative methodology for the determination of the main propylene polymerization kinetic constants under different conditions to better understand catalysts used by SABIC. The resulting constants can be used in mathematical models for process optimization, product development, process control, and operator training.

A unique feature of propylene polymerization using heterogeneous multiple-site Ziegler-Natta catalysts is the use of electron donors that control the fraction of atactic polypropylene made during polymerization. Electron donors also affect polymerization rate and polymer properties (Forte and Coutinho, 1996). The effect of electron donors will be quantitatively evaluated for commercial catalyst/electron donor systems similar to the ones used by SABIC.

In summary, this research project has the following objectives:

1. To validate experimentally the general trends of hydrogen and external electron donor effects predicted with a previously developed mathematical model for propylene polymerization kinetics and polypropylene microstructure, taking into consideration the effect of external electron donors.
2. To estimate polymerization kinetic constants of a commercial heterogeneous Ziegler-Natta catalyst for propylene polymerization under different external donor and hydrogen concentrations and temperatures.
3. To study the effect of electron donor type and concentration, and of their mixtures, on propylene polymerization kinetics and polypropylene tacticity distribution.

1.2. THESIS CONTENTS

Chapter 2 includes a literature review and background on Ziegler-Natta catalysts, propylene polymerization, and our previously developed mathematical model for propylene polymerization. Chapter 3 summarizes the polymerization experimental details. Chapter 4 describes the effect of the presence of hydrogen and/or electron donors on polymerization rate and polypropylene microstructure. Chapter 5 describes how varying the concentration of hydrogen and electron donor at two polymerization temperatures affects catalyst activity and polymer microstructure. In Chapter 6, the effect of several external donors suitable for the 4th generation Ziegler Natta catalyst used in this investigation on polymerization activity and polymer microstructure were compared. The donor which generated a catalyst with the highest activity was then mixed with another electron donor that has self-extinguishing properties in an optimum ratio to enhance the polymerization activation rate while maintaining excellent polymer tacticity. Finally, Chapter 7 summarizes the conclusions for the entire work.

Chapter 2

BACKGROUND AND LITERATURE REVIEW

2.1. ZIEGLER-NATTA CATALYSTS

Ziegler-Natta catalysts for propylene polymerization have improved much since their discovery in the fifties, including changes in catalyst precursors, cocatalysts, internal and external electron donors. Internal donors are used during catalyst manufacturing to maximize the fraction of stereospecific sites; external donors are added during the polymerization to replace internal donors lost due to alkylation and reduction reactions with the cocatalyst. In addition to its use for passivation (poison scavenging), the cocatalyst is used to activate the catalyst by the reduction and alkylation of the transition metal (Busico *et al.*, 1985; Barino and Scordamaglia, 1998; Chadwick *et al*., 2001).

First and second generation Ziegler-Natta catalysts were composed of crystalline $TiCl_3$ in four different geometries: α = hexagonal, β = fiber or chain, γ = cubic, and δ = alternating between hexagonal and cubic. Three of these geometries, α, γ and δ, have high steroselectivity and can be activated with a diethylaluminum cocatalyst. The δ-$TiCl_3$ complex has the highest activity towards propylene polymerization and is obtained as porous particles with relatively small diameters (20-40 μm). The controlled fragmentation of catalyst particles during polymerization was one of the major challenges to the development of heterogeneous Ziegler-Natta catalysts (Cerruti, 1999).

The introduction of electron donors (Lewis bases) during polymerization to increase catalyst stereoselectivity and productivity led to 2nd generation Ziegler-Natta catalysts. Because most of the potential active sites are located inside $TiCl_3$ crystals where they cannot promote polymerization, 1st and 2nd generation catalysts have poor productivities per mole of titanium,

and require post-reactor steps to remove catalyst residues (deashing). Their lower stereoselectivities also demand a post-reactor step to extract atactic polypropylene from the final product. The elimination of these two post-reactor steps was the main driving force behind the development of new types of heterogeneous Ziegler-Natta catalysts (Cerruti, 1999; Soga and Shiono, 1997).

A new catalyst generation came about when $TiCl_4$ was supported on porous $MgCl_2$ particles. These 3rd generation ($TiCl_4/MgCl_2$) Ziegler-Natta catalysts had very high activities and stereoselectivities. Shell (1960) produced the first 3rd generation catalyst using $TiCl_4$ supported on $MgCl_2$ with high activity and controlled stereoselectivity using several types of electron donors. The activity of 3rd generation catalysts can be as high as 27 kg-polypropylene per gram of catalyst, which is almost six times higher than that of a typical 2nd generation catalyst. Polypropylene resins made with 3rd generation catalysts have an isotacticity index (II) of 92-97%, while those produced with 2nd generation catalysts have only an II of 88-93%. (The isotacticity index measures the fraction of isotactic polypropylene – or, more correctly, the fraction of polypropylene insoluble in boiling heptane – in the resin.) Therefore, one of the biggest advantages of 3rd generation catalysts is the elimination of post-reactor steps for atactic polypropylene removal and catalyst deashing (Cerruti, 1999).

Fourth generation Ziegler-Natta catalysts are also composed of $TiCl_4$ supported on porous $MgCl_2$, but with controlled morphology and with slightly better productivity (Chang *et al.*, 2006; Kissin *et al.*, 2008).

In the early eighties, a new class of olefin polymerization catalyst appeared in the form of metallocene complexes. Metallocenes produce polyolefins with properties that are more uniform than those made with Ziegler-Natta catalysts, and have been used particularly for the production of differentiated commodity polyethylene and polypropylene resins (Cerruti, 1999).

2.1.1. $TiCl_4/MgCl_2$ Catalysts

A typical $TiCl_4/MgCl_2$ catalyst is prepared in four main temperature-controlled steps: digestion, activation, washing, and drying. The digestion step includes the reaction of an

organo-magnesium (MgOR) compound, $TiCl_4$, and an internal electron donor in a chlorinated organic solvent; $TiCl_4$ is dispersed in the precursor porous surface, forming $MgCl_2$ crystals and $TiCl_3$.OR. In the activation step, $TiCl_3$.OR is removed by further addition of $TiCl_4$ and solvent. The formed catalyst is washed with a volatile organic solvent in the washing step. Finally, hot nitrogen is used in the drying step to evaporate the solvent, obtaining a free-flowing $TiCl_4/MgCl_2$ powder (Chang et al., 2006).

Electron donors control the $TiCl_4$ distribution on the (100) and (110) faces of the $MgCl_2$ surface, as illustrated in Figure 2-1 (Busico *et al.*, 1985; Chadwick *et al.*, 2001). Ti_2Cl_8 species coordinate with the (100) faces through dinuclear bonds to form the isospecific polymerization sites, while the electron donor molecules tend to coordinate with the non-stereospecific and more acidic sites on the (110) faces. When aromatic monoesters and diesters are used as internal donors, the addition of alkylaluminums (alkylation) results in the partial removal of the internal donor; therefore, external donors are needed to maintain high stereoselectivity. During catalyst preparation, there is also a chance of the internal donor to coordinate with the (100) face, but it has been reported that, in the case of ethyl benzoate, $TiCl_4$ is able to remove the donor from the (100) stereospecific face during the titanation step (Busico *et al.*, 1985). However, when 1,3-diethers are used as internal donors, they coordinate strongly with the (110) faces and cannot be removed by alkylaluminums (Barino and Scordamaglia, 1998). As a consequence, Ziegler-Natta catalysts with excellent isospecificity are obtained with diether internal donors in the absence of external donors.

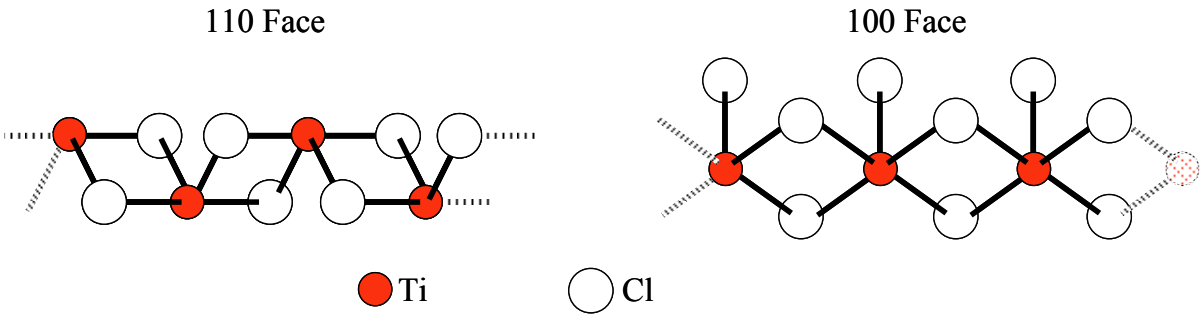

Figure 2-1. Lateral faces of a $TiCl_4/MgCl_2$ Ziegler-Natta catalyst (Busico *et al.*, 1985).

2.1.2. Polymerization Mechanism and Catalyst Geometry

According to the Cossee-Arlman's mechanism (Arlman and Cosee, 1964), propylene molecules require an activated catalyst site that has been alkylated by cocatalyst, as shown in Figure 2-2.

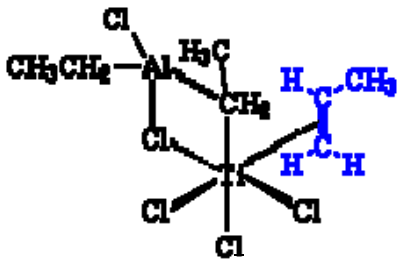

Figure 2-2. Catalyst, cocatalyst (alkylaluminum), and propylene complexation.

The π-bond electrons in the double bond of the incoming propylene are shared with the titanium atom during the coordination step. During the insertion step, the double bond breaks, forming a C-Ti bond between the monomer molecule and the Ti site, and a C-C bond between the monomer and the growing chain, restoring the vacant coordination site for further coordination and insertion steps, as illustrated in Figure 2-3.

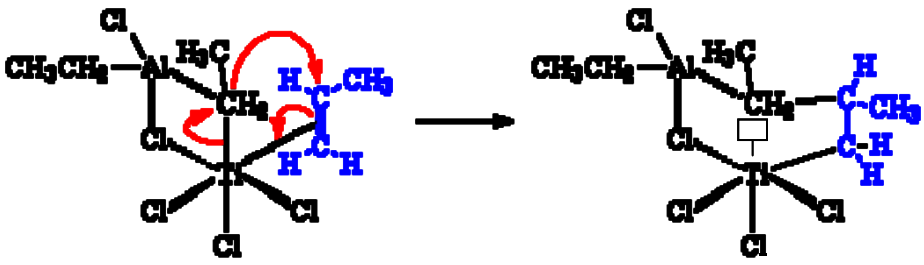

Figure 2-3. Transition state forming new vacant site.

Catalyst geometry is very important in propylene polymerization to ensure that the methyl group in the propylene molecule is aligned in the same plane, producing isotactic

polypropylene chains. Figure 2-4 shows molecular structural models for γ-$TiCl_3$ (Kakugo *et al.,* 1988). Three site structures were postulated: highly isotactic, low isotactic, and atactic. The highly isotactic site has one coordination vacancy, and is bonded to the alkyl-polymer chain site (blue molecule, on top), and four Cl atoms. Due to site symmetry, stereo- and regioregular insertions are favored. The low isotactic site, despite of also having only one coordination vacancy, has two Cl atoms not bonded to Ti atoms; since the site occupied by the growing chain and the vacant site are not symmetrical, stereo- and/or regiodefects, may occur during insertion. Finally, the two coordination vacancies of the atactic site allow for the random coordination of propylene molecules and the formation of atactic polypropylene chains.

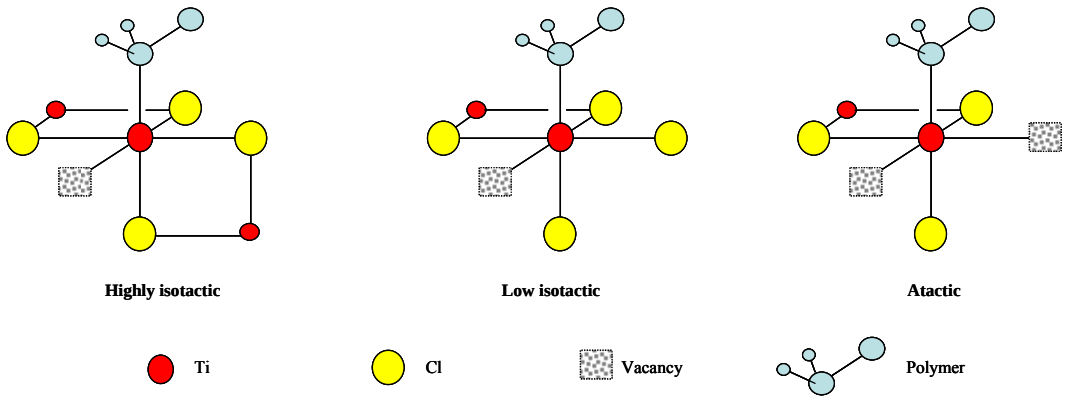

Figure 2-4. Active site models for γ-$TiCl_3$ (Kakugo *et al.,* 1988).

When $TiCl_4$ is supported on $MgCl_2$, the resulting structure is similar to that of β-$TiCl_3$ (Figure 2-5 and Figure 2-6). An electron donor molecule can complex with the Ti atom in the low isotactic site, blocking the coordination vacancy, and rendering the site inactive for polymerization, as illustrated in Figure 2-5. On the other hand, the atactic site has two vacancies to which an electron donor molecule may complex; if only one vacancy is occupied by the electron donor, as shown in Figure 2-6, the site is transformed into a highly isotactic site. In this case, the bulkiness of the electron donor provides steric hindrance, rendering the site isospecificity.

It is interesting to notice that some donors may kill the catalyst or reduce its activity when used in excess. This phenomenon, called self extinction, is used in some commercial processes to shut down the polymerization. Chen reported that esters derived from aromatic carboxylic acids, such as para-ethoxy-ethyl-benzoate (PEEB), were good example of such donors. However, not all donors are able to reduce the polymerization activity, even if an excess amount is added to the polymerization reactor, such as alkoxysilanes (Chen, 2008).

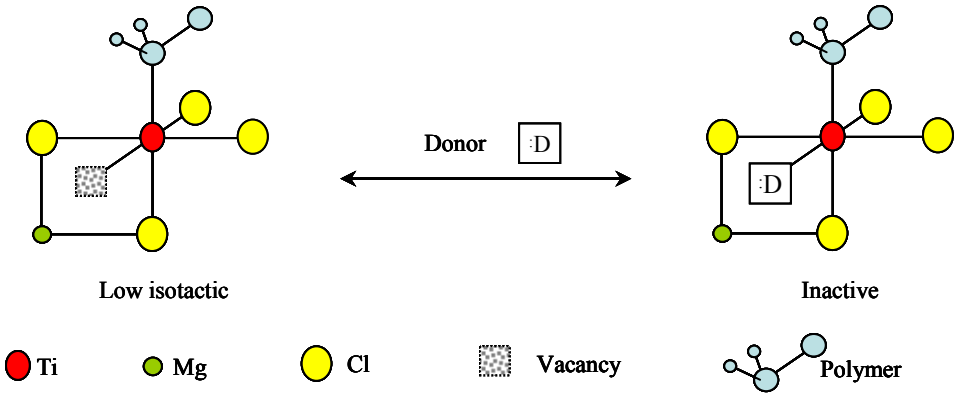

Figure 2-5. Donor addition to low isotactic site on $TiCl_4/MgCl_2$ (Kakugo *et al.,* 1988).

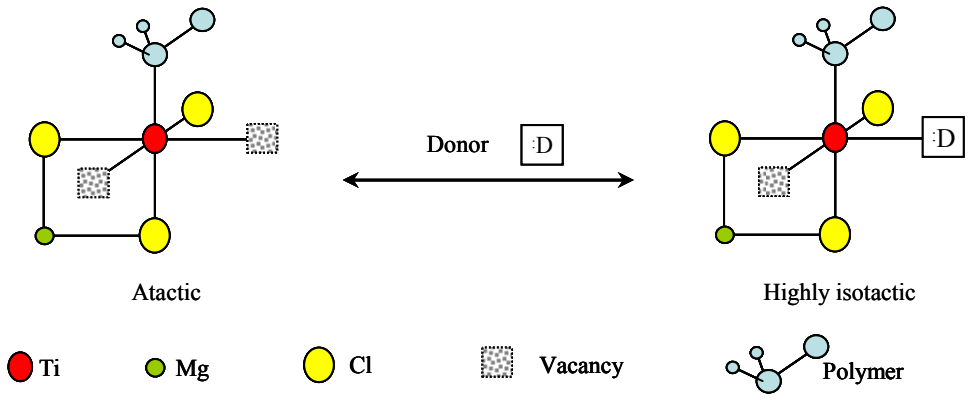

Figure 2-6. Donor addition to atactic site on $TiCl_4/MgCl_2$ (Kakugo *et al.,* 1988).

Busico *et al.* (1999) preferred to classify the catalyst sites according to the chains they produced as highly isotactic, poorly isotactic (or isotactoid), and syndiotactic, as shown in Figure 2-7. Atactic polypropylene is assumed to be produced in the isotactoid and syndiotactic sites. The highly isotactic site (a) has either two ligands (a chlorine or a donor atom), or one ligand with a strong steric hindrance to prevent the wrong insertion of monomer at position S2. The isotactoid site (b) has only one ligand. The syndiotactic propagation site (c) has two vacancies and no stereoselective control; it has been proposed that site (c) follows a chain end control mechanism rather than the most common site control mechanism for insertion. Busico *et al.* have proposed that losses of ligand L1 and/or L2 will result in a loss of the steric hindrance that may lead to the transformation of highly isotactic sites into isotactoid, and then to syndiotactic propagation sites.

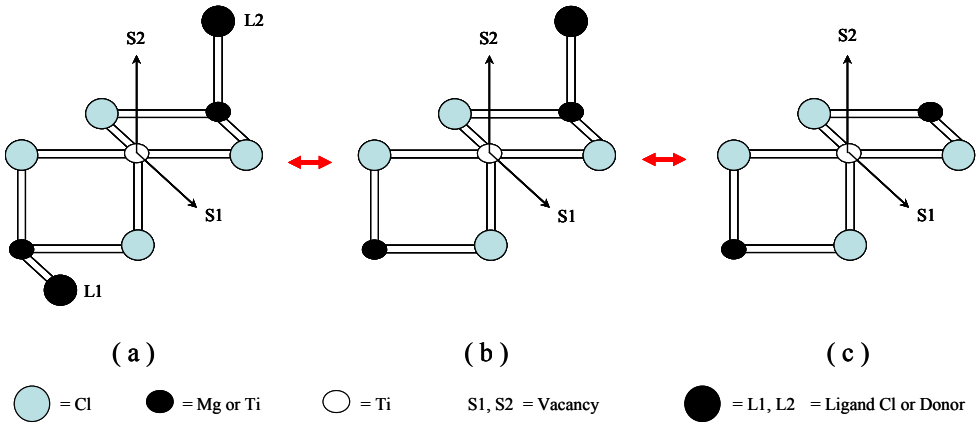

Figure 2-7. Active site models for $TiCl_4/MgCl_2$: (a) highly isotactic; (b) isotactoid; (c) syndiotactic (Busico *et al*., 1999).

2.2. METALLOCENE CATALYSTS

Kaminsky and Sinn (Sinn and Kaminsky, 1980; Kaminsky et al., 1985) discovered high activity metallocene catalysts for ethylene polymerization in the early eighties. The metallocenes studied initially were aspecific and produced only atactic polypropylene. Isotactic polypropylene was first synthesized with a metallocene catalyst in 1984 by Ewen (Ewen, 1984) using Cp_2TiPh_2/MAO. Since then, metallocene catalysts have improved continuously to produce polypropylene with higher molecular weight, tacticity and melting temperature. Metallocene catalysis has also allowed the production of specialty polyolefins with well designed microstructures, such as syndiotactic polypropylene (sPP) and isotactic−syndiotactic block polypropylene.

Metallocene ligand symmetry determines its stereospecificity. Coates classified metallocene catalyst according to their ligand symmetry as shown in Figure 2-8 (Coates, 2000). Catalysts with C_{2v} symmetry (Figure 2-8.a), such as Cp_2MCl_2, produce atactic chains with low *mmmm* pentad fraction. Catalysts with C_s symmetry, shown in Figure 2-8.b and 2-8.c, produce both isotactic and syndiotactic chains, and syndiotactic chains, respectively. C_2 symmetry (Figure 2-8. d) leads to the production of isotactic polypropylene. Finally, catalysts with C_1

symmetry (Figure 2-8.e) can make polypropylene chains with a variety of configurations, such as atactic–isotactic stereoblock, highly isotactic, and hemi–isotactic (Coates, 2000).

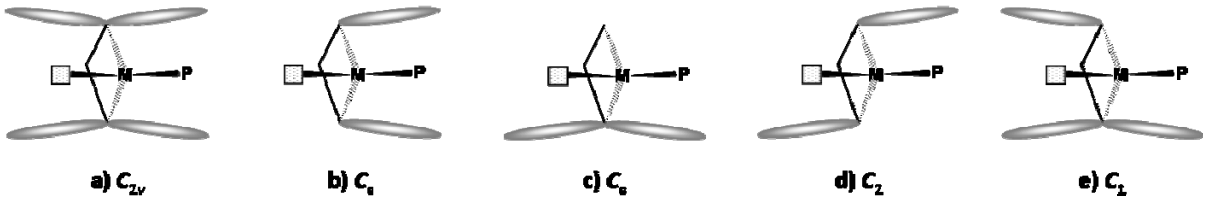

Figure 2-8. Classification of metallocene catalysts according to ligand symmetry (Coates, 2000). P stands for polymer chain and M for the transition metal.

The crystallinity degree of polypropylene increases by increasing its *mmmm* pentad content to up to when its melting temperature reaches 160°C $< T_m <$ 166°C, when it is then considered to be isotactic (The theoretical T_m for pure isotactic polypropylene is 171°C) (Maier and Calafut, 1998).

As described above, C_2 symmetric catalysts produce isotactic polypropylene because the incoming propylene molecule must be oriented in the way shown in Figure 2-9.a. This orientation is favored due to the non–bonding interaction between the incoming monomer and the ligand cloud (Pino et. al, 1987; Kaminsky and Arndt, 1997).

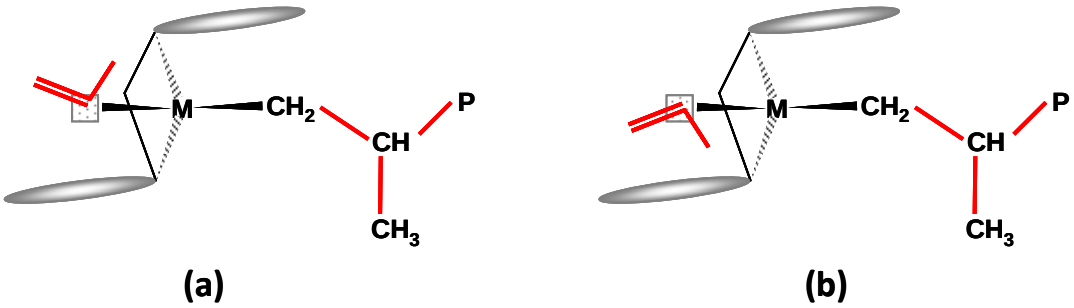

Figure 2-9. C_2 symmetric metallocene catalyst showing the most favored configuration (a), which leads to the stereospecific insertion. P stands for polymer chain.

Ewen (1984) reported the first synthesis of partially isotactic polypropylene using a metallocene catalyst with a mixture of the meso and racemic complexes; the racemic complex of this catalyst is shown in Figure 2-10.a. Ewen proposed that the isotactic polypropylene fraction was produced by the racemic C_2-symmetric complex shown in Figure 2-10.a. A year later, Kaminsky *et al.* (1985) supported this conclusion when they used the racemic C_2-symmetric zirconocene catalyst shown in Figure 2-10.b to produce isotactic polypropylene with a soluble fraction as low as 0.2 wt.%. Moreover, the catalyst activity was 2−3 times higher than that for the meso form of the same zirconocene, and it made polymer with a polydispersity in the range from 1.9 to 2.6.

ExxonMobil started the commercial production of isotactic polypropylene in 1995 using a metallocene catalyst specifically designed to produce resins for melt−blown applications with high melt flow rate and narrow molecular weight distribution.

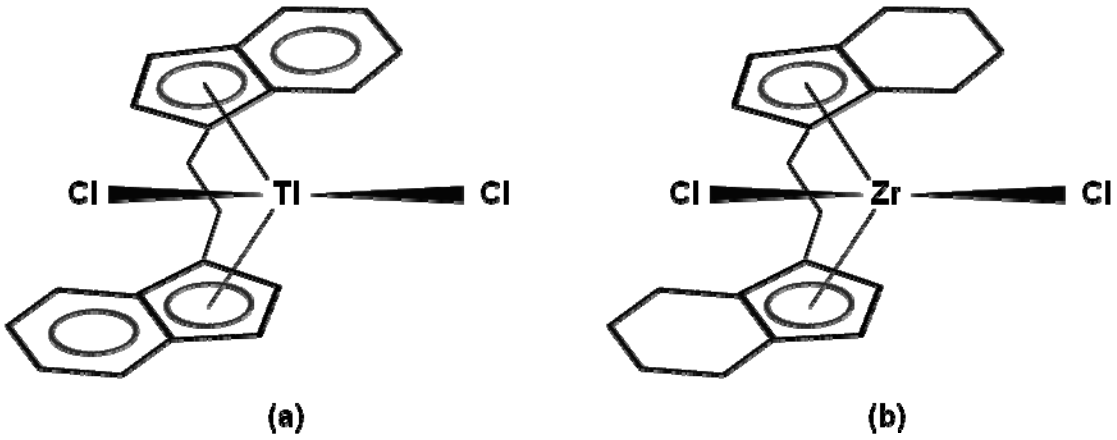

Figure 2-10. Bridged C_2-symmetric racemic metallocene catalysts: (a) used by Ewen, and (b) used by Kaminsky and Brintzinger.

The crystallinity degree of syndiotactic polypropylene increases by increasing its *rrrr* pentad content (Maier and Calafut, 1998); syndiotactic polypropylene with 83.6 % *rrrr* pentad content has a T_m of 133.2°C and with 94 % *rrrr* pentad content has a T_m of 155°C (Kaminsky and Arndt, 1997; Yoshino et al., 2003).

Ewen and coworkers (Ewen et al., 1988) used a C_s-symmetric catalyst, $[Me_2C(Flu)(Cp)]ZrCl_2$ (Figure 2-11), to make syndiotactic polypropylene with high activity and *rrrr* content as high as 86%. Razavi and Atwood (1995) were able to improve polypropylene syndiotacticity by replacing the Me_2C bridge with Ph_2C, to form $[Ph_2C(Flu)(Cp)]ZrCl_2$. A further significant syndiotacticity increase was achieved when using ligands that were bulkier than fluroenylidene (Figure 2-12), with *rrrr* pentad contents greater than 99% (Coates, 2000). Most recently, Muller et al. (2004) added *tert*-butyl groups to the fluoroenylidene ligand (Figure 2-13) to produce syndiotactic polypropylene with 99% of *rrrr* pentad content and with a moderate activity of 90 kg–PP/(mol–Zr·h·(mol/L–C_3)).

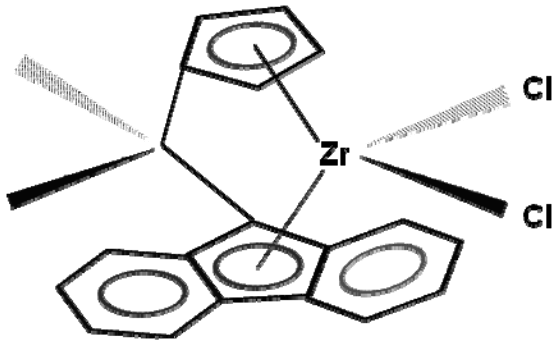

Figure 2-11. C_s–symmetric catalyst used by Ewen et al. (1988).

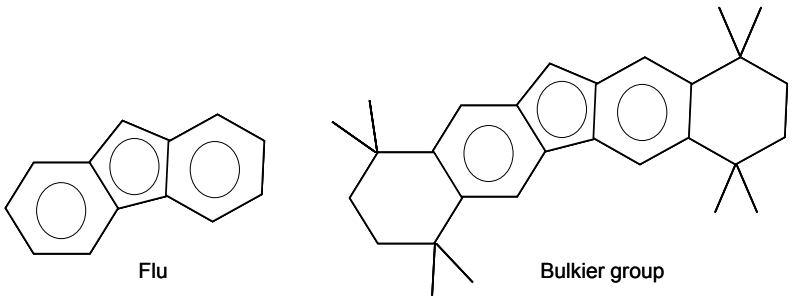

Figure 2-12. Bulkier group used in place of fluorenylidene (Flu) for increasing syndiotacticity in C_s catalyst.

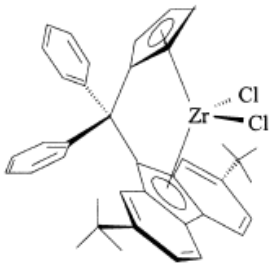

Figure 2-13. C_s–symmetric catalyst used by Muller *et. al* (2004).

Total Petrochemicals announced in 2002 (at that time, named Atofina Petrochemicals) the world's first commercial production of metallocene syndiotactic polypropylene. According to Atofina, this resin had higher clarity than conventional or metallocene isotactic polypropylene. Atofina also claimed other benefits when replacing random propylene/ethylene copolymers with syndiotactic polypropylene, such as softness (CMR report, February/March 2002).

Hemi–isotactic polypropylene has alternating isotactic and atactic placements, as shown in Figure 2-14. Farina et al. (1982) were the first to report such a structure. Ewen et al. (1991) reported the metallocene catalyst shown in Figure 2-15.a that has one stereospecific coordination site and one aspecific site. It is interesting to notice the slight difference between the configuration of this C_1-symmetric catalyst and the C_s-symmetric complex shown in Figure 2-11. Razavi et al. (1995) reported that a use of bulkier groups (such as *tert*-butyl), as shown in Figure 2-15.b, would increase the stereoselectivity of such a catalyst, leading to an increase of *mm* placements. Coates reported that the microstructure of polypropylene made with hemi–isotactic metallocene catalysts varied with propylene concentration (Coates, 2000).

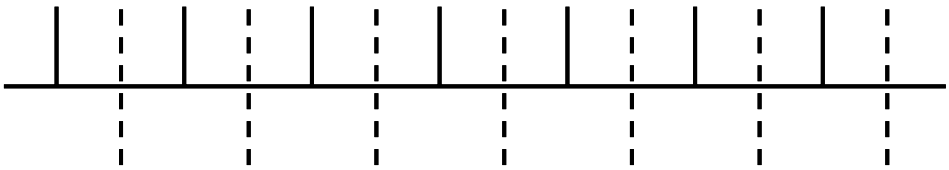

Figure 2-14. Hemi–isotactic polypropylene structure.

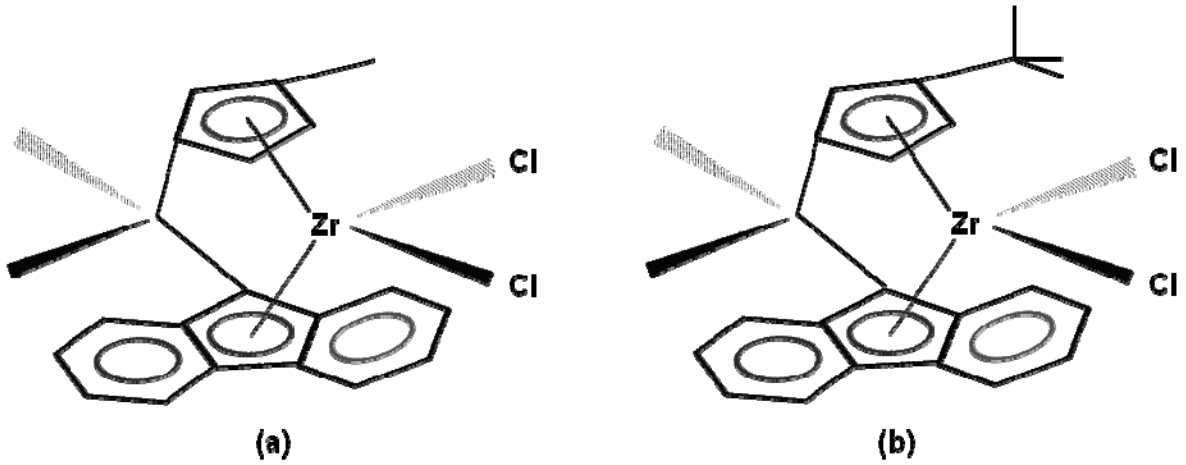

Figure 2-15. C_1-symmetric catalyst used for the production of hemi−isotactic polypropylene by (a) Ewen, and (b) by Razavi with a bulker group, *tert*-butyl.

Isotactic−atactic stereoblock polypropylene (Figure 2-16) can also be made with certain metallocene catalysts. These chains have elastomeric properties (Collete et al., 1989A; Collete et al., 1989B). This type of microstructure can be produced by C_1-symmetric catalysts, an oscillation catalyst (which will be discussed later in this section), or by a mixture of two types of catalyst (Coates, 2000). Chien et al. (1990) used the C_1-symmetric catalyst shown in Figure 2-17 to make stereoblock polypropylene with *mmmm* pentad content of 40 %. In this type of catalyst, the transition time between aspecific and stereospecific states (epimerization) is shorter than the average lifetime of a polymer chain. The distribution and average length of these stereoblocks depend on the propylene concentration and the polymerization temperature (Coates, 2000).

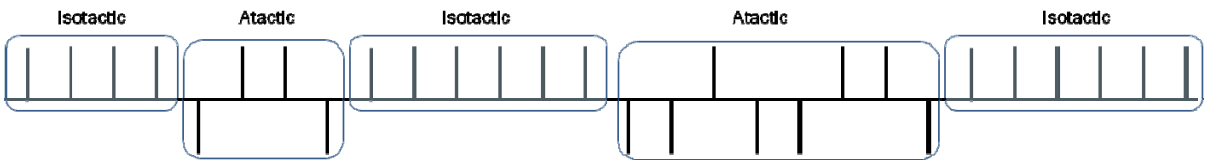

Figure 2-16. Illustration of an isotactic-atactic stereoblock polypropylene structure.

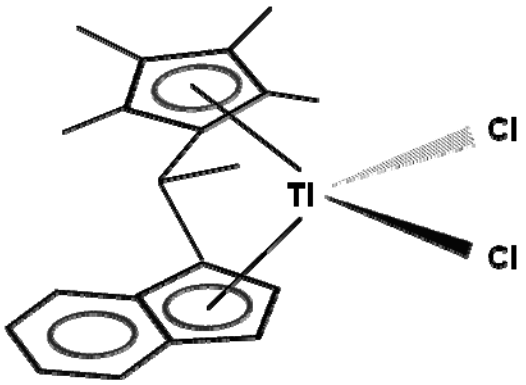

Figure 2-17. C_1-symmetric catalyst used to produce stereoblock polypropylene (Chien et. al, 1990).

Oscillation catalysts have been modified to increase isotactic block length for better elastomeric properties. In this type of catalyst, isomerization takes place during the lifetime of a polymer chain, as illustrated in Figure 2-18 (Coates and Waymouth, 1995; Busico et. al, 2003). Different ligands lead to polymers with different tacticities and elasticities (Hauptman et. al, 1995; Lin et. al, 1998).

The use of two types of metallocene with distinct stereospecifities is also an alternative way for preparing stereoblock polypropylene. Stereoblocks are produced when chain transfer occurs between the two catalysts using tri-isobutylaluminum (TIBA) as an activator and as a *chain crossover agent*. Chien et al. (1997) observed the formation of stereoblock polypropylene chains, in addition to pure isotactic and atactic chains, using a combination of two metallocene catalysts [$Et(Fl)_2ZrCl_2$ with $Et(Ind)_2ZrCl_2$ or $Me_2Si(Ind)_2ZrCl_2$] and attributed the formation of the stereoblock chains to the presence of TIBA acting as a chain crossover agent. This later observation guided Chien et al. (1999) to apply the same concept to synthesize syndiotactic−isotactic stereoblock polypropylene.

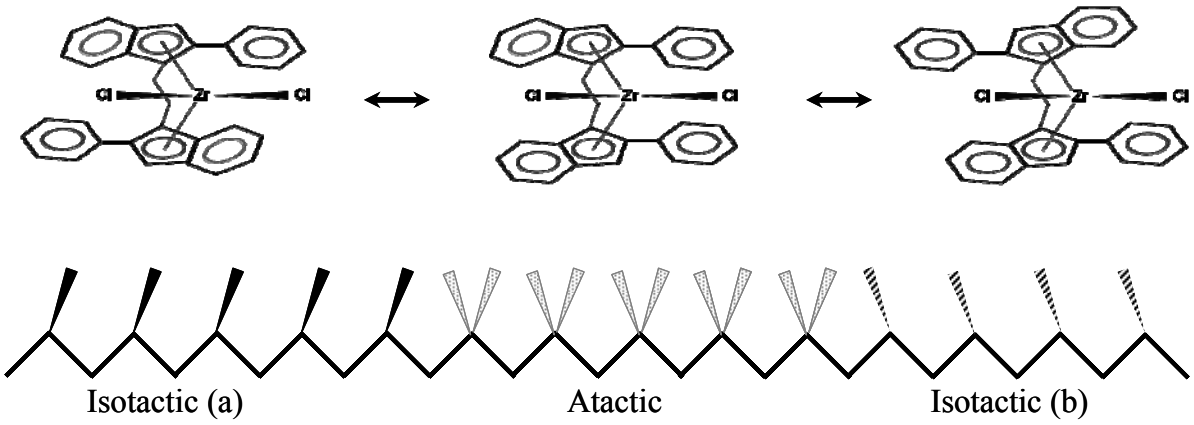

Figure 2-18. Oscillation catalyst isomers used for the production of stereoblock polypropylene (Busico et. al, 2003).

The existing heterogeneous Ziegler–Natta commercial polymerization processes use gas phase or slurry reactors that require supported catalysts. Therefore, metallocene catalysts must be supported on a carrier to be used in these processes. The most commonly used supports are SiO_2, Al_2O_3 and $MgCl_2$. Generally, the metallocene is supported either by direct synthesis on the selected support surface or by attaching it to the support using either chemical or physical means (Kaminsky and Arndt, 1997; Choi and Soares, 2010).

2.3. POLYPROPYLENE

2.3.1. Polypropylene Microstructure

Polypropylene microstructure can be classified (Chadwick *et al*., 1996) from a regioregularity point of view as regioregular (1,2 or primary insertions) and regioirregular (random 1,2 and 2,1 (secondary) insertions). From a stereoregularity point of view, polypropylene occurs as isotactic (with methyl groups aligned selectively on one side of the plane, Figure 2-19), atactic (with a random placement of methyl groups on either side of the plane, Figure 2-20), and syndiotactic (with methyl groups alternating on both sides of the plane). Isotactic regioregular chains are also called stereoregular chains, and atactic chains are

called stereoirregular chains. Other possible arrangements for isotactic and atactic regioirregular chains are illustrated in Figure 2-21 and Figure 2-22.

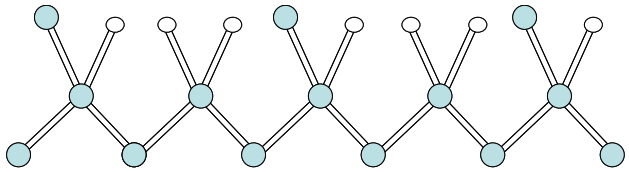

Figure 2-19. Isotactic regioregular chain (stereoregular).

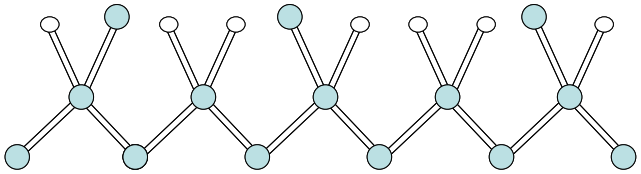

Figure 2-20. Atactic regioregular chain (stereoirregular).

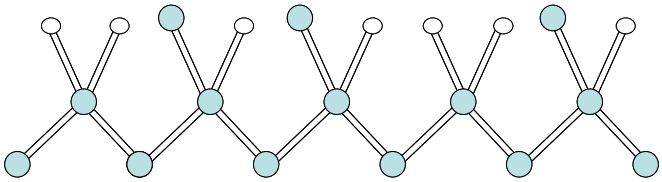

Figure 2-21. Isotactic regioirregular chain.

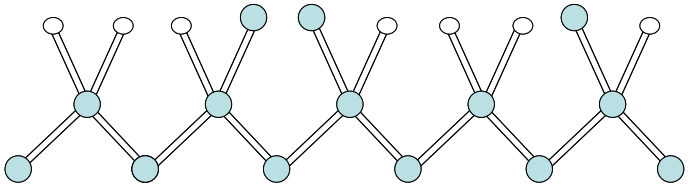

Figure 2-22. Atactic regioirregular chain.

Commercially, polypropylene is produced mainly as its isotactic isomer, with a small amount (around 2-5%) of atactic polypropylene (Moore, 1996). The fraction of isotactic chains in commercial polypropylene is quantified by the *isotacticity index*, generally measured as the mass fraction of polypropylene insoluble in boiling heptane. The microstructure of polypropylene is defined by its distributions of molecular weight (MWD) and chemical composition (CCD) for the case of propylene/ethylene copolymers. The MWD affects the mechanical and rheological properties of the polymer and the CCD affects its mechanical and thermal properties. Some analytical techniques commonly used to measure the microstructure of polyolefins will be discussed in the following sections.

2.3.1.1. Characterization Using TREF, CRYSTAF, CEF, and FIPA

Temperature rising elution fractionation (TREF), crystallization analysis fractionation (CRYSTAF), and crystallization elution fractionation (CEF), are analytical techniques that fractionate polyolefins according to their crystallizabilities in a dilute solution.

In TREF, a dilute polymer solution is injected into a packed column and the temperature is cooled down at a low rate (2.0 – 6.0 °C/h) until all, or most, of the polymer crystallizes. Chains with higher crystallizabilities precipitate first, followed by chains with lower crystallizabilities (Soares, 1994). These fractions are then eluted with a solvent (commonly trichlorobenzene, TCB) flowing at increasingly higher temperatures. An infrared (IR) detector measures the mass of polymer eluting from the column as a function of temperature, and a calibration curve is used to relate elution temperature to copolymer composition or stereoregularity (Soares *et al*., 2007). TREF can also be used as a preparative technique to collect polymer fractions that can be analyzed offline using GPC, ^{13}C NMR, and other analytical techniques (Soares, 1994). TREF may be used to determine the stereoregularity of polypropylene, but since atactic polypropylene is amorphous, it does not crystallize and is recovered as the first TREF fraction, soluble at room temperature. The broadness of the TREF peak is a qualitative indication of the structural defects in the polymer chain, and can be used to access donor effects on catalyst stereo- and regioselectivity. TREF has been used to identify the

three main chain populations present in polypropylene samples: amorphous, lowly crystalline, and highly crystalline (Soares, 1994).

TREF requires two fractionation steps: crystallization and elution; CRYSTAF was developed to eliminate the elution step (Monrabal, 1991; 1994). During CRYSTAF, the concentration of the polymer solution, initially added to a crystallization vessel at high temperature, is monitored as a function of the crystallization temperature using a mass detector, resulting in the cumulative CRYSTAF profile. The first derivative of the cumulative profile is called the derivative profile, and provides information that is similar to that measured by TREF, but at a considerably shorter analysis time. Unfortunately, CRYSTAF generally has lower resolution than TREF.

CEF is a newly developed technique that also uses two temperature cycles like TREF (Monrabal *et al*., 2007), as illustrated in Figure 2-23. In CEF, however, the crystallization step takes place under continuous solvent flow; therefore, fractions of different crystallizabilities precipitate in different sections of the column, reducing cocrystallization effects. After the completion of the crystallization step, the elution step, as in TREF, follows.

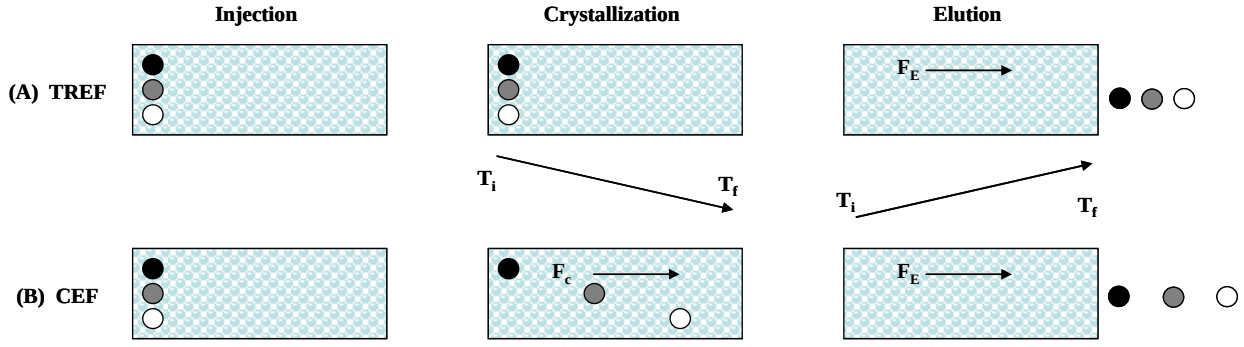

Figure 2-23. Fractionation by crystallinity using (A) TREF and (B) CEF (Monrabal *et al*., 2007)

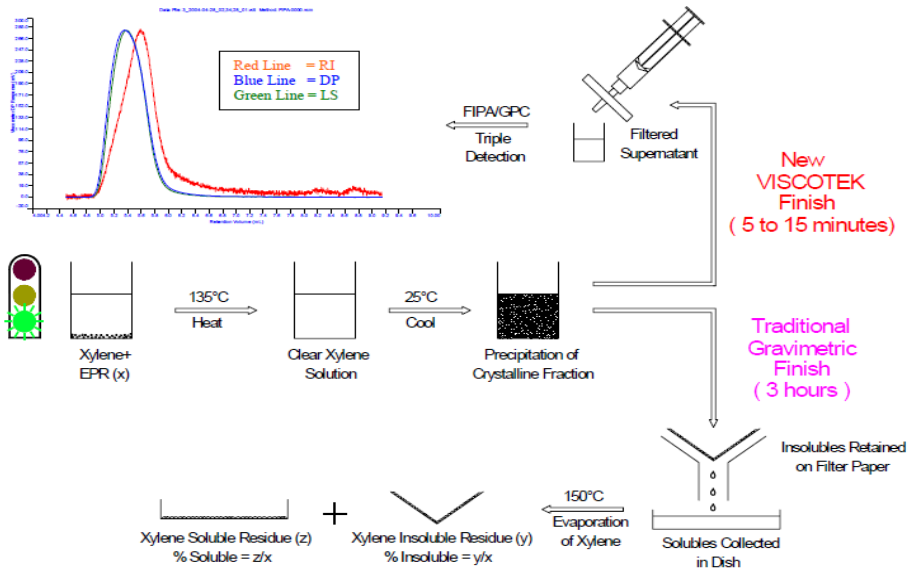

Figure 2-24. Xylene soluble analysis: FIPA versus the traditional method (Wong, 2008).

The most common xylene-soluble (XS) analysis requires dissolving approximately 1.0 g of polypropylene in 100 mL of xylene at 135°C; this is followed by a cooling step to precipitate the insoluble fraction. After the precipitation step, the sample is filtered and dried to record the soluble fraction (XS%) (SABIC, 2005). This technique takes around 3-4 hours to be completed, spent mainly on filtering and drying; it is also subjected to human error. A new automated technique, called flow injection polymer analysis (FIPA), uses the same concept of the traditional xylene-soluble analysis, but requires only 0.25 g of polypropylene and 25 mL of xylene. This method replaces the most time-consuming steps in the standard method, filtering and drying, with a FIPA/GPC step, which takes only 5 to 15 minutes to complete, as illustrated in Figure 2-24. The FIPA/GPC step consists of an automated sampler, filter to separate the insoluble fraction, pump to transfer the soluble fraction, GPC column, and a set of detectors. The detector set consists of an IR detector for concentration measurements, a light scattering detector for molecular weight measurements, and a viscometer for the measurement of the intrinsic viscosity (IV). Therefore, FIPA analysis provides average MW, IV, and XS%.

2.3.1.2. Carbon-13 Nuclear Magnetic Resonance (^{13}C NMR)

Carbon-13 nuclear magnetic resonance can be used to measure the sequence distribution of meso (isotactic, *m*) and racemic (syndiotactic, *r*) placements of the methyl groups along the polypropylene chain. Figure 2-25 shows these dyad arrangements. Triads, tetrads, pentads and higher sequences are similarly defined, as illustrated for a particular sequence in Figure 2-26 (Busico and Cipullo, 2001). These sequences follow well-established mathematical relationships (Odian, 2004).

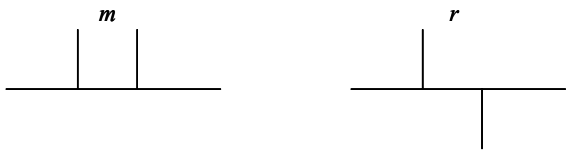

Figure 2-25. Propylene dyad arrangements (*m* = meso, *r* = racemic).

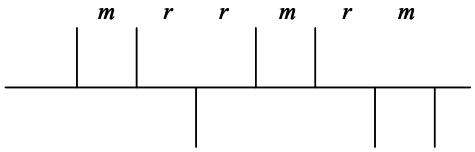

Figure 2-26. Higher propylene meso and racemic sequence distributions.

Polypropylene has only three functional groups: methyl (CH_3), methine (CH), and methylene (CH_2). The methyl region, which is used to determine the sequences in Figure 2-25 and Figure 2-26, lies between 19.7 to 22.0 ppm downfield of the tetramethylsilane (TMS) standard; the methine region between 27.90 to 28.5 ppm; the methylene region between 44.80 to 47.75 ppm (Busico *et al.*, 2001). These regions are comprised within a chemical shift region spreading 30 ppm, as shown in Figure 2-27 (Inoue *et al.*, 1972). The methyl region has nine major peaks, corresponding to the ten possible pentad configurations depicted in Figure 2-28, where the *mmrm* and *rmrr* pentads are superimposed.

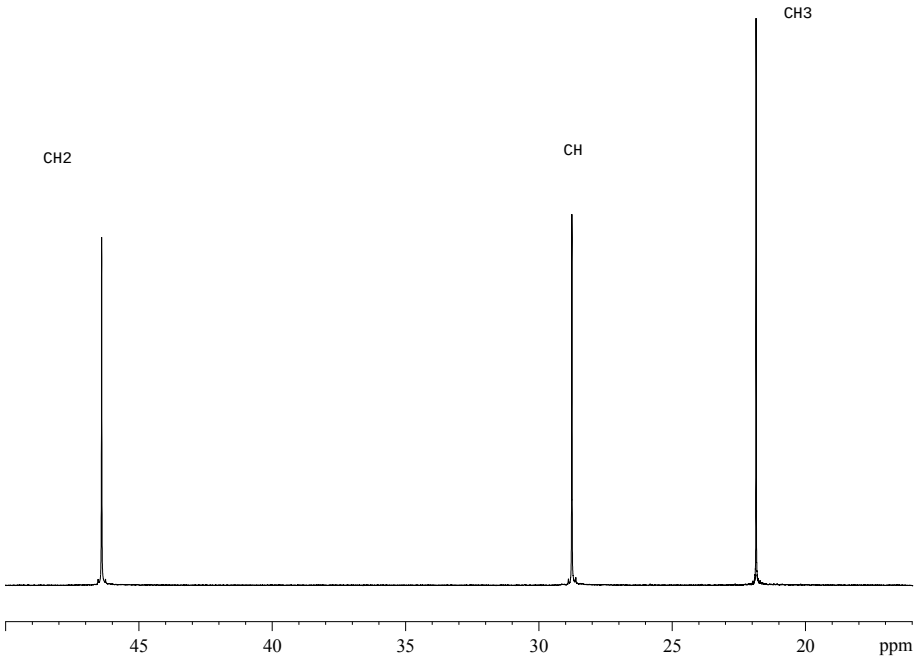

Figure 2-27. ^{13}C NMR spectral regions (proton-decoupled) for polypropylene made with 4th generation Ziegler Natta $TiCl_4/MgCl_2$ catalyst (measured in tetrachloroethane-1,2-d_2 at 120°C and 125MHz).

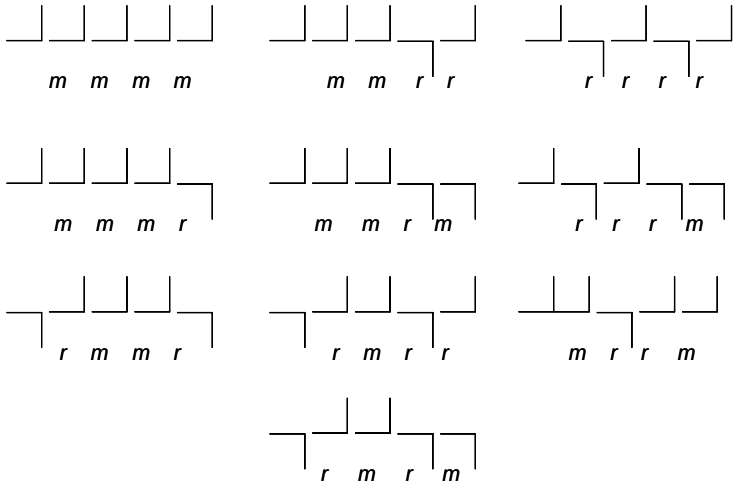

Figure 2-28: The ten possible pentad configurations for polypropylene.

One of the first reported ^{13}C NMR assignments for all polypropylene pentads were published by Zamelli *et al.* (1975) using a 22.63 MHz ^{13}C NMR. High field spectrometers (150 MHz ^{13}C NMR) allowed Busico *et al.* (1997, 1998) to achieve heptad to decad resolution for

regioregular polypropylene. The pentad chemical shift range using high field spectrometers (150 MHz ^{13}C NMR) has been reported by Busico *et al.* (2001), and is reproduced in Table 2-1.

Table 2-1. Experimental chemical shift values (δ) using 150MHz ^{13}C NMR (in tetrachloroethane-1,2-d_2 at 70°C; ppm downfield of TMS), reported by Busico *et al.*(2001).

Pentad	*mmmm*	*mmmr*	*rmmr*	*mmrr*	*mmrm + rmrr*	*rmrm*	*rrrr*	*rrrm*	*mrrm*
δ	22.0-21.7	21.7-21.4	21.4-21.2	21.2-21.0	21.0-20.7	20.7-20.5	20.5-20.25	20.25-20.0	20.0-19.7

2.3.2. Effect of External Electron Donors on Propylene Polymerization

The type and concentration of the external electron donor affect propylene polymerization kinetics and polypropylene properties. Forte and Coutinho (1996) have studied these effects on the molecular weight of polypropylene made in slurry and bulk polymerizations at 25°C using $MgCl_2$·$TiCl_4$·diphthalate ester / triethylaluminum·alkoxyilne. They investigated four different external donors: diisopropyl-dimethoxysilane (DIPDMS), diphenyl-dimethoxysilane (DPDMS), dicyclopentyl-diethoxysilane (DCPDMS), and cyclohexyl-methyl-dimethoxysilane (CHMDMS). Propylene bulk polymerizations were carried out in a two-liter reactor for two hours at a pressure of 30 atm, temperature of 70°C, with 0.006 g of catalyst (0.003 mmol Ti), with an aluminum/titanium ratio of 1400, and aluminum/external donor ratio of 20. Each type of external donor generated catalysts that produced polypropylene with different molecular weight averages, xylene insoluble fractions, and oligomer contents at the same polymerization conditions. Table 2-2 shows the molecular weight averages and intrinsic viscosities for polypropylenes made with the four different external donors. Table 2-3 shows how the external donor type influenced catalyst activity, hydrogen response, and xylene-insoluble fraction (X.I.%).

Table 2-2. Effect of external donor (ED) type on the molecular weight and intrinsic viscosity of polypropylene made by bulk propylene polymerization (Forte and Coutinho, 1996).

	Intrinsic Viscosity	M_n	M_w	M_w/M_n
ED	g/dl	g/mol	g/mol	
DIPDMS	1.97	65,100	405,200	6.22
		69,600	402,700	5.78
DPDMS	1.24	55,100	202,400	3.67
		55,500	212,800	3.83
DCPDMS	2.26	76,600	453,600	5.92
		83,500	436,550	5.22
CHMDMS	1.63	67,400	368,400	5.46
		64,600	350,400	5.42

Table 2-3. Effect of the external donor (ED) type on catalyst activity, hydrogen response, and xylene insoluble fraction (Forte and Coutinho, 1996).

ED	Cat. Activity (Kg PP/mol Ti·2h)	Melt Flow Index (MFI) (g/10 min)	*X.I.* (%) w/w
Without ED	15.2	6.2	68.0
DIPDMS	20.7	12.0	97.0
DPDMS	14.4	65.4	97.9
DCPDMS	22.7	5.5	96.6
CHMDMS	15.8	15.6	96.9

They also compared the properties of polypropylene produced by slurry polymerization at 60^{o}C and a propylene partial pressure of 1 atm, using DIPDMS and DPDMS at different concentrations and Al/external donor ratios. They observed that the molecular weight averages of polypropylene made when DIPDMS was used were higher than when DPDMS was used, at the same Al/external donor ratio, as shown in Table 2-4. Based on this observation, they claimed that external donors with bulkier groups (in this case, DIPDMS) had a stabilizing effect on the stereospecific centers, resulting in the production of polymer with higher molecular weights. They also observed that DIPDMS led to a catalyst with higher activity: 20.7 kg PP/mole Ti·(2 hr), compared to 14.4 kg PP/mole Ti·(2 hr) when DPDMS was used. When DIPDMS was used, the xylene insoluble fraction was slightly lower (97.0 × 97.9 %w/w).

Several polymerizations were also done for each external donor at a constant Al/Ti ratio. Catalysts that used DIPDMS had higher activity and *X.I.* %. The catalyst activity reached its maximum at Al/ DIPDMS of 20. When DPDMS was used the activity reached a maximum at Al/ DPDMS = 10 and then started to decrease as shown in Table 2-5.

Table 2-4. Effect of external donor (ED) concentration on polypropylene molecular weight (Forte and Coutinho, 1996).

Molar ratio Al/ED	M_n (g/mol)	M_w (g/mol)	M_w/M_n
DPDMS			
1	36,000	359,000	10.0
10	37,300	431,000	11.6
50	38,000	296,000	7.8
DIPDMS			
1	104,000	955,000	9.2
10	67,000	518,000	7.7
20	40,000	376,000	9.4
50	42,300	475,000	11.2
Without ED	30,400	185,000	6.1

Table 2-5. Effect of external donor (ED) type, Al/ED, and Al/Ti on catalyst activity and X.I.% of polypropylene (Forte and Coutinho, 1996).

Molar ratio		ED = DIPDMS		ED = DPDMS	
Al/ED	Al/Ti	Activity Kg PP/mole Ti· 2 hr	*X.I.* (%) w/w	Activity Kg PP/mole Ti· 2 hr	*X.I.* (%) w/w
1	170	0.9	98.4	0.85	96.5
10	170	1.07	97.5	1.05	96.8
15	170	1.10	96.9	1.03	95.4
20	170	1.14	96.1	1.00	95.1
50	170	1.06	94.7	0.99	91.0
Without ED	170	0.97	91.7	0.97	91.7
10	50	0.96	96.1	1.03	95.7
10	85	1.09	96.4	1.04	96.7
10	340	0.85	97.5	0.94	96.8

Xu *et al.* (1998) used preparative TREF (p-TREF) to study the effect of internal and external donors on the tacticity distribution of polypropylene made with heterogeneous Ziegler Natta catalysts. The polymerizations were carried out using a $MgCl_2/TiCl_4$-$AlEt_3$ catalyst in four different scenarios: (A) without internal and external donors; (B) with internal donor only;

(C) with external donor only; and (D) with internal and external donor. They used di-n-butyl phathalate (DNBP) as internal donor and diphenyldimethoxysilane (DPDMS) as external donor. Figure 2-29 shows that the p-TREF curves are relatively broad, and some have more than one peak. Preparative TREF was used to collect fractions in temperature intervals: < 80ºC, 80-103ºC, 103-115ºC, and > 115ºC. In addition to the obvious finding that the use of internal and external donors reduces the formation of chains with low isotacticity, Xu *et al.* observed that both internal and external donors reduced the *mmmm* frequency in the amorphous, room temperature-soluble TREF fraction as shown in Table 2-6.

The fractions collected at temperatures higher than 115ºC had almost 100% *mmmm* frequency. The authors proposed that the aspecific sites on the 110 $MgCl_2$ face had one more vacant site than the aspecific sites on the 100 face, and that the site on the 110 face produced polypropylene with higher *mmmm* pentads; they claimed that the electron donors changed only the sites on the 100 face to isospecific sites (Xu *et al.*, 1998). However, it is also possible that, in the absence of external or internal donors, the *mmmm* pentad content of chains made in the low isotactic sites is not high enough to make them crystallize, and therefore they are recovered in the TREF soluble fraction. When donor is added to the catalyst, it blocks one of the vacancies on the low isotactic or atactic sites, enabling them to make chains with higher *mmmm* frequencies. These chains become semicrystalline and crystallize above room temperature; therefore, they are not recovered in the soluble fraction. As a consequence, the *mmmm* % in the soluble fraction decreases with the addition of electron donors.

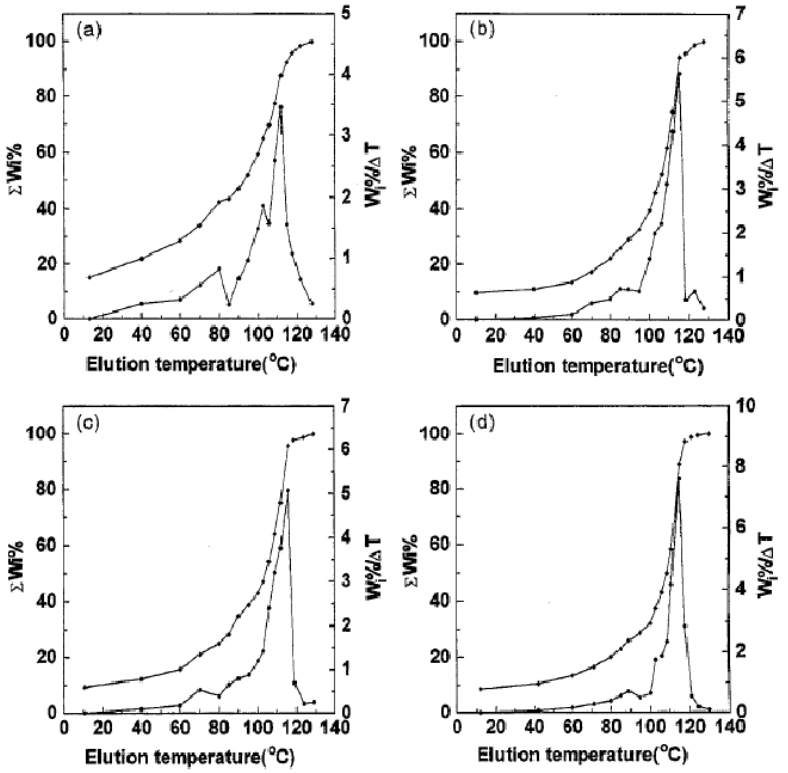

Figure 2-29. TREF profiles for polypropylene prepared (a) without internal and external donors, (b) with internal donor only, (c) with external donor only, and (d) with internal and external donors. Internal donor = DNBP and external donor = DPDMS (Xu *et al.*, 1998).

Table 2-6. Pentad *mmmm* % for the first three fractions for each samples using ^{13}C NMR (100.7 MHz at 370K in $C_6D_4Cl_2$) (Xu *et al.*, 1998).

Sample	*mmmm* %			
	A (no ID, no ED)	B (ID, no ED)	C (no ID, ED)	D (ID, ED)
R.T	41.7	33.7	29.7	22.9
80ºC	75.8	72.6	77.1	73.6
103ºC	91.7	89.3	92.4	91.9

TREF was also used by Chadwick *et al.* (2001) to show stereoselectivity differences among different donors. Three internal donors were used: ethyl benzoate (EB), di-iso-butyl-phthalate (DIBP), and diether. *p*-Ethoxy-ethyl-benzoate (PEEB) was used as external donor with the EB-modified catalyst, and three different external donors were used with the DIBP-modified catalyst: 3,3,3-tri-fluro-propyl-(methyl)-dimethoxy-silane (TFPMDMS), cyclohexyl-

methyl-dimethoxysilane (CHMDMS), and dicyclopentyl-dimethoxysilane (DCPDMS). The diether-modified catalyst did not require an external donor. They observed that higher crystallinity fractions also had higher molecular weights and higher *mmmm* pentad frequencies for all systems studied, as shown in Figure 2-30 and Table 2-7. Polypropylene made with the DIBP-modified catalyst was the most influenced by external donor type: when TFPMDMS was used, the polypropylene made had the lowest crystallinity of all polymers produced, with peak elution temperature of 110ºC, but it also had the highest crystallinity when DCPDMS was used, with peak elution temperature at 118-119ºC. Interestingly, the EB/PEEB system made polypropylene with a bimodal TREF profile, with elution peak temperatures at 111-114ºC and 115-117ºC.

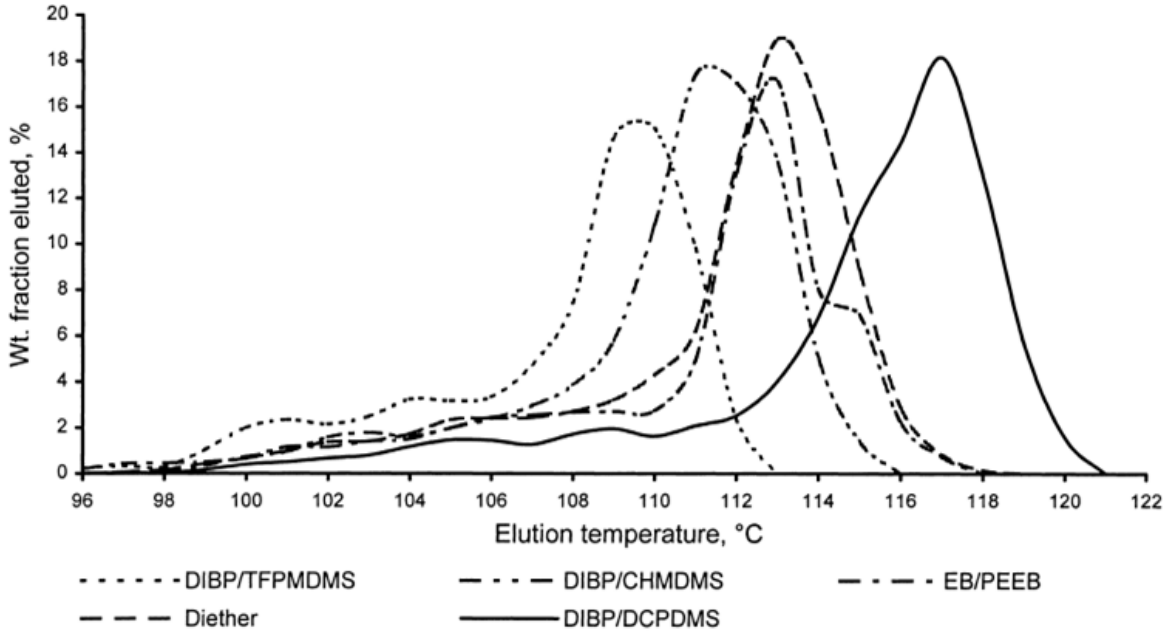

Figure 2-30. TREF curves for polypropylene made with different donor systems (Chadwick *et al.*, 2001).

Table 2-7. MWD and *mmmm* pentad frequency for the propylene TREF fractions made with different internal/external donor (ID/ED) systems (Chadwick *et al.*, 2001).

ID/ED	TREF		Molecular weight distribution					
	El. Temp ºC	Wt. % Eluted	M_n x 10^{-3} g/mol	M_w x 10^{-3} g/mol	M_z x 10^{-3} g/mol	M_w/M_n	M_z/M_w	*mmmm*%
EB/PEEB	26-95	19.2	25	84	211	3.4	2.5	79.9
	113-114	43.2	283	722	1538	2.6	2.1	97.1
	115-117	9.9	415	998	2018	2.4	2.0	98.3
DIBP/TFPMDMS	26-95	21.4	21	73	210	3.4	2.9	84.1
	113-114	15.1	141	332	746	2.4	2.2	97.0
DIBP/CHMDMS	26-95	7.2	16	67	206	4.3	3.1	77.6
	113-114	18.9	163	494	1173	3.0	2.4	97.3
DIBP/DCPDMS	26-95	4.6	7	28	98	3.9	3.6	80.3
	113-114	10.9	80	162	288	2.0	1.8	97.4
	116	14.5	144	345	743	2.4	2.2	98.2
	118-119	18.6	266	718	1793	2.7	2.5	99.7
Diether/-	26-95	5.9	10	42	143	4.2	3.4	83.6
	113-114	35.0	92	234	465	2.5	2.0	98.0

It has also been proposed that behavior differences among aloxysilane electron donors are due to their electron density, complexation with catalyst surfaces, bulkiness, and their stability or ability to protect their hydrocarbon parts (Harkonen *et al.*, 1995).

External donor mixtures can be used to combine the desired features of each individual external donors and achieve better process control during polymerization. Miro and Ohkura (2000) used mixtures of 2.5 to 50 mol % of dicyclopentyldimethoxysilane (DCPDMS) and propyltriethoxysilane (PTES) to improve the impact resistance and processability of polypropylenes. Ishimaru *et al.*(1997) reported that the use of two electron donor types produced polypropylene with broader MWDs. Miro et al. (2003) used two different organosilicon electron donors with magnesium-supported catalysts to produce polypropylene

with reasonably broad MWDs, desirable melt flow rates, low melting points, and low decalin-soluble fractions.

For some $MgCl_2$/internal donor·Al/external donor catalysts, where the internal and external donors are aromatic mono-esters (such as internal donor = EB and external donor = PEEB), PEEB could be used to self-extinguish the polymerization during normal plant shutdown. Newer catalyst generations use different internal donors (aromatic di-esters, such as DIPB) and external donors (aloxysilanes, such as n-propyltrimethoxysilane or NPTMS). This system produces polypropylene with high activity and high isotactic index; however, the advantage of self-extinguishing is lost. In this case, a selective poison such as CO is used to kill the polymerization. However, restarting the reactor back to its normal operation requires the complete removal of the CO, which is an expensive and time consuming task.

The use of donor mixtures to improve polymerization activity and to make polypropylene with high isotactic index, while maintaining the self extinguishing property, is an interesting area of research. Campbell and Chen (2008) and Chen (2008) reported that when esters or diesters of aromatic dicarboxylic acids were selected as internal donors, the use of a combination of esters and aloxysilanes as external donors resulted in good catalyst activity and very good process stability while maintaining the self-extinguishing property. Chen and Nemzek (2006) used a mixture of external donors, where at least one of them was a normally dominating donor and the other was a single normally dominated donor or a mixture of them. The normally dominating donor is used because it promotes high catalyst activity and has a positive effect on one or more polypropylene properties, including molecular weight averates and distribution, xylene-insoluble fraction, and melt flow index. The normally dominated donor, or mixture of donors, is used to add additional properties to the catalyst without influencing those promoted by the normally dominating donor. For instance, a silane external donor can be used as dominating donor (DCPDMS, DIBDMS, DCHDMS, or NPTMS), and a carboxylic acid ester, such as PEEB, can be added as dominated donor to improve the catalyst activity while maintaining the advantage of self-extinguishing. Chen and Nemzek (2006) claimed that the best results were achieved with silanes of C_5 and C_6 cyclic groups when mixed with PEEB.

2.4. MATHEMATICAL MODELING AND SIMULATION OF PROPYLENE POLYMERIZATION IN THE PRESENCE OF ELECTRON DONORS*

In this section, a summary of a previously developed model for propylene polymerization that accounts for the effect of external donors will be given. The model takes into consideration the effect of hydrogen and external electron donor on polypropylene microstructure and propylene polymerization rate. The model also accounts for the reversible transformation of aspecific to stereospecific sites during chain growth promoted by external donors, as proposed by Busico *et al.* (1995). Table 2-8 lists the main polymerization kinetic steps considered in the model, where the active sites may either in stereospecific (*I*) or aspecific (*II*) states.

* The subjects discussed in this chapter have been published in Alshaiban, A. and J.B.P. Soares, *Macromol. React. Eng.* **2011**, *5*, 96−116 and Alshaiban, A. and J.B.P. Soares, *Macromol. Symp.* **2009**, *285*, 8−22.

Table 2-8: Elementary steps for the propylene polymerization mechanism with 4th generation Ziegler-Natta catalysts in the presence of external electron donors (*j=I* or *II*, and $P_{C*}^{j} = P_0^{j}, P_H^{j}$, or P_{Et}^{j}).

Step	Equation		Step	Equation	
Activation	$C_j + Al \xrightarrow{k_a^j} P_0^i$	(2.1)	Propagation	$P_{r,i}^{j} + M \xrightarrow{k_p^j} P_{r+1,i}^{j}$	(2.11)
Initiation	$P_0^j + M \xrightarrow{k_i^j} P_{1,1}^j$	(2.2)	Termination by		
	$P_H^j + M \xrightarrow{k_{iH}^j} P_{1,1}^j$	(2.3)	β-hydride elimination	$P_{r,i}^{j} \xrightarrow{k_\beta^j} P_H^j + D_{r,i}^j$	(2.12)
	$P_{Et}^j + M \xrightarrow{k_{iR}^j} P_{1,1}^j$	(2.4)	Hydrogen	$P_{r,i}^{j} + H_2 \xrightarrow{k_H^j} P_H^j + D_{r,i}^j$	(2.13)
Transformation by Donor			Monomer	$P_{r,i}^{j} + M \xrightarrow{k_M^j} P_{1,1}^j + D_{r,i}^j$	(2.14)
	$P_{C*}^{II} + Do \xrightarrow{k_{Do}^+} P_{C*}^I$	(2.5)	Aluminum	$P_{r,i}^{j} + Al \xrightarrow{k_{Al}^j} P_{Et}^j + D_{r,i}^j$	(2.15)
	$P_{C*}^I \xrightarrow{k_{Do}^-} P_{C*}^{II} + Do$	(2.6)	Deactivation	$P_{r,i}^{j} \xrightarrow{k_d^j} C_d + D_{r,i}^j$	(2.16)
	$P_{r,i}^{II} + Do \xrightarrow{k_{Do}^+} P_{r,i+1}^I$	(2.7)	Poisoning	$P_{r,i}^{j} + I \xrightarrow{k_{d,I}^j} C_d + D_{r,i}^j$	(2.17)
	$P_{r,i}^I \xrightarrow{k_{Do}^-} P_{r,i+1}^{II} + Do$	(2.8)			
	$P_{r,i}^{II} + Do \xrightarrow{k_{Do}^+} B_r^{II} + P_{0,i+1}^I$	(2.9)			
	$P_{r,i}^I \xrightarrow{k_{Do}^-} B_r^I + P_{0,i+1}^{II} + Do$	(2.10)			

Each step of the polymerization mechanism shown in Table 2-8 is described in the next paragraphs.

Activation: Catalyst at state *I* or *II* (C_I and C_{II}) is activated (alkylated and reduced) by reaction with the alkylaluminum cocatalyst (*Al*) – typically triethylaluminum – according to Equation (2.1), forming monomer-free active sites, P_0^I and P_0^{II}, where the subscript 0 indicates that there are no monomer molecules attached to the active site.

Initiation: Monomer-free sites, either resulting from catalyst activation (P_0^I, P_0^{II}) or chain transfer reactions ($P_H^I, P_H^{II}, P_{Et}^I, P_{Et}^{II}$), are initiated by insertion of the first monomer molecule (*M*), according to Equations (2.2) to (2.4). The following nomenclature convention was adopted to keep track of polymer chain length, number of blocks per chain, and catalyst state: $P^{state}_{chain\ length,\ number\ of\ blocks}$

Site transformation by electron donor: The inclusion of the reversible site transformation from the stereospecific state *I* to the aspecific state *II* in the presence of the electron donor (*Do*) is the new feature of this model. As the site state changes from *II* to *I* (by coordination with a *Do* molecule) or from *I* to *II* (by release of a *Do* molecule), the polymer chain length (*r*) is not altered (*r* remains the same), but the number of stereoblocks increases by 1 (*i*+1), as shown in Equations (2.5) to (2.10). Equations (2.7) and (2.8) keep track of the number of blocks and length of the whole polymer chain. It is also useful to track the size distribution of isotactic (*I*) and atactic (*II*) blocks; for this distribution, we have to reformulate the model equations to describe the concentration of blocks of length *r* (B_r^I and B_r^{II}), according to Equations (2.9) and (2.10). After a site transformation step, the length of the living polymer is reset to zero, since a new block starts being formed at this moment. With these expressions, in addition to the overall balances, we are able to follow the length of all isotactic and atactic segments in the reactor without considering to which chain (isotactic, atactic, or stereoblock) they belong.

Propagation: Propagation is the most common step during polymerization. The addition of monomer to sites in state *I* or *II* increases the length of the chain by one unit (*r*+1), as indicated in Equation (2.11).

Chain transfer: The four most common chain transfer steps in propylene coordination polymerization are β-hydride-elimination, transfer to hydrogen, transfer to monomer, and transfer to cocatalyst. These chain transfer steps are described in more details below.

> **β-Hydride elimination:** During β-hydride elimination, one of the hydrogen atoms attached to the β carbon atom is transferred to the titanium active site,

forming a metal hydride Ti-H site (P_H^I or P_H^{II}) and a dead chain with an unsaturated chain end ($D_{r,i}^I$ or $D_{r,i}^{II}$), as shown in Equation (2.12).

Transfer to hydrogen: This is the main transfer step in industrial-scale propylene polymerization, generating a metal hydride Ti-H site, and a dead chain with a saturated chain end, as shown in Equation (2.13). Varying hydrogen concentration in the reactor is the main technique to control the molecular weight averages of industrial polypropylene resins.

Transfer to monomer: Transfer to monomer takes place when a monomer molecule coordinated to the active site "fails" to insert into the growing polymer chain, but instead terminates chain growth, forming a living polymer chain of unity length and a dead chain with a terminal unsaturated end, as shown in Equation (2.14).

Transfer to cocatalyst: In some reactor operation conditions, especially at elevated polymerization temperatures, the frequency of transfer to cocatalyst may be considerable. It is, however, generally negligible at normal polymerization temperatures with $TiCl_4/MgCl_2$ catalysts. When this transfer step occurs, an active site bonded to the alkyl group of the alkylaluminum compound (an ethyl group in the case of triethylaluminum) and a dead polymer chain with a saturated chain end will be formed, as illustrated in the Equation (2.15).

Site deactivation: Most Ziegler-Natta catalysts deactivate according to first or second order kinetics, generating a dead polymer chain and a deactivated site (C_d) that is unable to catalyze polymerization. First order deactivation kinetics was adopted for simplicity, as shown in Equation (2.16).

Catalyst poisoning: The presence of catalyst poisons in the polymerization system is undesirable. One of the functions of alkylaluminum cocatalysts is to passivate the system by removing most of the polar poisons from the reactor. Catalyst poisoning will result in an inactive catalyst and a dead polymer chain. Even though the kinetics of

catalyst poisoning is not well understood, we have adopted the simple bimolecular mechanism step with a polar impurity (*I*), as shown in Equation (2.17).

The proposed model can describe the MWD and molecular weight averages of purely isotactic, purely atactic, and stereoblock chains; it can also describe the MWD and molecular weight averages of isotactic and atactic segments. Three types of population balances were formulated to monitor different aspects of the polypropylene chain microstructure: 1) for the whole chains, without monitoring the number or type of stereoblocks per chain, 2) for purely isotactic, purely atactic, and stereoblock chains, and 3) for chain segments (Alshaiban and Soares, 2009; 2011).

Two methods were used to solve this model: the method of moments was used to obtain average properties, and Monte Carlo simulation to recover the complete microstructural distributions. Applications of both modeling approaches, and model development details, have been reported by Alshaiban and Soares (2009; 2011).

2.5. DECONVOLUTION OF THE MOLECULAR WEIGHT DISTRIBUTION

Heterogeneous Ziegler-Natta catalysts make polypropylene with broad MWD because of the presence of several different site types. The polymer MWD can be deconvoluted into two or more Flory's most probable distributions (Flory, 1953), one for each site type on the catalyst. Flory's distribution is expressed as,

$$w(\log MW) = 2.3026 MW^2 \tau^2 \exp(-MW\tau) \tag{2.18}$$

$$\tau = \frac{1}{M_n} \tag{2.19}$$

where M_n is the number average molecular weight and MW is the polymer molecular weight. The MWD of polymers made with Ziegler-Natta catalysts can be conveniently described with a summation of different Flory's distributions (Kissin, 1993; Kissin, 1995; Soares and Hamielec, 1995; Beigzadeh *et. al*, 2000; Alghyamah and Soares, 2009),

$$w(\log MW) = 2.3026 MW^2 \sum_{j=1}^{n} w_j \tau_j^2 \exp(-MW\tau) \qquad (2.20)$$

where, w_j is the weight fraction of the polymer made on site type j and n is the total number of site types in the catalyst.

Therefore, 2(n-1) independent parameters $(\tau_1, \tau_2 .... \tau_n, w_1, w_2 .... w_{n-1}, w_n = 1 - \sum_{j=1}^{n-1} w_j)$ need to be estimated to describe the MWD of polyolefins made with a Ziegler-Natta catalyst that has n site types. These parameters can be estimated by minimizing the sum of the square of the differences between the experimental and predicted MWDs using the objective function below,

$$\sum \Delta^2 = \min \left[\sum_{i=1}^{m} w(\log MW_i)_{\exp} - \left\langle 2.3026 MW_i^2 \sum_{j=1}^{n} w_j \tau_j^2 \exp(-MW_i \tau) \right\rangle \right]^2 \qquad (2.21)$$

where m is the number of data points in the experimentally measured MWD.

Chapter 3

POLYMERIZATION EXPERIMENTS

3.1. EXPERIMENTAL DESIGN

One of the objectives of this research was to estimate the main polymerization rate constants for the model developed by Alshaiban and Soares (2009; 2011) considering the influence of donor to catalyst ratio (*Do*/*Ti*), hydrogen concentration (H_2), and polymerization temperature (*T*), on the polymer molecular weight distribution (MWD), tacticity distribution, and polymerization activity. The catalyst selected for this investigation was an industrial 4th generation $TiCl_4/MgCl_2$ heterogeneous Ziegler-Natta catalyst activated with triethylaluminum. Dicyclopentyldimethoxysilane (DCPDMS, also known as D-donor) was the main external donor used during the polymerizations, unless otherwise mentioned.

Two sets of experiments were performed. Design A involved three factors (*Do*/*Ti*, H_2, and *T*) at two levels (with and without *Do*, with and without H_2, and T = 60 or 70^{o}C) with a constant *Al/Ti* = 900 mol/mol, as shown in Figure 3-1. This design requires 2 × 8 = 16 distinct experiments, including replicates.

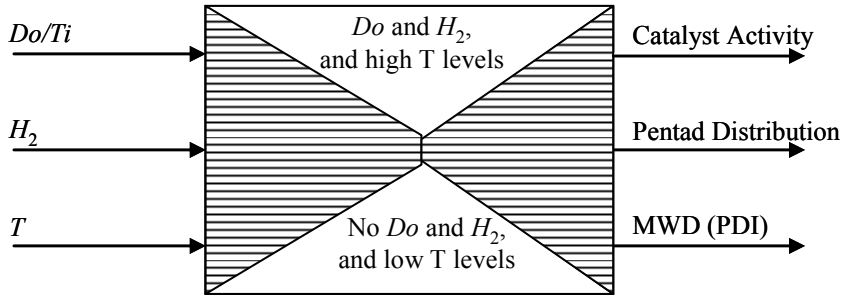

Figure 3-1. Three factors, two levels, and three responses for experimental Design A.

Design B was used to investigate two additional levels of the same three factors (*Do*/*Ti*, H_2, and *T*), resulting in 8 experiments. In addition, two replicates for the central experiments were carried out at *Al*/*Ti* = 900 mol/mol, *Do*/*Ti* = 1.4 mol/mol, P_{H_2} = 16 psi, and *T* = 60 °C, adding up to a total of 10 experiments.

Another set of polymerization experiments were conducted using different types of external electron donors and their binary mixtures. The external donors used were D donor, N donor (NPTMS), P donor (DIPDMS), and PEEB. The chemical structures of these donors are shown in Figure 3-2. The donor that gave the catalyst with best activity (D donor) was selected to be mixed with PEEB to generate a system with self-extinguishing capabilities. The molar ratio D donor/PEEB was constrained by a maximum drop in polymerization activity of 5 %. PEEB is known for decreasing the polymerization activity, but it is advantageous in commercial processes because of its stability and self-extinguishing properties (Chen, 2008).

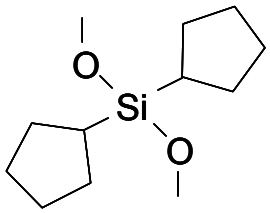

DCPDMS (D-Donor)
Dicyclo pentyl dimethoxy silane

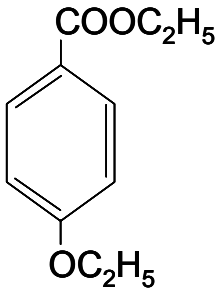

PEEB
Para ethoxy ethyl benzoate

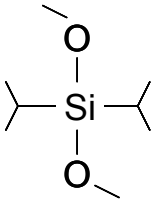

DIPDMS (P-Donor)
Diiso propyl dimethoxy silane

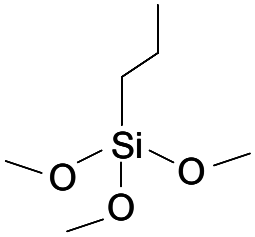

NPTMS (N-Donor)
n-Propyl trimethoxy silane

Figure 3-2. Chemical structures of external electron donors used in this research.

In order to decompose the error associated with our GPC and ^{13}C NMR analysis results, a hierarchical design of experiments into the three levels shown in Figure 3-3 was employed. The 95 % confidence intervals estimated from these analyses were generalized for the rest of the runs in all groups.

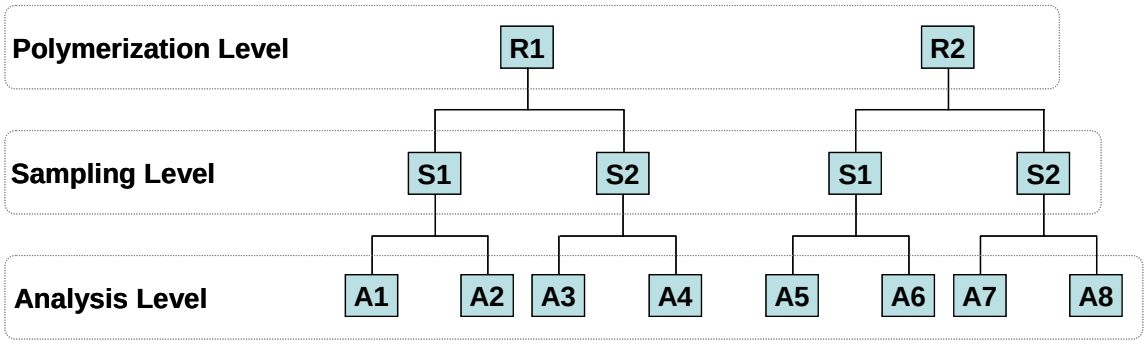

Figure 3-3. Hierarchical design of experiment chart used for GPC and ^{13}C NMR analyses for 2 polymerization replicate runs (R), 2 samples (S) per run, and two analyses (A) for each sample.

3.2. EXPERIMENTAL PROCEDURES

All polymerizations were carried out in a 300 mL stainless steel semi-batch stirred reactor (PARR Instrument Company). The reactor was equipped with a temperature control loop that consisted of an external electrical heater and an internal cooling coil, capable of keeping the temperature within ± 0.3 °C of the set point during polymerization, as shown in Figure 3-4. The stirrer speed could be increased up to 650 rpm.

All operations were performed under nitrogen atmosphere (99.999%, from Praxair) using standard Schlenk techniques or inside a glove-box. Polymer grade propylene (99.5 %, Matheson) and nitrogen were purified by passing through columns packed with R3-11 copper catalyst, activated alumina, and 3 Å/4 Å mixed molecular sieves. Triethylaluminum (2 M in hexane) was purchased from Aldrich and used without further purification. D donor was donated by SABIC. Solvents for catalyst synthesis and polymerization were purified by passing through columns packed with activated alumina and molecular sieves (Zeolum Type F-9, Tosoh). All purified solvents were stored in Schlenk flasks with 3A/4A mixed molecular sieves.

Prior to polymerization, the reactor was conditioned to remove impurities by three cycles of purging with nitrogen and heating to 150°C under vacuum. Then, the reactor was allowed to cool under dry nitrogen flow. A volume of 125 mL of dry *n*-hexane and the desired amount of triethylaluminum (TEAL) were charged to the reactor using a double-tipped needle under nitrogen pressure through a septum inlet. After that, the stirrer was turned on and the

reactor contents were kept under stirring for approximately 10 minutes. The reactor gas space was then vented through an oil bubbler. If needed, the desired volume of hydrogen was fed to its predefined pressure. Then, the reactor temperature control was turned on to achieve the required polymerization temperature. When the temperature set point was reached, propylene was fed to the reactor until reaching its desired partial pressure. The catalyst suspension (catalyst powder suspended in 25 mL dry *n*-hexane) was injected into the reactor by flowing propylene through the catalyst cylinder, pushing the catalyst suspension into the reactor. The propylene flow was monitored by an online flow meter and recorded through a data acquisition system. The polymerization was stopped when approximately 7 grams of polymer (5 % of the suspension concentration) were produced to minimize mass or heat transfer resistances. The polymerization was terminated by turning off the stirrer, closing the propylene feed line, and depressurizing the reactor quickly. The reactor was then opened and the catalyst was quenched with 150 mL of acidified ethanol (2 % HCl by volume). The polymer was washed with ethanol, filtered, and left to dry at 60ºC in an oven overnight, prior to weighing.

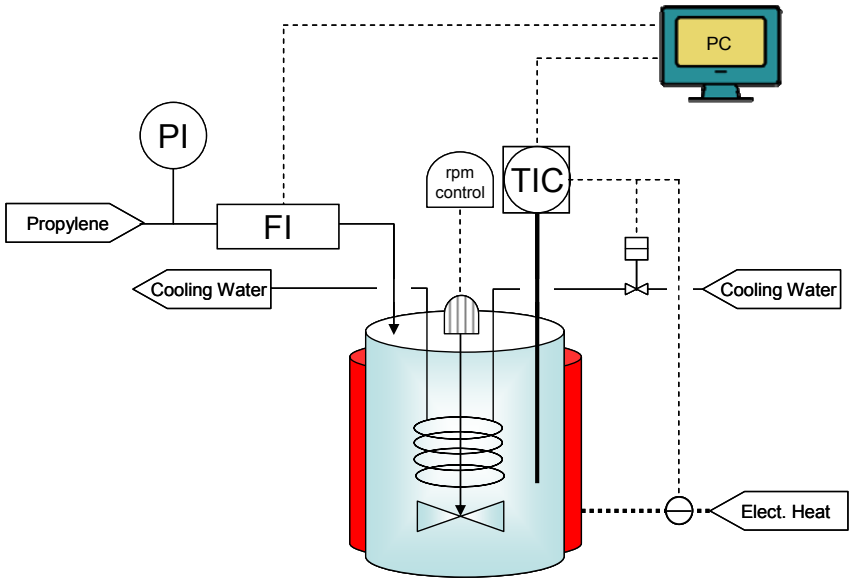

Figure 3-4. Polymerization reactor setup.

A Polymer Char high-temperature gel permeation chromatography (GPC) was used to determine the MWD of the polypropylene samples according to ASTM D3536. The polymer sample was prepared by dissolving a maximum of 18 mg of polymer in 9 mL of 1,2,4-trichlorobenzene (TCB) in a 10 mL vial. The vial was then placed in an oven at 160°C for an hour, and then visually inspected to assure that the polymer solution was uniform and contained no impurities. The sample was then placed in the GPC auto-sampler and ready for analysis. GPC analysis was performed at 145°C with a TCB flow rate of 1 mL/min. The GPC was equipped with a linear column (Polymer Labs Columns) and three detectors in series (infra-red, light scattering, and differential viscometer). The GPC was calibrated using polystyrene narrow standards.

Crystallization elution fractionation (CEF, Polymer Char) was used to analyze the stereoregularity distribution of polypropylene. A mass of approximately 15−20 mg of polymer was added into a 10 ml vial and placed in the autosampler which automatically added the required quantity of trichlorobenzene (TCB). The analyses started by heating the dissolved sample to 160°C, after which the sample was maintained at 140°C for 20 minutes. The polymer solution was then pumped through the CEF column while being cooled to 35°C at a cooling rate of 0.7°C/min and crystallization flow rate of 0.0075 mL/min. After the sample was completely deposited in the CEF column, the elution cycle stared with a heating rate of 3.0°C/min to 140°C and an elution flow rate of 1.0 mL/min.

A high resolution 500 MHz Bruker instrument was used for the ^{13}C NMR analysis. A sample of 100 mg of polymer was transferred into the 7” long NMR tube filled with tetrachloroethane-1,2-d_2 (TCE) as solvent. The sample was then dissolved in the solvent at 120°C for 24 hours. The analysis was then started using the interface computer at 120°C and 125 MHz. The pulse angle was 90°, the pulse repetition was 10 seconds, the spectral width was 5000 Hz, the number of scans was 6000, and 32 thousand data points were collected for each sample analyzed.

3.3. SCREENING POLYMERIZATION EXPERIMENTS

3.3.1. Mass Transfer Limitations

Screening experiments were performed to evaluate the effect of external mass transfer limitations during polymerization and to measure the concentration of propylene in the diluent (hexane) at different temperatures and pressures.

Even though they are not crucial for the estimation of apparent polymerization kinetic constants, mass transfer limitations are preferably kept at a minimum level in our experiments, since they would bias the MWD deconvolution procedure by generating an internal radial MWD profile along the polymer particle (McKenna and Soares, 2001).

There are two main ways of studying whether mass transfer limitations are significant or not. The first is to conduct polymerizations with varying stirring rates; if no differences in polymerization rate are observed, external mass transfer limitations can be assumed to be negligible. The second involves the fractionation of the polymer or catalyst particles by size (through sieving); if the MWD is independent of particle size, internal mass transfer limitations are not significant. According to extensive simulations with the multigrain model, internal mass transfer limitations are generally negligible for most heterogeneous Ziegler-Natta catalysts (McKenna and Soares, 2001).

The catalyst used in this work is a commercial 4th generation Ziegler-Natta catalyst with well controlled morphology that produces spherical polymer particles with uniform morphology, as shown in Figure 3-5.

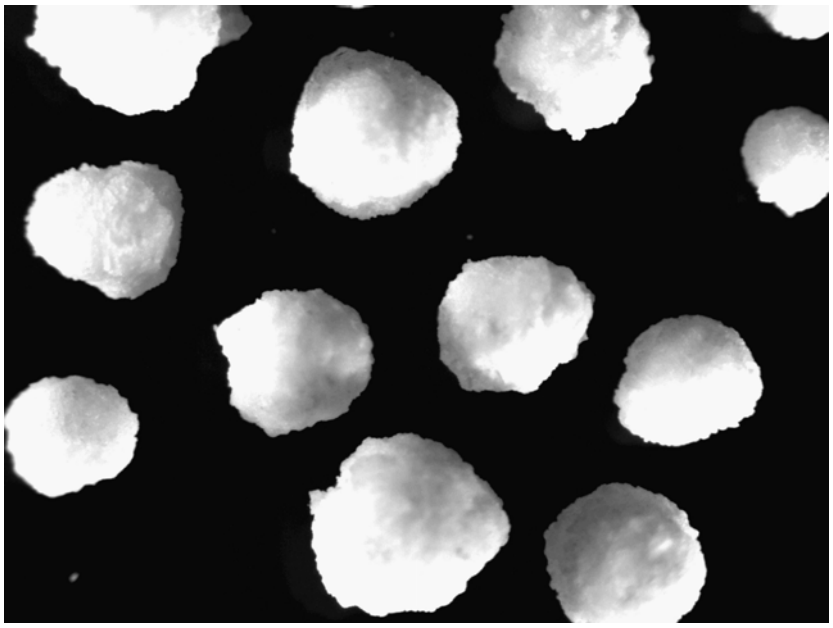

Figure 3-5. Polypropylene particles produced at 60ºC, run (D, H)-1 (For details, refer to Table 4-2).

Figure 3-6 shows propylene uptake curves for two replicate polymerizations at different stirring rates, indicating that external mass transfer limitations are not significant. The experiments started with a stirring rate of 500 rpm; after 22 minutes of polymerization, corresponding to the production of approximately 2 grams of polypropylene, the stirring rate was increased to 650 rpm, and kept at this rate for approximately 15 minutes; finally, the stirring rate was reduced to its original value of 500 rpm, and kept for another 15 minutes before stopping the polymerization. The propylene uptake rate was not affected by the changes in stirring rate throughout the experiment. If external mass transfer limitations were important, the monomer uptake rate should have increased when the stirring rate increased from 500 to 650 rpm, and decreased when it was reduced from 650 rpm back to 500 rpm.

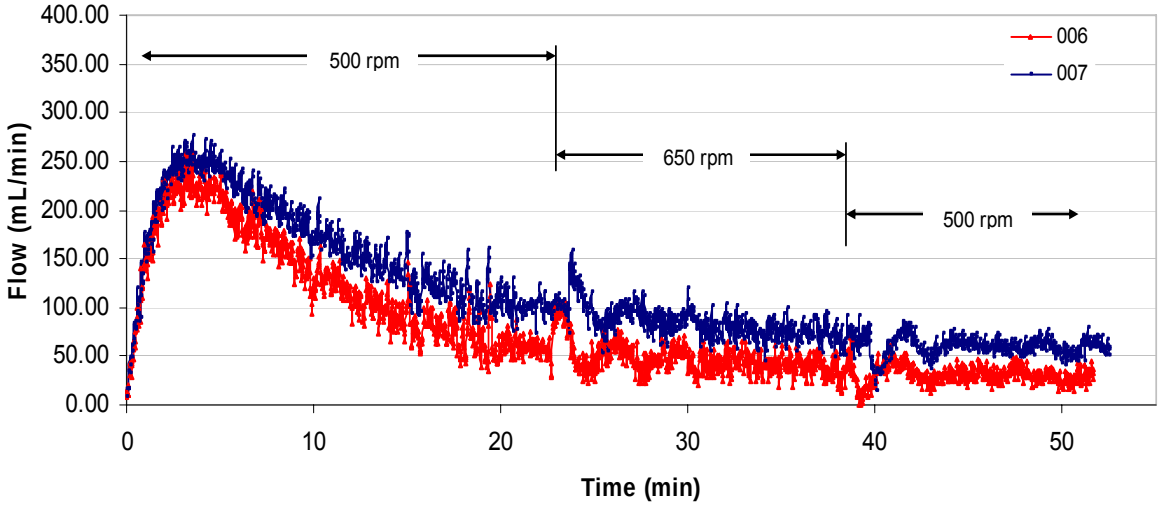

Figure 3-6. Effect of stirring rate on the propylene polymerization rate for two replicate runs (Runs 006 and 007, Table A.1, Appendix A)

3.3.2. Estimation of Propylene Concentration in Hexane

The concentration of propylene in hexane, needed to estimate the polymerization kinetics parameters, was calculated at different temperatures and propylene pressures by recording the total mass of propylene fed to the reactor. These runs were conducted in the same 300-ml reactor used for the polymerization experiments, with a hexane volume of 150 ml. Propylene was fed to the reactor until the set point pressure was reached and the propylene flow rate was recorded using an online flowmeter. The total propylene mass fed to the reactor is simply the area under the flow × time curve.

Propylene concentration in hexane is given by the expression,

$$\text{Propylene concentration} = \frac{M_{liquid}}{V_{liquid}} \tag{3.1}$$

where M_{liquid} is the mass of propylene dissolved in hexane, calculated as follows,

$$M_{liquid} = M_{total} - M_{gas} \tag{3.2}$$

The total mass of propylene fed to the reactor, M_{total}, is obtained by integrating the mass flow rate of propylene fed to the reactor,

$$M_{total} = \int_0^{\infty} \dot{m}_{C_3} \mathrm{d}t \tag{3.3}$$

where $\dot{m}_{C_3}$ is the propylene mass flow rate (mass/ time), and t is the time.

Assuming a constant liquid volume, the mass of propylene in the reactor gas space was estimated using the ideal gas law,

$$M_{gas} = \frac{(P - P_{hexane})(V_{reactor} - V_{liquid})MW_{propylene}}{RT} \tag{3.4}$$

where M_{gas} is the mass of propylene in the reactor gas phase, P is the reactor pressure, P_{hexane} is hexane vapor pressure, $V_{reactor}$ is the reactor volume, V_{liquid} is the reactor liquid phase volume, R is the gas constant, and T is the reactor temperature.

The hexane vapor pressure (P_{hexane}) was calculated using Equation (3.5) (Reid *et al.*, 1987) with A = −7.46765 , B = 1.44211, C = −3.28222, D = −2.50941, T_C= 507.5K , and P_C= 30.1 bar,

$$\begin{aligned} \ln(P_{hexane}/P_C) = (T/T_C)[&A(1-T/T_C) + B(1-T/T_C)^{1.5} \\ &+ C(1-T/T_C)^3 + D(1-T/T_C)^6] \end{aligned} \tag{3.5}$$

The propylene concentration in hexane was measured at three temperatures (50, 60, and 70^{o}C) and four propylene pressures (40, 55, 70, and 85 psi), as shown in Figure 3-7. The experimental estimates agree well with ASPEN predictions using the Peng-Robinson equation of state. The values of the experimental propylene concentrations obtained from this plot were used in the estimation of the polymerization parameters in Chapters 4 and 5.

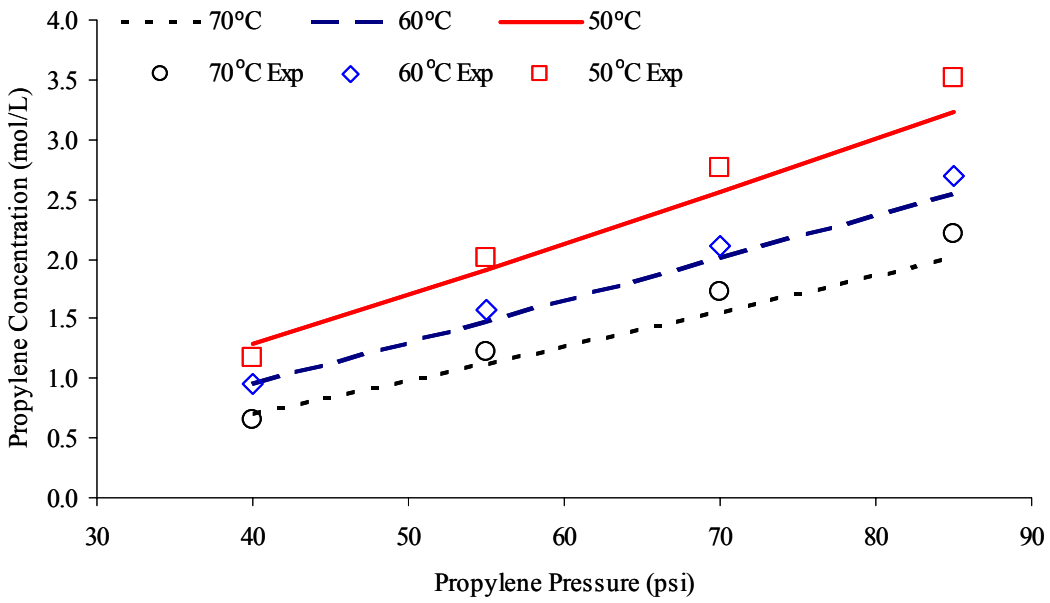

Figure 3-7. Propylene concentrations at different temperatures and pressures. The solid lines are concentrations calculated using ASPEN with the Peng-Robinson equation of state.

Chapter 4

EFFECT OF HYDROGEN AND EXTERNAL DONOR ON PROPYLENE POLYMERIZATION KINETICS AND POLYPROPYLENE MICROSTRUCTURE WITH A 4TH GENERATION ZIEGLER-NATTA CATALYST

4.1. INTRODUCTION

A unique feature of propylene polymerization with heterogeneous Ziegler-Natta catalysts is the use of electron donors that control the fraction of atactic polypropylene in the final product. Electron donors also affect polymerization rate and polymer properties such as molecular weight distribution. Different external donor types produce polypropylene with distinct M_n, M_w, and tacticity at the same polymerization conditions (Forte and Coutinho, 1996). The addition of a silane external donor, (cyclo-$C_5H_9)_2Si(OMe)_2$, doubled the M_w of polypropylene when compared with samples made without external donor with $TiCl_4$/dialkyl phatalate/$MgCl_2$ (Kissin and Rishina, 2008). Different internal/external donor systems also affect polypropylene stereoregularity (Chadwick et al., 2001). It has been proposed that the donor effect on stereoselectivity is related to their electron density (Harkonen et al., 1995): the higher the electron density, the more effective the electron donor.

On the other hand, hydrogen enhances the rate of propylene polymerization when using high activity $TiCl_4$-based catalysts (Guastalla and Giannini, 1983; Shaffer and Ray, 1997). Recent studies with $TiCl_4$/dialkyl phatalate/$MgCl_2$ showed a significant increase in polymerization rate when hydrogen was added (Pater *et al*., 2002; Kissin and Rishina, 2008). Busico *et al*. (1992) explained this rate enhancement effect by the freeing-up of 2-1 terminated dormant sites. This finding was further supported by end group analyses (Tsutsui *et al*., 1990;

Chadwick *et al*., 1994). In our previous publications (Alshaiban and Soares, 2009; 2011), hydrogen was also noticed to increase the tacticity of polypropylene in the simulation results.

The polymerization rate with $TiCl_4/MgCl_2$ catalysts is highest from 60 to 70°C, starting to decrease beyond 70°C (Keii, *et al*., 1982; Spitz *et al*., 1984; Albizzati *et al*., 1995). Polymerization temperature also affects polypropylene stereoregularity (Kissin, 2008). One may classify how regular polypropylene chains are into three main fractions based on their crystallizability: low, intermediate, and high crystallinity. Interestingly, Kissin *et al*. has shown that when the polymerization temperature is increased, the high crystallinity fraction increases but the average *mmmm* pentad for the overall polymer sample decreases (Kissin *et al.*, 2004; Kissin, 2008).

Matos et al. (2001) estimated kinetic constants for propylene polymerization using a first generation Ziegler-Natta catalyst and developed a mathematical model for polypropylene microstructure and properties. The model fits the experimental data well, but did not include the effect of electron donors. They also did not estimate the activation energies for activation, propagation, or deactivation steps.

In this chapter, the effect of electron donor and hydrogen on propylene polymerization kinetics was evaluated quantitatively for a commercial 4^{th} generation Ziegler-Natta catalyst. The polymerizations were carried out in the presence or absence of external donor and hydrogen at two temperatures (60 and 70°C), according to experimental Design A described in Section 3.1. Since most heterogeneous Ziegler-Natta catalysts have multiple active site types that produce polypropylene with different molecular weight and tacticity averages, kinetic constants per site type are very hard to estimate. Therefore, apparent polymerization kinetic constants were obtained instead.

Moreover, a systematic study on the effect of hydrogen and/or external donor on polypropylene microstructure produced at 60 and 70ºC was conducted to try to better understand how these factors affect polypropylene microstructure and propylene polymerization kinetics.

4.2. EXPERIMENTAL

All polymerization experiments were conducted in the 300 mL stainless steel reactor described in Section 3.2 according to the design conditions summarized in Table 4-1. The polymer molecular weight distribution was determined using Polymer Char GPC, Polymer Char CEF was used for the crystallinity analysis, and ^{13}C NMR was used to measure the pentad distribution, according to the procedures explained in Section 3.2.

Table 4-1. Experimental conditions for Design A.

Experiment number	Factors		
	Do/Ti (mol/mol)	P_{H_2} (psi)	*T* (ºC)
1	0	0	60
2	0	0	70
3	0	16	60
4	0	16	70
5	1.4	0	60
6	1.4	0	70
7	1.4	16	60
8	1.4	16	70

4.3. KINETIC STUDY *

4.3.1. Model Development

The polymerization rate of Ziegler-Natta catalysts can be described with the activation, propagation and deactivation reactions described below,

$$C + Al \xrightarrow{k_a} P_0 \tag{4.1}$$

$$P_r + M \xrightarrow{k_p} P_{r+1} \tag{4.2}$$

$$P_r \xrightarrow{k_d} C_d + D_r \tag{4.3}$$

where C is the catalyst precursor, Al is the alkylaluminum, k_a is the activation rate constant, P_0 is the activated monomer-free catalyst site, M is the monomer, P_r is a living chain with length r, k_p is the propagation rate constant, C_d is a deactivated catalyst site, D_r is a dead polymer chain with length r, and k_d is the first order catalyst deactivation rate constant.

The polymerization rate, R_p, is given by the expression,

$$R_p = V\frac{\mathrm{d}[M]}{\mathrm{d}t} = Vk_p[M]\sum_{r=0}^{\infty} P_r = Vk_p[M]Y^0 \tag{4.4}$$

where V is the reaction volume in liters, $[M]$ is the monomer concentration in moles per liter, and Y^0 is the total number of moles of living chains in the reactor, which can be calculated with the following molar balance,

* The contents of this chapter have been submitted for publication (A. Alshaiban and J. B. P. Soares, "Effect of Hydrogen and External Donor on the Propylene Polymerization Kinetics with a 4th Generation Ziegler-Natta Catalyst", *Macromol. Chem. Phys.*, **2011**).

$$\frac{dY^0}{dt} = K_A C - k_d Y^0 \tag{4.5}$$

where $k_a[Al] = K_A$.

The molar balance for the catalyst precursor is shown below,

$$\frac{d[C]}{dt} = -k_a[Al][C] \tag{4.6}$$

Since, the cocatalyst is usually present in large excess, the product $k_a[Al] = K_A$ may be assumed to be constant. Integration of Equation (4.6) with the initial condition $[C]\big|_{t=0} = [C]_0$, will result in,

$$[C] = [C]_0 e^{-K_A t} \tag{4.7}$$

Equation (4.7) can be substituted into Equation (4.5) to eliminate the unknown term *C*, as illustrated in Equation (4.8),

$$\frac{dY^0}{dt} = K_A [C]_0 e^{-K_A t} - k_d Y^0 \tag{4.8}$$

Integrating Equation (4.8) using the initial condition $Y^0\big|_{t=0} = 0$ leads to,

$$Y^0 = \frac{[C]_0 \left[1 - e^{-K_A t\left(1 - k_d / K_A\right)}\right] e^{-k_d t}}{1 - k_d / K_A} \tag{4.9}$$

Finally, substituting Equation (4.9) into Equation (4.4), the expression for the rate of polymerization is obtained,

$$R_p = Vk_p[M][C]_0 \frac{\left[1 - e^{-K_A t(1-k_d/K_A)}\right] e^{-k_d t}}{1 - k_d/K_A} \tag{4.10}$$

The propylene concentration in the diluent, [*M*], was estimated experimentally at different temperatures and propylene pressures as explained in Section 3.3.2.

Experimentally, the polymerization rate is measured as the monomer uptake in mole/time, as shown in Equation (4.11), where *M* is the number of monomer moles fed to the reactor,

$$R_{p,Exp} = \frac{\mathrm{d}M}{\mathrm{d}t} \tag{4.11}$$

Equation (4.10) can be fitted to the experimental monomer uptake rate to estimate the apparent activation, propagation and deactivation rate constants (K_a, k_p and k_d) by minimizing the sum of the squares of the differences between the experimental and simulated monomer uptake rates,

$$\min_{\substack{k_p \\ K_a \\ k_d}} \sum [R_{p,Exp} - R_p]^2 = \min_{\substack{k_p \\ K_a \\ k_d}} \sum \Delta^2 \tag{4.12}$$

Furthermore, Equation (4.12) may be combined with Arrhenius law to estimate the activation energies (E_j) and pre-exponential constants (A_j) for activation, propagation, and deactivation steps, as indicated below,

$$k_j = A_j e^{(E_j/RT)} \tag{4.13}$$

$$\min_{\substack{A_j \\ E_j}} \sum \{[(R_{p,Exp} - R_p)\big|_{60°C}]^2 + [(R_{p,Exp} - R_p)\big|_{70°C}]^2\} = \min_{\substack{A_j \\ E_j}} \sum \Delta^2 \tag{4.14}$$

where the subscript j stands for activation (a), propagation (p), or deactivation (d).

The initial catalyst concentration, $[C]_0$, was calculated with the expression,

$$[C]_0 = \frac{M_{Cat} f_{Ti}}{MW_{Ti}\ V} \tag{4.15}$$

where V is the reaction volume, M_{Cat} is the mass of the catalyst added to the reactor, f_{Ti} is the weight fraction of titanium in the catalyst, and MW_{Ti} is the molar mass of titanium.

Finally, the polypropylene number average molecular weight, M_n, is given by the ratio of the propagation reaction rate, R_p, to the overall rate of chain transfer, R_t,

$$M_n = (42\ \text{g/mol}) \times \frac{R_p}{R_t} \tag{4.16}$$

where R_p is given in Equation (4.4) and R_t is given by the expression,

$$R_t = V(k_{tH}[H_2] + k_{tAl}[Al] + k_{tM}[M] + k_{t\beta})Y^0 = VK_T Y^0 \tag{4.17}$$

where, k_{tH}, k_{tAl}, k_{tM}, and k_β are the chain transfer rate constants by hydrogen, cocatalyst, monomer, and β-hydride elimination, respectively, and $[H_2]$, $[Al]$, and $[M]$ are the concentrations of hydrogen, cocatalyst, and monomer, respectively. Therefore, K_T can be estimated by substituting the definitions for R_p and R_t in Equation (4.16) and rearranging as follow,

$$K_T = (42\ \text{g/mol}) \times \frac{k_p[M]}{M_n} \tag{4.18}$$

4.3.2. Results and Discussion

Table 4-2 lists the polymerizations conditions for all experiments. Two replicate runs were conducted at each polymerization condition. Four polymer sample groups are listed in Table 4-1, classified according to the presence or absence of hydrogen or donor. To help identification of the four groups, they are followed by the identifier (−, −), where the first placeholder indicates the presence of donor, and the second the presence of hydrogen. For instance, (D, −) indicates samples made in the presence of donor and absence of hydrogen, and (−, H) in the presence of hydrogen and absence of donor.

For each experimental group, reaction rate constants were estimated at 60 and 70ºC. Since there are two replicate runs at each polymerization temperature, four combinations are available to estimate activation energies and pre-exponential factors: 1) Replicate 1 at 60ºC with Replicate 1 at 70ºC, 2) Replicate 1 at 60ºC with Replicate 2 at 70ºC, 3) Replicate 2 at 60ºC with Replicate 1 at 70ºC, and 4) Replicate 2 at 60ºC with Replicate 2 at 70ºC. The resulting four values were used to find approximate estimates of the 95 % confidence intervals for the activation energies and pre-exponential factors for activation, propagation, and deactivation.

Table 4-2. Summary of experimental conditions and catalyst productivities for Design A.

Pol. Temp. ºC	Group	Run #	*Al*/*Ti* mol/mol	*Do*/*Ti* mol/mol	C_o [(1)] mol/L x 10^{-5}	P_{H_2} psi	P_{C_3} [(2)] Psi	Productivity g-PP/ (g-cat· min)
60	(D, −)	(D, −)-1	904	1.5	3.8	0	70	7.44
		(D, −)-2	964	1.5	3.6	0	70	8.14
	(−, −)	(−, −)-1	945	0.0	3.7	0	70	6.45
		(−, −)-2	917	0.0	3.8	0	70	6.35
	(D, H)	(D, H)-1	852	1.4	4.1	17	86	17.73
		(D, H)-2	831	1.4	4.3	15	85	16.85
	(−, H)	(−, H)-1	964	0.0	3.6	15	85	7.81
		(−, H)-2	965	0.0	3.6	16	86	8.89
70	(D, −)	(D, −)-1	859	1.3	4.2	0	74	7.96
		(D, −)-2	910	1.3	4.0	0	74	6.86
	(−, −)	(−, −)-1	889	0	3.9	0	74	7.07
		(−, −)-2	918	0	3.8	0	74	6.25
	(D, H)	(D, H)-1	815	1.3	4.2	16	90	16.84
		(D, H)-2	771	1.3	4.5	16	90	15.79
	(−, H)	(−, H)-1	838	0	4.1	16	90	7.62
		(−, H)-2	793	0	4.4	16	90	9.91

(1) The weight fraction of titanium in the catalyst added to the reactor was 0.017 Ti for all runs [see Equation (4.15)].

(2) Propylene pressure was adjusted to maintain the propylene concentration in hexane at 2.1 mol/L for all runs, as described in Section 3.3.2.

The reproducibility of the polymerization experiments was excellent, as illustrated in Figure 4-1 for two replicate polymerizations, runs (D, −)-1 and (D, −)-2.

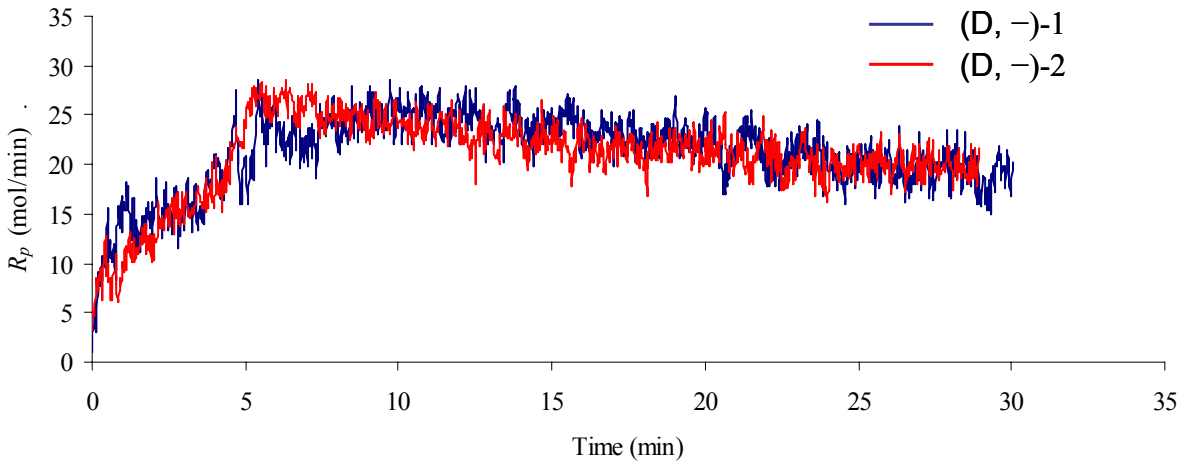

Figure 4-1. Typical propylene uptake curve (rate of polymerization) replicates for experimental conditions of Group (D, −) at 60°C.

Figure 4-2 shows model fits for the propylene uptake curves in Group (−, −) and Table 4-3 lists the equivalent model parameters. A similar approach was applied to estimate the kinetic constants for the polymerization runs in the other three groups. Figure 4-3 shows that the model adequately describes the polymerization rates for all four groups, and Table 4-4 lists model parameters for all four experimental groups. The estimated activation energies, when using the individual fit shown in Appendix B, are not adequate because of the experimental noise that led to lower values on the reaction rate constant at higher polymerization temperature (i.e. reaction rate constant of activation and deactivation of (D, H) at 70°C is lower than those of (D, H) at 60°C).

Interestingly, when using simultaneous solution, the values estimated for the activation energies for activation, propagation, and deactivation do not vary much among groups, implying that H_2 and donor do not have an appreciable effect on them. On the other hand, the pre-exponential constant for catalyst activation decreases by adding donor and even more by adding hydrogen. The pre-exponential constants for propagation and deactivation increase by adding donor. Adding hydrogen to the catalyst in the absence of donor has no effect on the pre-

exponential constants for propagation and deactivation, but in the presence of donor, significant increase was observed in both pre-exponential constants.

Since the activation energies are not significantly affected by hydrogen or donor, it is likely that they do not influence the nature of the active sites significantly. However, both donor and hydrogen seem to change the balance between site types, which can be quantified as a change in the pre-exponential terms of the kinetic constants. Since these are only apparent kinetic constants, this interpretation must be considered as only tentative, but it seems to agree well with our observations.

The activation energy for propagation for all groups varies from 8.1 – 8.6 kcal/mol, which is close to the values reported in the literature for other heterogeneous Ziegler-Natta catalysts used for propylene polymerization (Table 4-5).

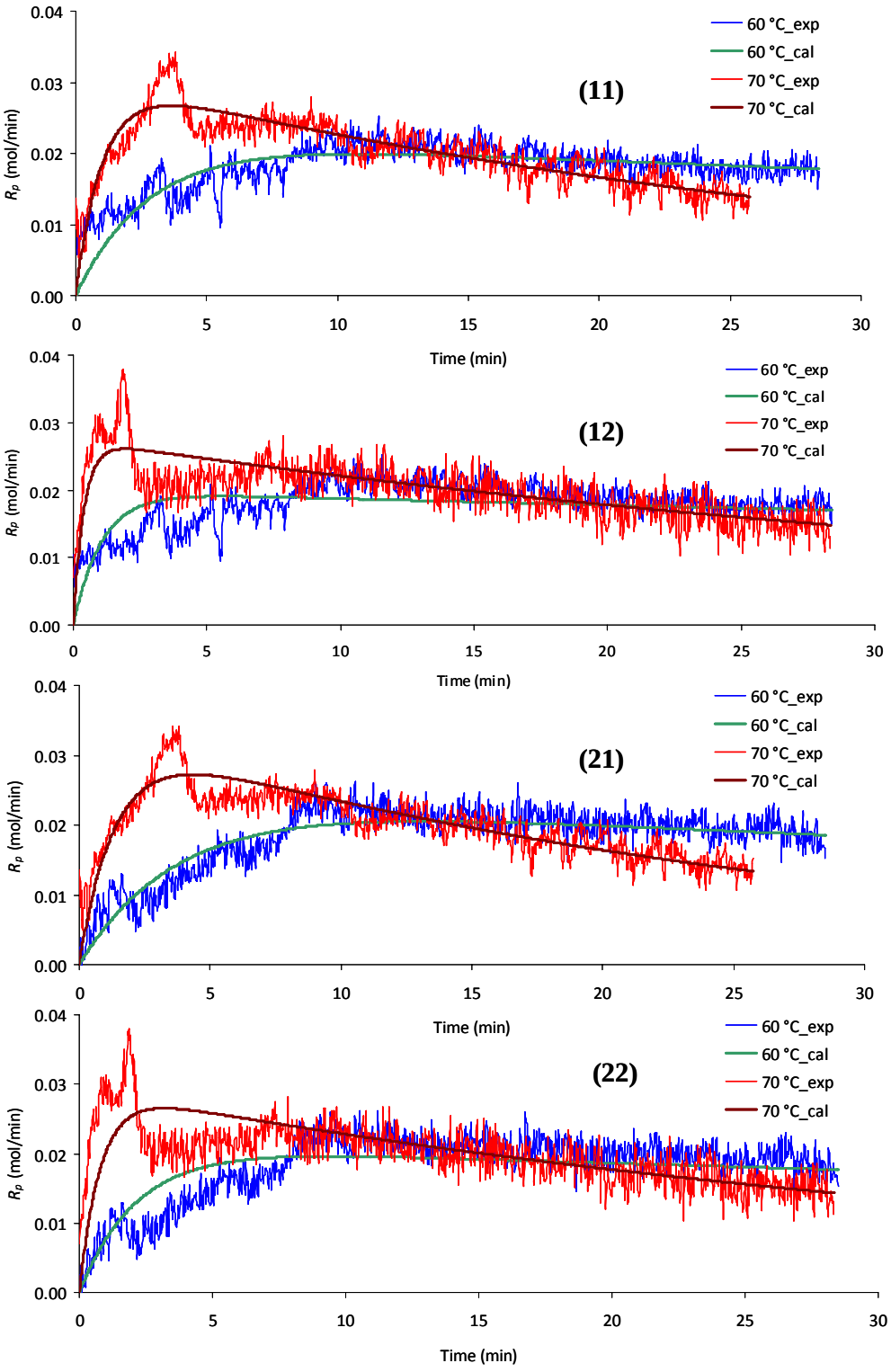
(11)
60 °C_exp
60 °C_cal
70 °C_exp
70 °C_cal
R_p (mol/min)
Time (min)
(12)
(21)
(22)

Figure 4-2. Model fit of experimental data in Group (−, −). The notation (12) represents Replicate-1[(−, −)-1] and Replicate-2 [(−, −)-2] at 60°C and 70°C, respectively.

Table 4-3. Activation energies estimated for run replicates in Group (−, −).

Energy (kcal/mol)	(11)*	(12)	(21)	(22)	Average	Standard Deviation	95 % Confidence
E_A	22.73	22.10	22.93	22.57	22.58	0.353	± 0.346
E_p	8.51	8.58	8.47	8.54	8.52	0.044	± 0.043
E_d	32.03	32.27	31.94	32.17	32.10	0.148	± 0.145

* The notation (12) represents Replicate-1[(−, −)-1] and Replicate-2 [(−, −)-2] at 60 and 70°C, respectively.

Table 4-4. Activation energies and pre-exponential constants for site activation, propagation, and deactivation for all groups.

Energy	Group			
(kcal/mol)	(D, −)	(−, −)	(D, H)	(−, H)
E_a	21.5 (± 0.60)	22.6 (± 0.35)	21.8 (± 0. 38)	19.3 (± 0.31)
E_p	8.6 (± 0.07)	8.5 (± 0.04)	8.1 (± 0.01)	8.2 (± 0.09)
E_d	31.9 (± 0.08)	32.1 (± 0.14)	32.5 (± 0.34)	31.4 (± 0.10)
Pre-exponential constant				
A_A (min^{-1})	2.5×10^{14}	3.0×10^{14}	2.1×10^{14}	5.0×10^{13}
A_p ($L \cdot mol^{-1} \cdot min^{-1}$)	7.5×10^{8}	7.0×10^{8}	9.0×10^{8}	7.0×10^{8}
A_d (min^{-1})	8.25×10^{18}	8.0×10^{18}	1.1×10^{19}	8.0×10^{18}

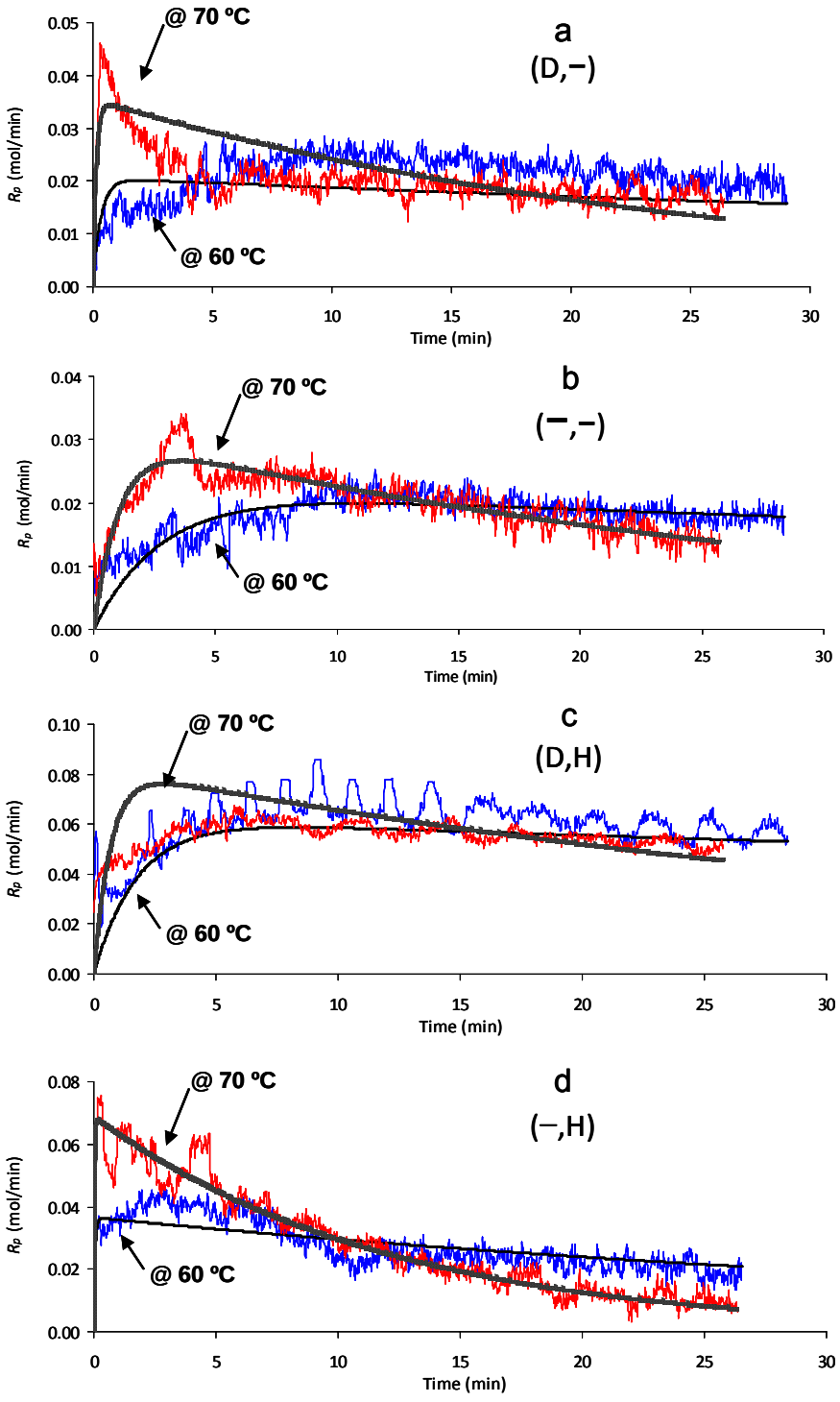
a
(D,−)
@ 70 ºC
@ 60 ºC
R_p (mol/min)
Time (min)
b
(−,−)
@ 70 ºC
@ 60 ºC
R_p (mol/min)
Time (min)
c
(D,H)
@ 70 ºC
@ 60 ºC
R_p (mol/min)
Time (min)
d
(−,H)
@ 70 ºC
@ 60 ºC
R_p (mol/min)
Time (min)

Figure 4-3. Experimental and calculated propylene uptake curves: a) Runs (D, −)-1 and (D, −)-2, b) Runs (−, −)-2 and (−, −)-1, c) Runs (D, H)-1 and (D, H)-2, and d) Runs (−, H)-2 and (−, H)-1.

Table 4-5. Propagation activation energies reported in the literature.

Propagation activation energy (kcal/mol)	Reference	Note
10.0	Keii *et al.* (1967)	
13.9 and 12.0	Xu *et al.* (2001)	
3 − 6	Zakharov (1978)	Theoretically
13.8	Soares and Hamielic (1996)	Without H_2
15.6	Soares and Hamielic (1996)	With H_2
9.5 − 11.9	Keii *et al.* (1984)	

The lumped chain termination term, K_T, was calculated for all samples using Equation (4.18) and the GPC data shown in Table 4-6. Estimates for K_T are tabulated in Table 4-7. In the absence of hydrogen, adding external donor decreases K_T, as seen by examining the data from Group (−, −) to (D, −) at 60 and 70ºC. However, when hydrogen is fed to the reactor, the addition of donor increases K_T at 60ºC, but decreases it at 70ºC, as indicated by data from group (−, H) to (D, H).

Table 4-6. Molecular weight averages used to calculate lumped chain transfer constants (K_T).

	Group							
	(D, −)		(−, −)		(D, H)		(−, H)	
Temp. (ºC)	60	70	60	70	60	70	60	70
M_n (g/mol)	30,070	84,080	22,480	13,660	18,030	27,510	18,990	9,410
M_w (g/mol)	151,550	499,400	140,280	72,535	82,990	95,460	77,290	32,560
PDI	5.04	5.94	6.24	5.31	4.60	3.47	4.07	3.46

Table 4-7. Estimated K_T (min^{-1}) values.

	Group			
Polymerization Temperature (°C)	(D, −)	(−, −)	(D, H)	(−, H)
60	4.9	7.0	23.0	13.9
70	2.6	16.7	21.5	40.2

Figure 4-4 shows the predicted propylene polymerization curves using the model parameters listed in Table 4-4. The polymerization rates predicted for Group (−, −) are the lowest of all experimental conditions. When donor is added in Group (D, −), a slight increase in both activation and polymerization rates is observed. On the other hand, when hydrogen is added in the absence of donor, Group (−,H), a significant increase in the activation and polymerization rates results; K_a increases by 20 times and k_p by 1.6 times at both 60 and 70ºC, as compared to the rate constants for Group (−, −). An increase in the catalyst activation rate by hydrogen is a common phenomenon in propylene polymerization (Guastalla and Giannini, 1983; Busico *et al.*, 1992). Finally, when both electron donor and hydrogen are used, Group (D, H), the activation rate term decreases, compared to Group (−, H), but k_p increases substantially.

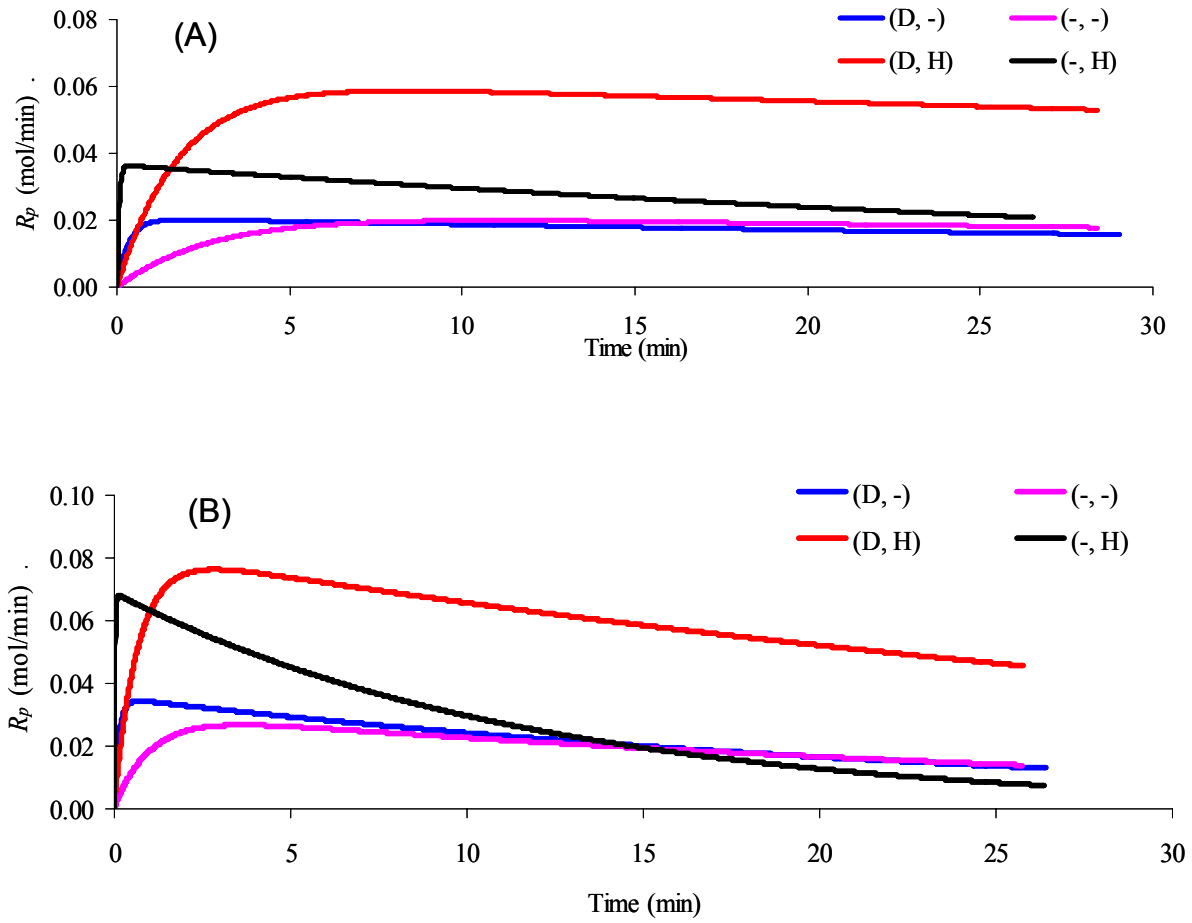

Figure 4-4. Rates of polymerization predicted for the four experimental condition groups at (A): 60°C, and (B): 70°C.

Figure 4-5 to Figure 4-7 compares the values estimated for K_A, k_p, and k_d for all experimental groups. When hydrogen is present, adding donor increases k_p and decreases k_d, likely because the external donor reduces the fraction of aspecific sites that have higher deactivation rates. The addition of hydrogen significantly increases K_A and k_p, and has almost no effect on k_d. It has been proposed that hydrogen frees-up 2-1 terminated sites (Busico *et al.*, 1992; Tsutsui *et al.*, 1990; Chadwick *et al.*, 1994; Shafer and Ray, 1996) that are considered to

be dormant or either have a lower propagation rate constant due to the steric hindrance effect of the methyl group placed close to the transition metal site.

Interestingly, a sharper change in the value of K_A is seen when hydrogen in added to the catalyst without external donor − compare results from Group (−, −) and Group (−, H) – than when it is added in the presence of donor − Group (D, −) and Group (D, H). Since the fraction of aspecific sites in the absence of external donor is higher than in its presence, one may suggest that a higher fraction of 2-1 terminated sites is freed up (higher K_A) when H_2 is added to the donor-free catalyst than when external donor is used during the polymerization. Groups (−, −) and (−, H) also have the highest deactivation rate constants, indicating that the deactivation rate of the aspecific sites is higher than that of the specific sites, regardless of the presence of hydrogen.

The estimated kinetic parameters can be incorporated within process simulators used by commercial plants for better prediction of polymer properties and to optimize process conditions. For instance, if the polymer grade being produced with a certain tacticity (xylene soluble percent) and molecular weight (melt flow index) is to be changed to another grade with different properties, donor and hydrogen concentrations must be changed. During this grade transition, most process simulators will not predict accurate polymer properties due to the lack of catalyst/donor kinetic information. If detailed polymerization kinetic parameters, such as the ones estimated in this chapter, are incorporated within these process simulators, an expected improvement in their property prediction capabilities and optimal grade transition time could be achieved.

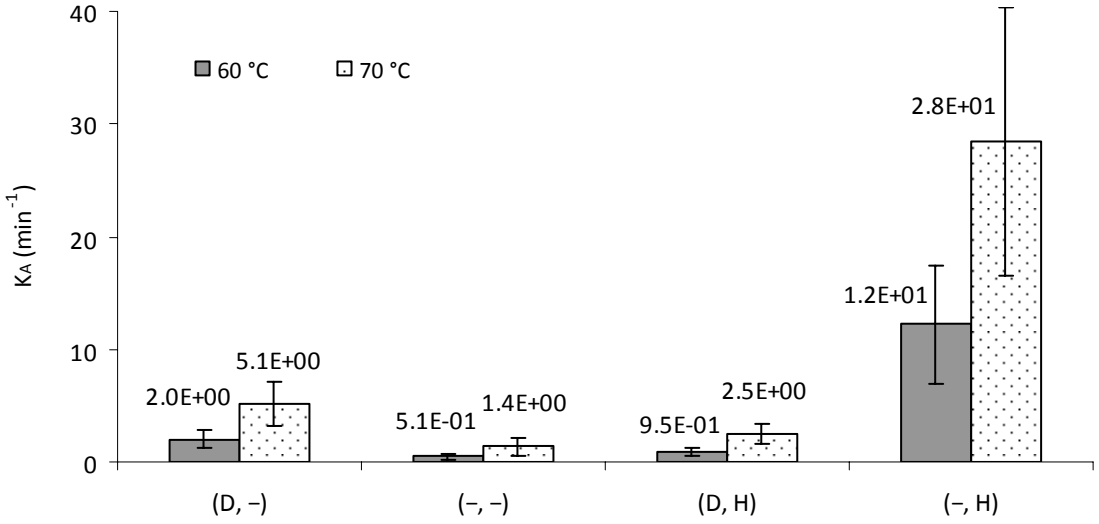

Figure 4-5. Activation rate constants (K_A).

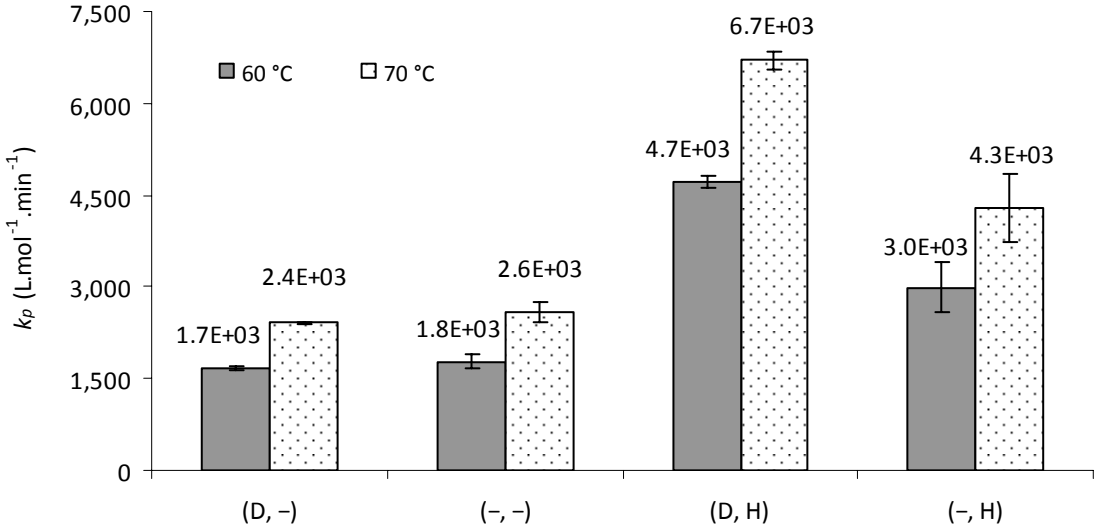

Figure 4-6. Propagation rate constants (k_p).

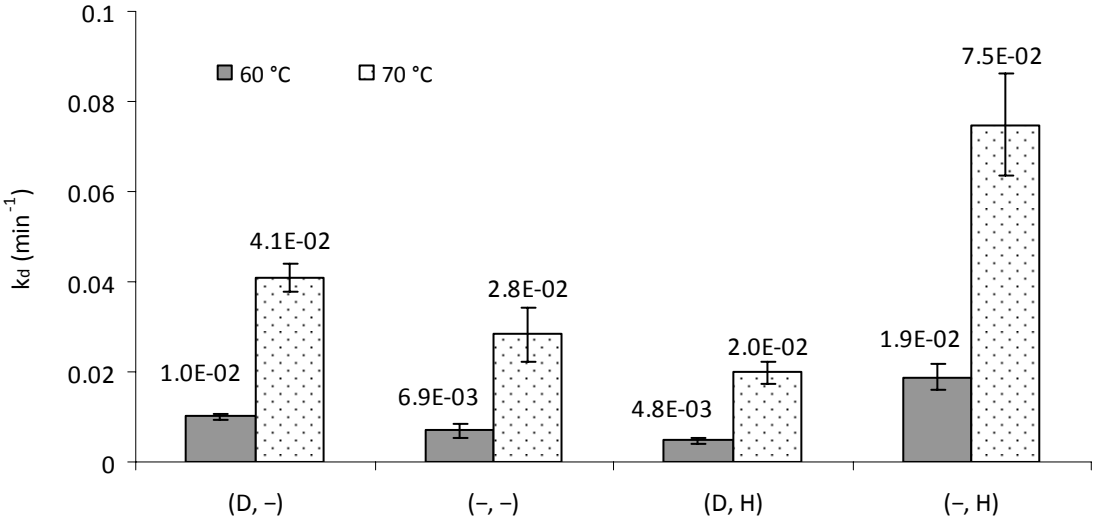

Figure 4-7. Deactivation rate constants (k_d).

4.4. MICROSTRUCTURAL STUDY *

4.4.1. Molecular Weight Averages and Distribution

The hierarchal design of experiments shown in Figure 3-3 was applied to analyze number and weight average molecular weights and polydispersity (M_n, M_w, and PDI) in Table 4-8. Replicate of polymerization runs (D, H)-1 and (D, H)-2 were sampled twice and each sample was analyzed two times to investigate errors coming from polymerization replicates, sampling, and analysis replicates. Averages for M_n, M_w and *PDI* for these samples, as well as their 95 % confidence intervals, are shown in Table 4-8. The F-test showed that run to run and sample to sample deviations were not significant, as illustrated in Table 4-9, where the $F_{observed} < F_{critical}$ for polymerization runs and sampling levels. Therefore, the polymer samples have reproducible MWDs that are not influences by run replicates or sampling.

* Part of the results discussed in this section have been accepted for publication (A. Alshaiban and J. B. P. Soares, ""Effect of Hydrogen, Electron Donor, and Polymerization Temperature on Polypropylene Microstructure", *Macromol. Symp.*, **2011**).

Table 4-8. Hierarchal design of experiments according to Figure 3-3 for GPC data.

Run	Sample	Analysis	M_n	M_w	PDI
(D, H)-1	S1	A1	28,300	135,100	4.8
		A2	29,300	130,150	4.4
	S2	A3	27,900	142,350	5.1
		A4	28,000	140,000	5.0
(D, H)-2	S1	A5	27,100	139,600	5.2
		A6	27,000	140,000	5.2
	S2	A7	27,500	135,000	4.9
		A8	27,500	135,100	4.9
Average			27,800	137,150	5.0
Standard Deviation			750	4,000	0.24
95 % Confidence Interval			500	2,750	0.17

Table 4-9. ANOVA table for the GPC data presented in Table 4-8 for polymerization runs (D, H)-1 and (D, H)-2 at polymerization temperature of 70°C.

Source of Variation	Sum of Squares	Degree of Freedom	Mean Square	Expected Value of Mean Square		$F_{critical}$	$F_{observed}$	P-value
Average	6.2×10^9	1						
Run	2.4×10^6	1	2.4×10^6	602,528	F(1,2,0.05)	18.50	5.4	0.05003
Sample	898,911	2	449,456	224,728	F(2,4,0.05)	6.94	3.5	0.05005
Analysis	515,600	4	128,900	128,900				

The MWD of a sample of each group was analyzed by GPC and deconvoluted using Flory's distributions to identify the minimum number of active site types needed to describe

their MWD, as discussed in Section 2.5. Table 4-10 and Table 4-11 list the molecular weight averages and number of site types for samples in each group made at 60 and 70°C, respectively.

The minimum number of active site types needed to describe the polymer MWD, shown in Table 4-10 and Table 4-11, was estimated for representative samples belonging to the four groups. The number of active site types was obtained by minimizing the objective function defined in Equation (2.21), by systematically increasing the number of site types and watching how the fit error decreased until adding more site types did not improve the fit any further. Figure 4-8 shows the best fit with 3 site types for the MWD of sample (D, H)-1 made at 60°C. Since the fit was not satisfactory, 4 site types were tried to improve the MWD description (Figure 4-9), and then 5 site types (Figure 4-10). This procedure was repeated for all other resins by introducing additional site types until the sum of the squares of the differences between the experimental and predicted MWDs ($\sum \Delta^2$) did not vary significantly. No significant error reduction takes place by adding more than 4 or 5 site types for any sample investigated in this study, as shown in Figure 4-11. Five site types seem to be an adequate choice for this catalyst system under all polymerization conditions investigated, except for samples made at 70°C in the presence of hydrogen, where only four site types were required to describe the narrower MWDs obtained at these conditions. MWD deconvolution results, including M_n and the weight fraction of polymer made on each site type, w_i, are shown in Table 4-10 and Table 4-11 for polymer made at 60 and 70°C, respectively.

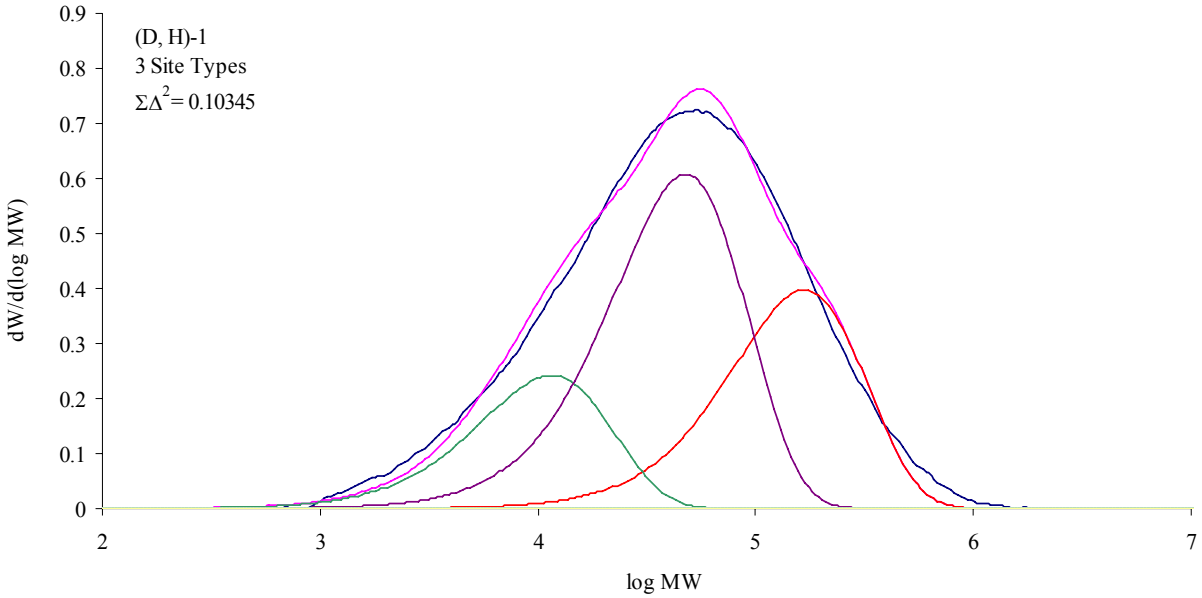

Figure 4-8. MWD deconvolution of sample (D, H)-1 assuming 3 active site types.

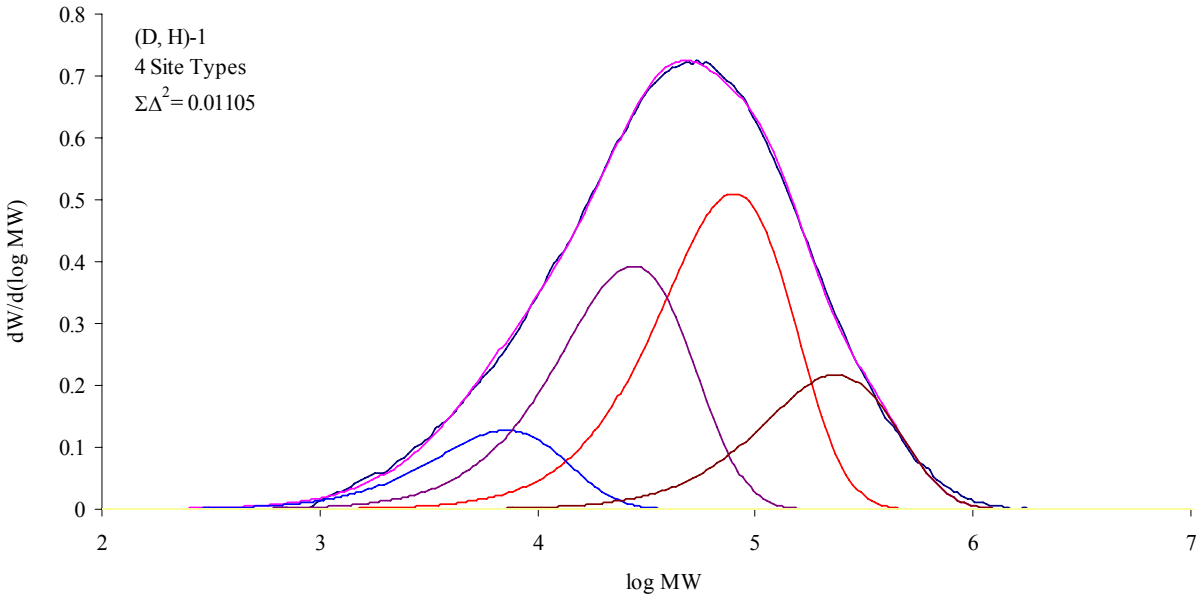

Figure 4-9. MWD deconvolution of sample (D, H)-1 assuming 4 active site types.

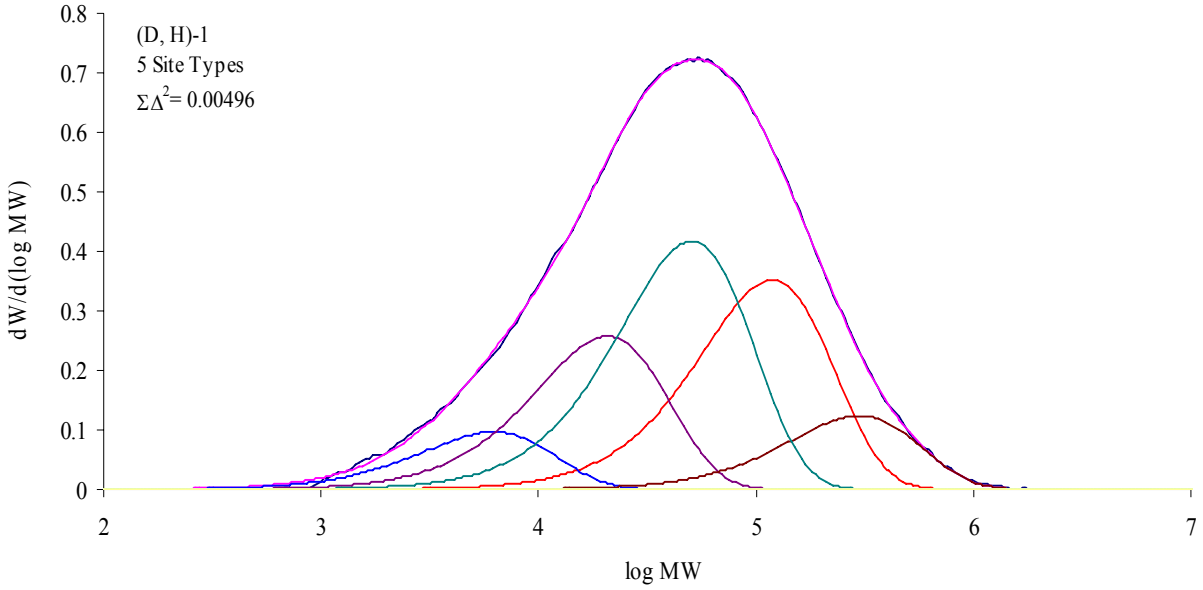

Figure 4-10. MWD deconvolution of sample (D, H)-1 assuming 5 active site types.

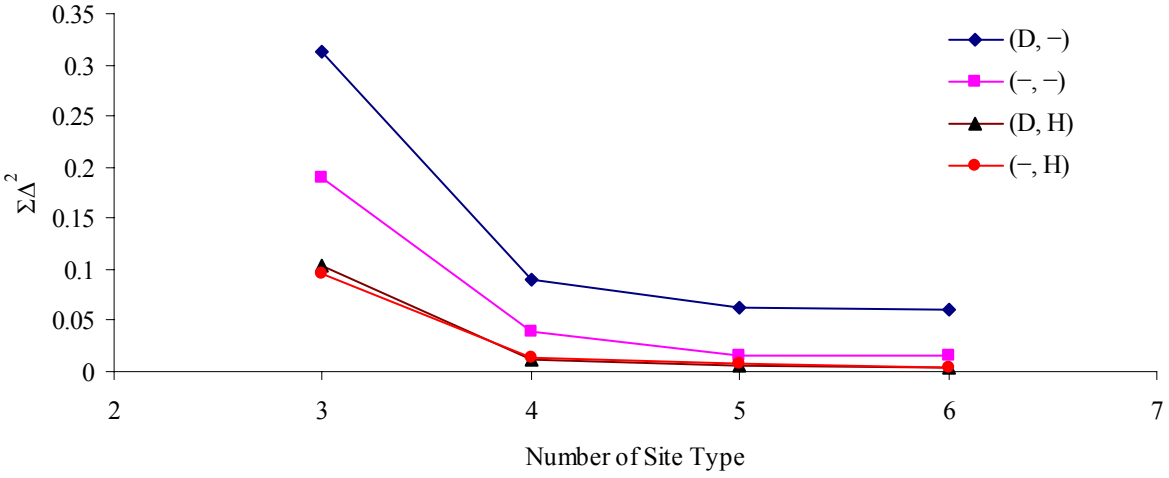

Figure 4-11. Sum of the squares of the differences between predicted and measured MWD for Groups (D, −), (−, −), (D, H), and (−, H) made at 60 °C as a function of the number of site types.

Table 4-10. Estimated weight fraction (w_i) and number average molecular weight (M_n) for each site type for polymer in all the four groups made at 60°C.

		n					M_n	M_w	*PDI*
Group	*Parameter*	1	2	3	4	5			
(D, −)	w_i	0.0689	0.1906	0.3135	0.2517	0.1753			
	M_n ($g \cdot mol^{-1}$)	4680	16×10^3	45×10^3	14×10^4	45×10^4	34×10^3	13×10^4	3.7
(−, −)	w_i	0.0849	0.2573	0.3482	0.2185	0.0910			
	M_n ($g \cdot mol^{-1}$)	5000	17×10^3	46×10^3	13×10^4	39×10^4	29×10^3	15×10^4	5.1
(D, H)	w_i	0.1064	0.2821	0.3636	0.1906	0.0573			
	M_n ($g \cdot mol^{-1}$)	3400	12×10^3	33×10^3	93×10^3	26×10^4	17×10^3	91×10^3	5.3
(−, H)	w_i	0.1193	0.3037	0.3713	0.1694	0.0363			
	M_n ($g \cdot mol^{-1}$)	3500	12×10^3	29×10^3	73×10^3	22×10^4	15×10^3	72×10^3	4.5

Table 4-11. Estimated weight fraction (w_i) and number average molecular weight (M_n) for each site type for polymer in all the four groups made at 70°C.

		n					M_n	M_w	*PDI*
Group	*Parameter*	1	2	3	4	5			
(D, −)	w_i	0.0899	0.2272	0.2763	0.2809	0.1257			
	M_n ($g \cdot mol^{-1}$)	15×10^3	46×10^3	13×10^4	32×10^4	87×10^4	84×10^3	50×10^4	5.9
(−, −)	w_i	0.1593	0.2779	0.3137	0.1718	0.0775			
	M_n ($g \cdot mol^{-1}$)	3×10^3	10×10^3	26×10^3	66×10^3	17×10^4	14×10^3	73×10^3	5.3
(D, H)	w_i	0.1151	0.3058	0.3810	0.1981				
	M_n ($g \cdot mol^{-1}$)	6×10^3	20×10^3	45×10^3	12×10^4		28×10^3	96×10^3	3.5
(−, H)	w_i	0.2105	0.3630	0.3137	0.1127				
	M_n ($g \cdot mol^{-1}$)	3×10^3	8×10^3	21×10^3	51×10^3		9×10^3	33×10^3	3.5

Figure 4-12 shows that adding hydrogen to the reactor causes M_n to decrease, as expected, but, more interesting, adding an external donor causes M_n to increase at 60°C and even more significantly at 70°C, likely because aspecific sites produce chains with lower M_n. The number average molecular weight decreases when the polymerization temperature is raised from 60 to 70°C for the polymerizations done in the absence of external donor, but increases when external donor is added to the reactor. Therefore, it seems that the electron donor molecules stabilize the active sites and make them less susceptible to chain transfer reactions, perhaps by blocking the transition state that leads to β−hydride elimination or transfer to monomer. Figure 4-13 illustrates this point more clearly.

Figure 4-14 shows that no unequivocal trends are observed for PDI as hydrogen and donor are added to the reactor. The fact that PDI varies among the different polymerization runs indicates that the active site ratio is significantly affected by the introduction of hydrogen and electron donor during polymerization. For instance, Figure 4-15 depicts the weight fractions of polymer made on each active site type at 60°C. Site type 1 produces polymer with the lowest molecular weight, and site type 5 with the highest. The presence of donor favors the production of polymer at high molecular weight sites (Figure 4-15). A similar behavior is observed for polymer made at 70°C (Figure 4-16). On the other hand, the weight fractions of the site types that produce low molecular weight chains increases by adding hydrogen. Indeed, at 70°C, hydrogen eliminated one site type, reducing them from 5 to 4 site types.

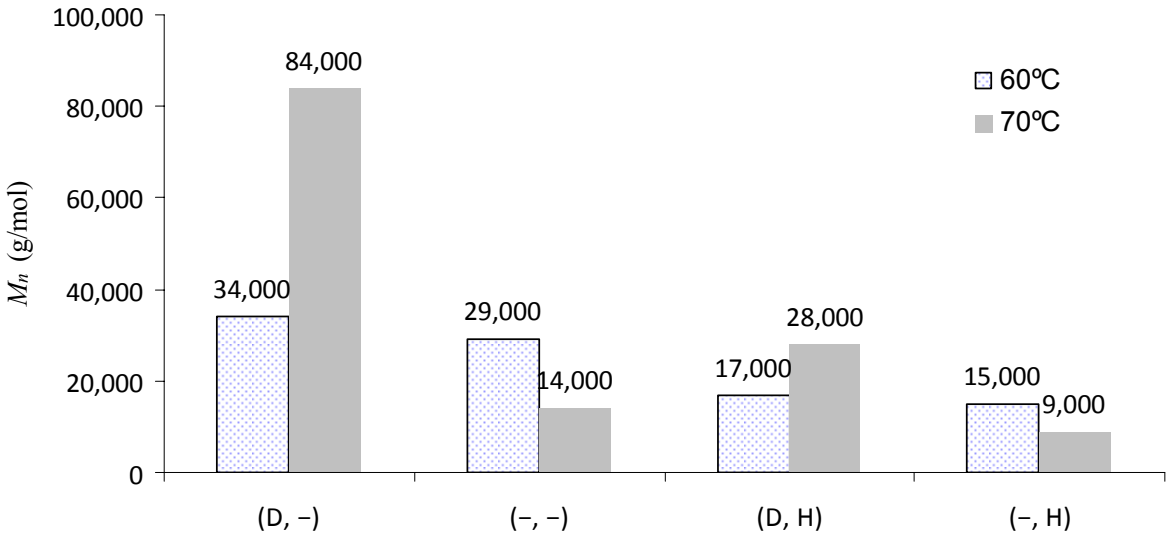

Figure 4-12. Effect of hydrogen and donor concentration on M_n.

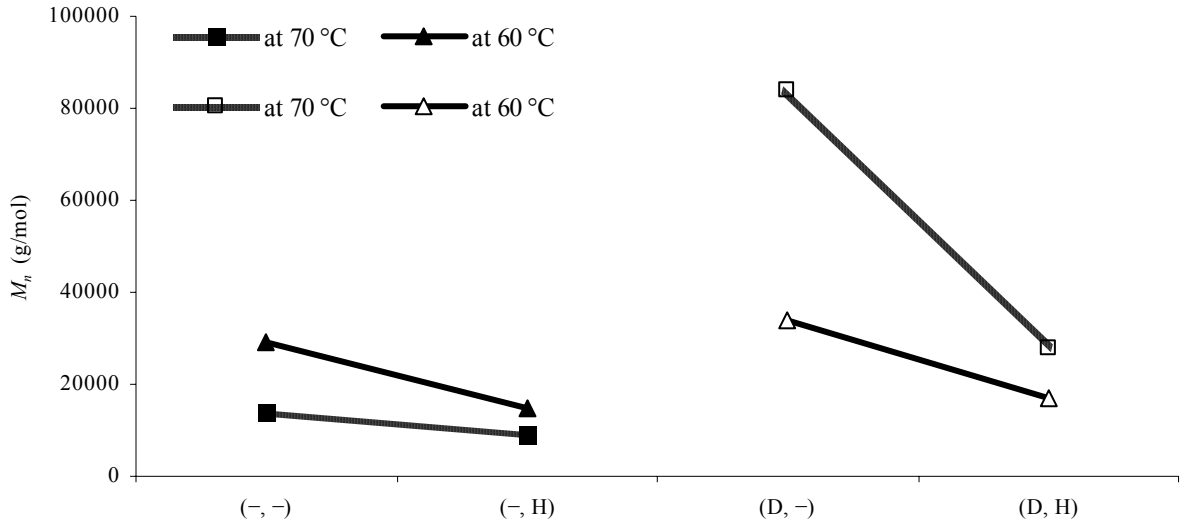

Figure 4-13. Effect of hydrogen addition on M_n in the presence and absence of electron donor.

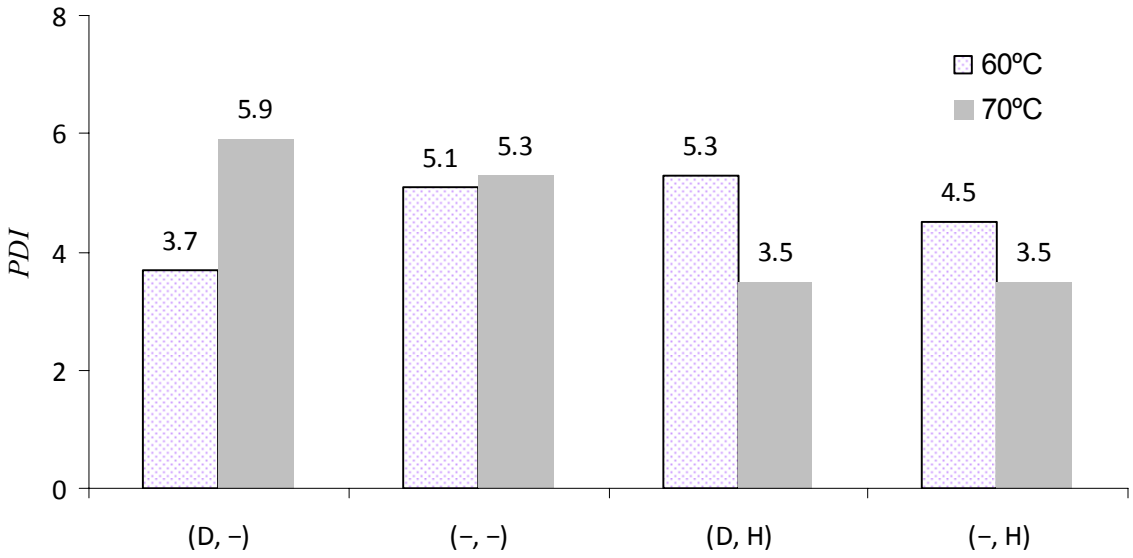

Figure 4-14. Effect of hydrogen and donor concentration on PDI.

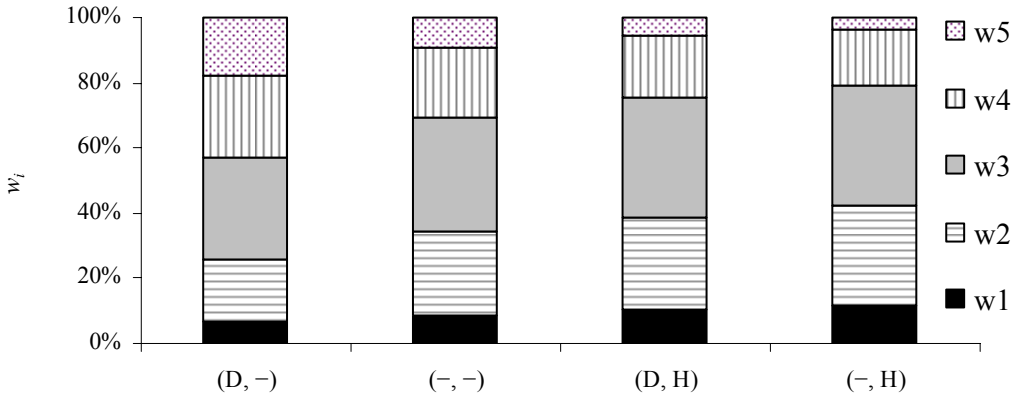

Figure 4-15. Weight fraction of each site type at 60°C.

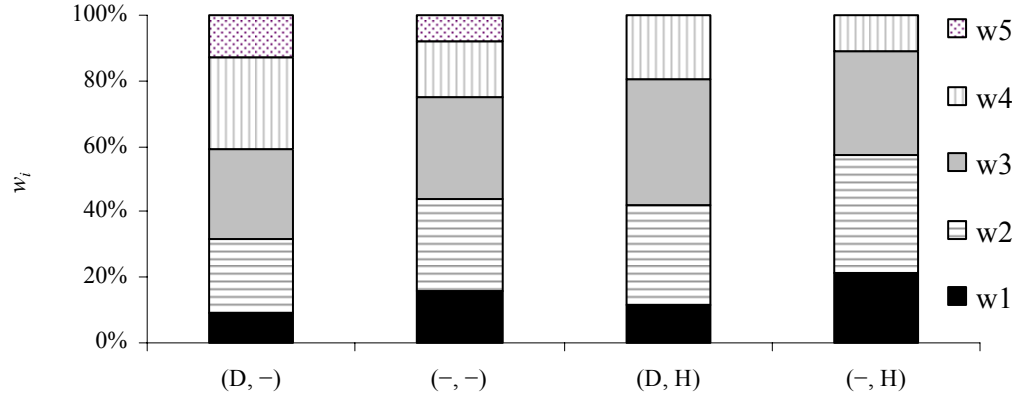

Figure 4-16. Weight fraction of each site type at 70°C.

Figure 4-17 shows that adding donor at 60°C in the presence or absence of hydrogen slightly increases the M_n of all of site types, but this increase is more pronounced for sites that produces polymer with higher M_n. On the other hand, at 70°C, the M_n of chains made on each site type increased significantly by donor addition, as shown in Figure 4-18, which seems to indicate that the donor can complex more effectively with the active sites at 70°C than at 60°C.

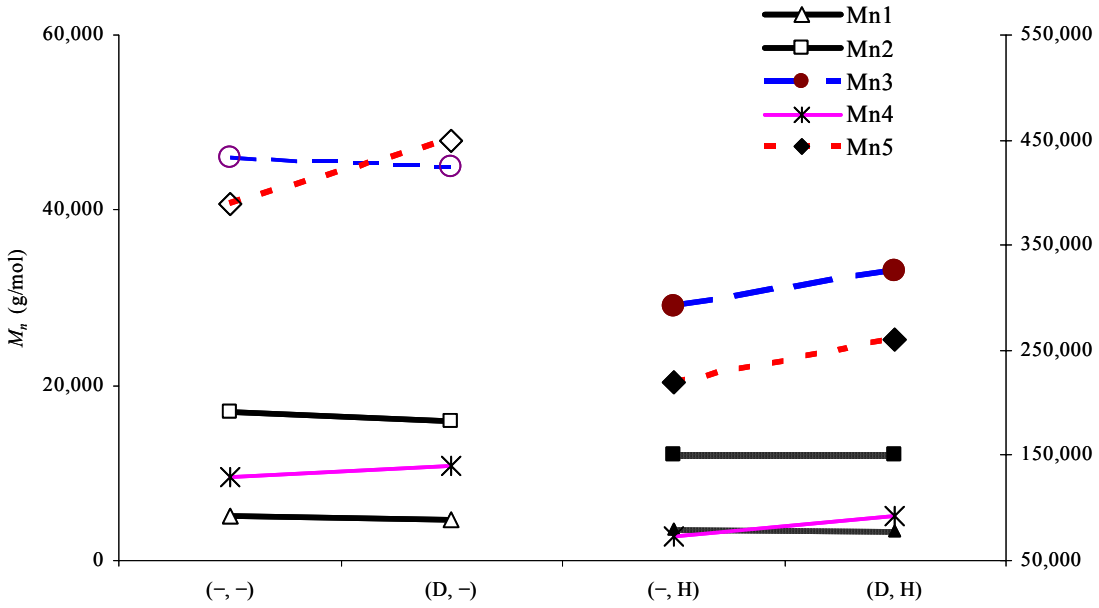

Figure 4-17. Changes in M_n per site type when donor is added to the reactor at 60°C polymerization temperature (Secondary axis is for M_{n4} and M_{n5} only).

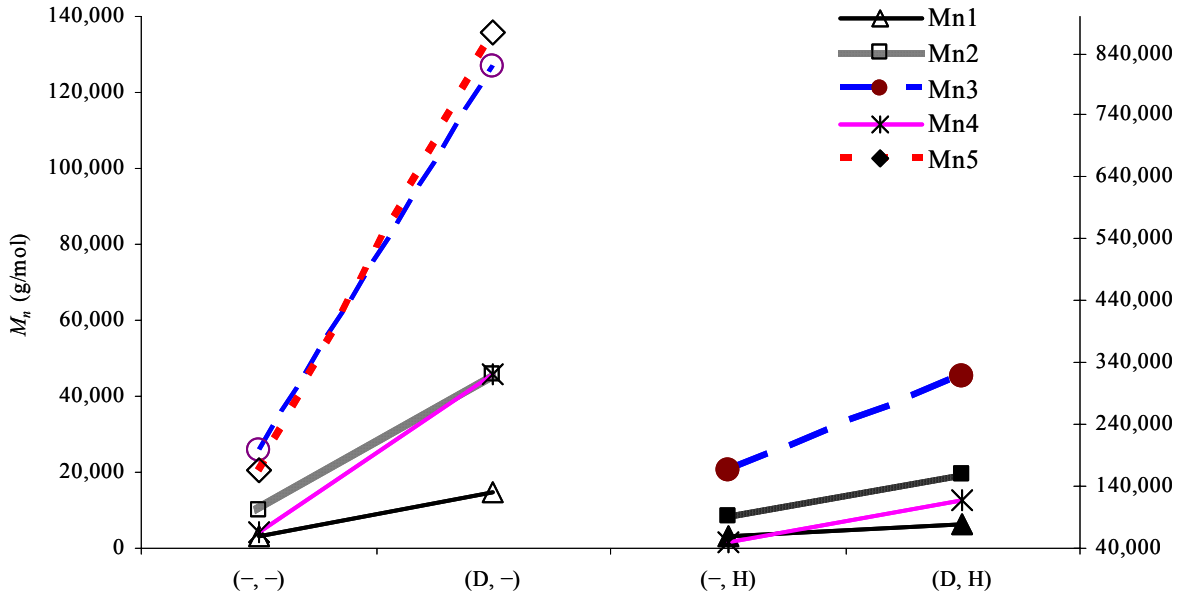

Figure 4-18. Changes in M_n per site type when donor is added to the reactor at 70°C (Secondary axis is for M_{n4} and M_{n5} only).

4.4.2. Tacticity and Crystallinity

The hierarchal design of the experiments shown in Figure 3-3 was also applied to analyze the *mmmm* pentad distribution measured by ^{13}C NMR. Polymerization replicate runs (D, H)-1 and (D, H)-2 at 70°C were used, with two aliquots from each sample being analyzed twice. The eight analyzed samples had an average *mmmm* pentad of 94.7 ± 0.55 %. The confidence interval calculated for the *mmmm* pentad of this sample was used for all the other samples analyzed by ^{13}C NMR. The F-test showed that run to run and sample to sample deviations were negligible, as indicated in the Table 4-13, where $F_{observed} < F_{critical}$ for both polymerization runs and sampling levels. Therefore, the polymer samples have reproducible *mmmm* pentads that are not influenced by run replicates or sampling.

Table 4-12. Hierarchal design according to Figure 3-3 for ^{13}C NMR data for runs (D, H)-1 and (D, H)-2 made at 70 °C (for full assignments please refer to Table A- 1).

Run	Sample	Analysis	*mmmm*
(D, H)-1	S1	A1	94.29
		A2	94.33
	S2	A3	96.32
		A4	94.92
(D, H)-2	S1	A5	94.18
		A6	94.89
	S2	A7	94.60
		A8	93.67
Average			94.7
Standard Deviation			0.79
95 % Confidence			0.55

Table 4-13. ANOVA table for *mmmm* pentad (2 × 2 × 2) for polymerization samples (D, H)-1 and (D, H)-1 made at 70°C.

Source of Variation	Sum of Squares	Degree of Freedom	Mean Square	Expected Value of Mean Square		$F_{critical}$	$F_{observed}$	P-value
Average	71,663	1						
Run	0.768	1	0.768	0.192	F(1,2,0.05)	18.5	0.8	0.05003
Sample	1.915	2	0.958	0.479	F(2,4,0.05)	6.94	2.3	0.05005
Analysis	1.674	4	0.419	0.419				

Table 4-14 and Table 4-15 show the normalized pentad assignments for polypropylene samples of the four groups made at 60°C and 70°C, respectively. Figure 4-19 compares the *mmmm* pentad fractions for polymers made in groups (D, −), (−, −), (D, H), and (−, H). The

mmmm pentad fractions were nearly insensitive to polymerization temperature, except when only donor was present, when it increased from 83.78% (60°C) to 95.50% (70°C). As expected, adding external donor to the catalyst increased the *mmmm* pentad fraction of all samples significantly. The highest *mmmm* pentad content was obtained at 70°C in the presence of donor but in the absence of hydrogen; this seems to agree with the results discussed in Figure 4-18 that showed that the donor effect on M_n per site type was more pronounce at 70°C. One may propose that the more effective donor-catalyst site coordination at 70°C affected both the *mmmm* pentad and M_n per site type. The lowest *mmmm* pentad content was observed when both hydrogen and donor were absent.

The positive hydrogen effect on the *mmmm* pentad fraction for all but one (Group (D, −), at 70°C) experimental cases is an important finding in this research that was also reported in some earlier publications by other researchers (Chadwick et al., 1995; 1996; 2000). We have also shown previously with a mathematical model that such behavior was indeed expected (Alshaiban and Soares, 2009; 2011) and the present results confirm our simulations. Figure 4-20 shows a steady-state simulation result of the hydrogen effect on the population of the isotactic, atactic, and stereoblock chains. This hydrogen enhancement effect on the *mmmm* pentad fraction is accounted for in the model by assuming that hydrogen preferentially terminates chains growing on low stereospecific sites after racemic or 2-1 insertions. The exceptional case seen when hydrogen was added in the presence of donor at 70°C will be further investigated in Chapter 5.

Table 4-14. Normalized pentad assignments for polypropylene samples made at 60°C.

		Range	Run #			
Seq.#		(δ)*	(D, −)-2	(−, −)-1	(D, H)-1	(−, H)-2
1	*mmmm*	22.0 − 21.7	83.78	61.25	93.77	76.46
2	*mmmr*	21.7 − 21.4	3.73	9.51	3.06	6.73
3	*rmmr*	21.4 − 21.2	0.53	1.87	0.00	0.00
4	*mmrr*	21.2 − 21.0	4.17	7.76	2.48	4.96
5	*mmrm* + *rmrr*	21.0 − 20-7	2.01	6.39	0.00	4.60
6	*rmrm*	20.7 − 20.5	0.00	1.67	0.00	0.00
7	*rrrr*	20.5 − 20.25	2.90	3.55	0.00	2.61
8	*rrrm*	20.25 − 20.0	1.67	5.18	0.00	2.29
9	*mrrm*	20.0 − 19.7	1.21	2.82	0.69	2.35

* Range of δ reported by Busico *et al.*(2001)

Table 4-15. Normalized pentad assignments for samples made at 70°C.

Seq.#		Range (δ)*	Run # (D, −)-1	(−, −)-1	(D, H)-2	(−, H)-2
1	*mmmm*	22.0 − 21.7	95.50	63.00	94.60	74.85
2	*mmmr*	21.7 − 21.4	2.20	7.53	3.53	6.94
3	*rmmr*	21.4 − 21.2	0.00	1.21	0.00	1.04
4	*mmrr*	21.2 − 21.0	1.30	8.18	1.04	6.13
5	*mmrm* + *rmrr*	21.0 − 20-7	0.19	4.99	0.58	4.44
6	*rmrm*	20.7 − 20.5	0.00	1.32	0.00	0.00
7	*rrrr*	20.5 − 20.25	0.50	5.27	0.00	2.39
8	*rrrm*	20.25 − 20.0	0.00	4.55	0.13	2.37
9	*mrrm*	20.0 − 19.7	0.31	3.94	0.12	2.84

* Range of δ reported by Busico *et al.*(2001)

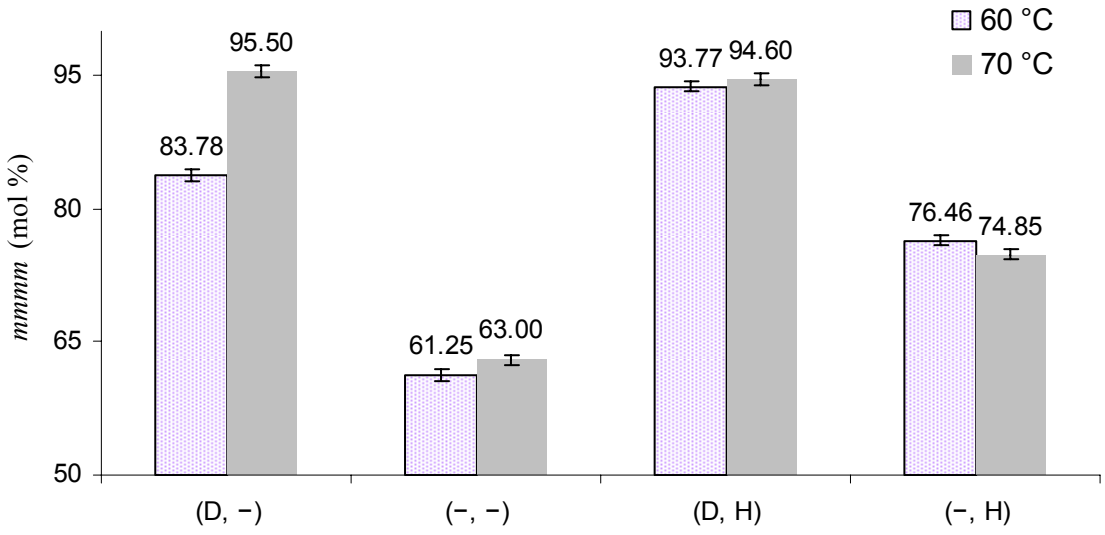

Figure 4-19. Effect of hydrogen and donor concentration on *mmmm* pentad percentages.

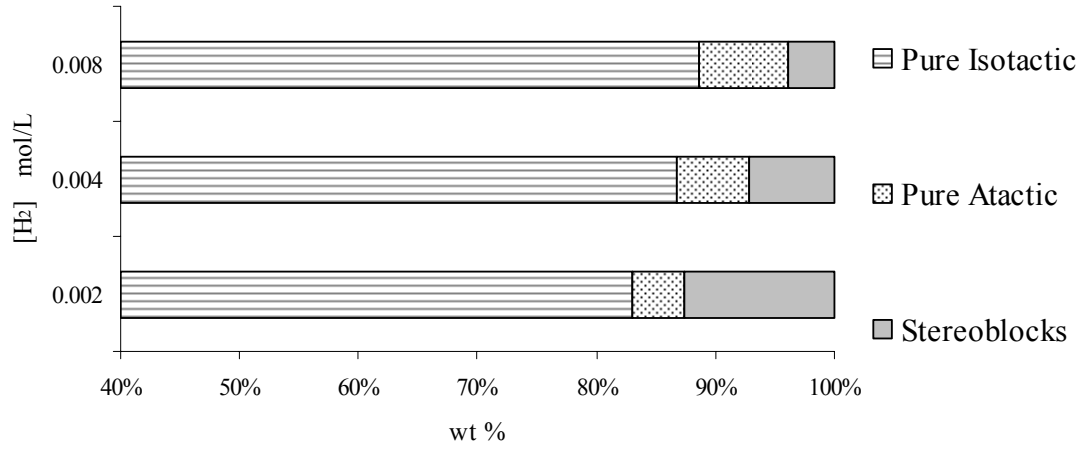

Figure 4-20. Simulation results for hydrogen effect on polypropylene tacticity (Alshaiban and Soares, 2009; 2011)

The crystallizability distribution of the produced polypropylene samples was investigated with crystallization elution fractionation (CEF). Figure 4-21 shows the excellent reproducibility of CEF profiles of two polypropylene samples made in replicate polymerization runs at 70°C. Similar results were obtained for all samples discussed in this chapter.

Representative CEF profiles for Group (D, −), (−, −), (D, H), and (−, H) samples made at 60 and 70°C are displayed in Figure 4-22 and Figure 4-23, respectively.

The CEF profiles can be divided in three main regions: 1) room-temperature elution peak, represented by the CEF purge peak at room temperature, 2) medium-temperature elution peak, appearing as an intermediate peak or shoulder, and 3) high-temperature elution peak, as the peak at the highest CEF elution temperature range. The room-temperature peak is associated with polymer chains with very low tacticity and/or molecular weight that remain soluble in TCB at room temperature; the medium-temperature peak is related to polypropylene with lower tacticity; finally, the high-temperature elution peak collects polypropylene with the highest tacticity in the sample.

Figure 4-24 demonstrates that adding hydrogen to the reactor at 60°C in the presence of external electron donor shifts the high-temperature elution peak to a higher value, albeit both samples retain their intermediate crystallinity shoulders. In contrast, Figure 4-25 shows that the high-temperature elution temperature peak does not change peak position upon hydrogen addition in the presence of donor at 70°C but, interestingly, the area under the medium-temperature shoulder increases. A similar behavior is also observed for polypropylene made in the absence of electron donor at 70°C: the highest peak temperature remains at approximately 111°C, as shown in Figure 4-26, but the fraction of the intermediate crystallinity material increases upon hydrogen addition. A similar trend was also observed upon hydrogen addition in the absence of electron donor at 60°C, as shown in Figure 4-27.

The increase of the intermediate crystalline fraction for polymers made at 70°C when adding hydrogen in the presence of donor shown in Figure 4-25, agrees with the decrease in *mmmm* pentad fraction from 95.5 to 94.6 described in ^{13}C NMR results in Figure 4-19. It may be tentatively proposed that at 70°C hydrogen disrupts the complexation of donor molecules to the less stereo and/or regioregular sites, leading to the formation of polymer with lower tacticity, but more experiments are needed to prove this hypothesis.

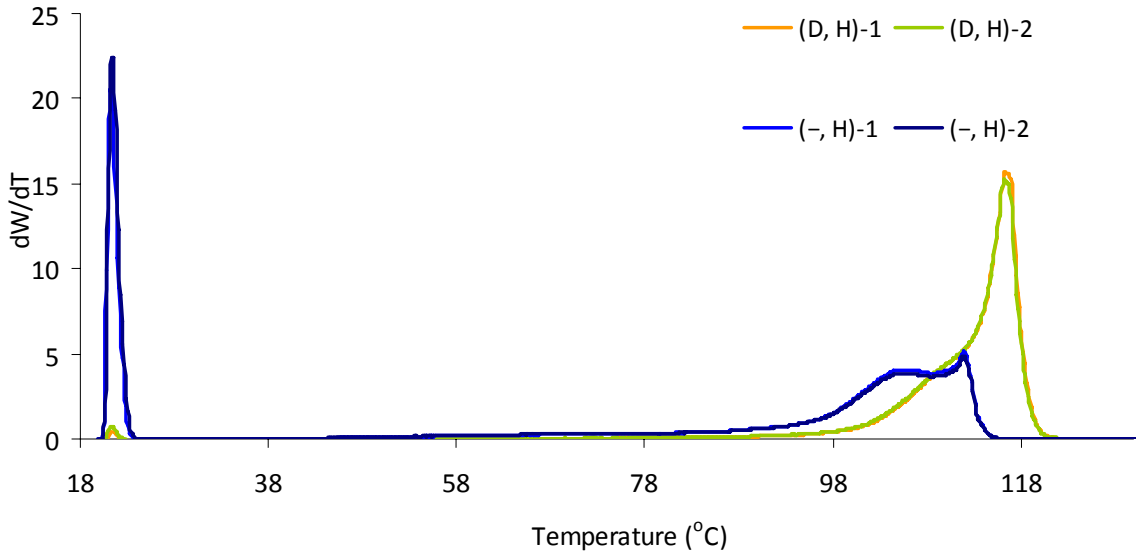

Figure 4-21. CEF profiles for two polymerization replicates of Group (D, H) [(D, H)-1 and (D, H)-2] and Group (−, H) [(−, H)-1 and (−, H)-2]; both polymerizations were done at 70°C.

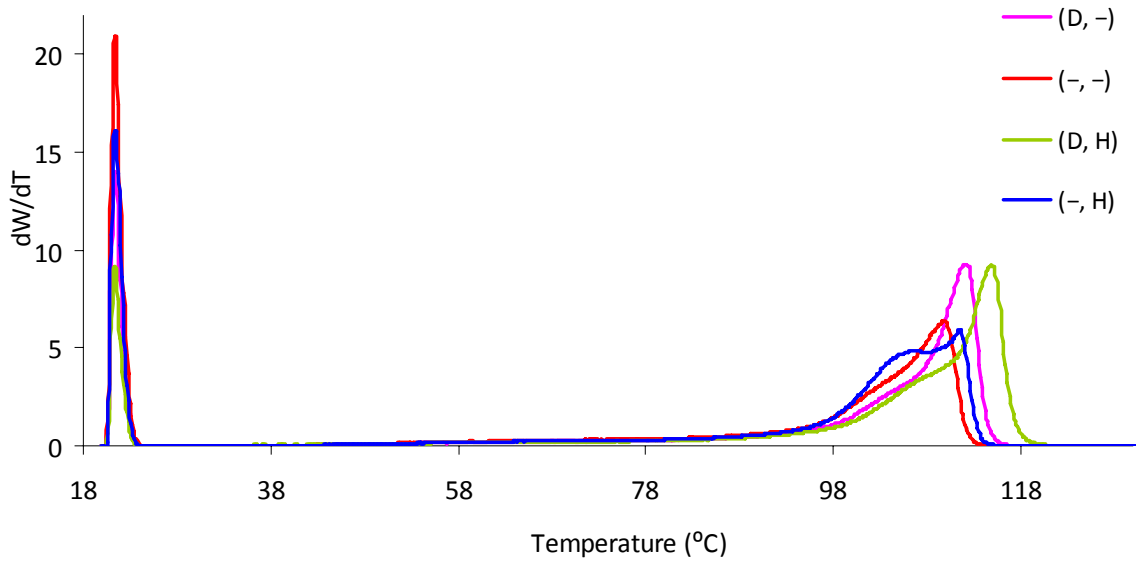

Figure 4-22. CEF profiles of polypropylene samples produced at 60°C.

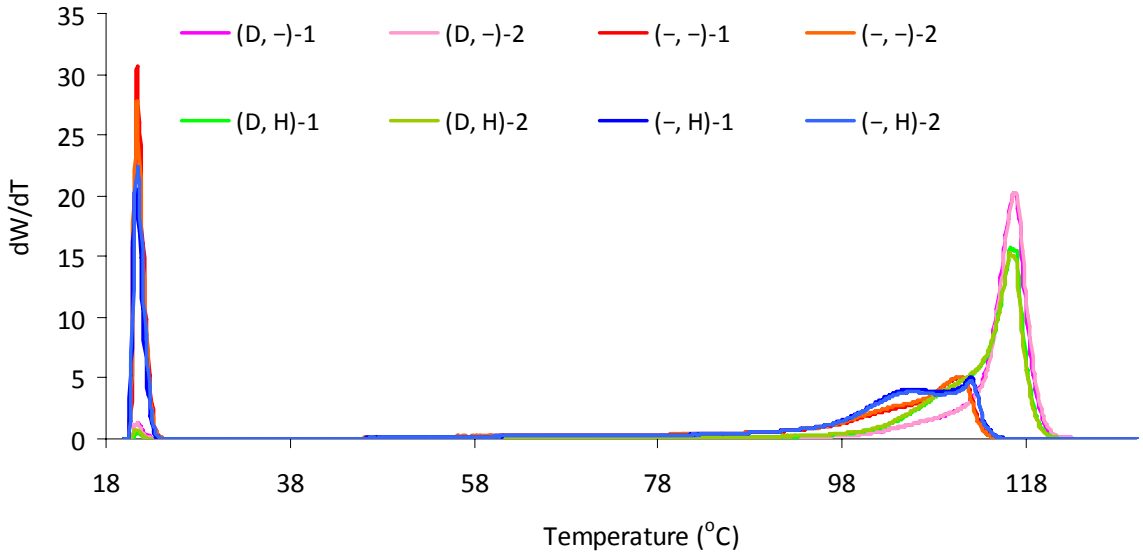

Figure 4-23. CEF profiles of polypropylene samples produced at 70°C.

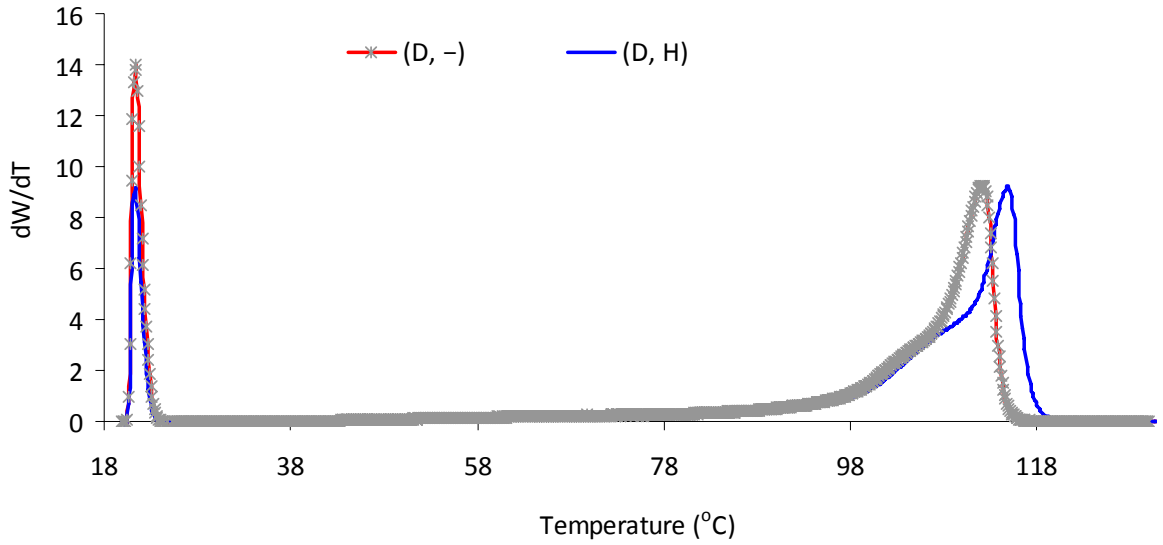

Figure 4-24. Comparison between polypropylene produced at 60°C in the presence of donor only (D, −) and in the presence of both donor and hydrogen (D, H).

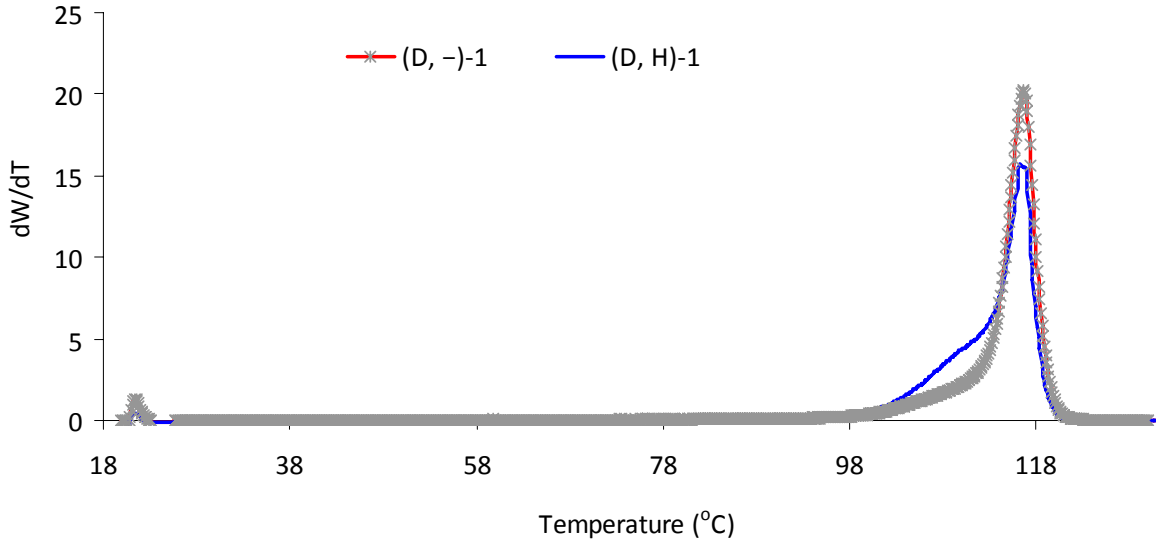

Figure 4-25. Comparison between polypropylene produced at 70°C in the presence of donor only (D, −) and in the presence of both donor and hydrogen (D, H).

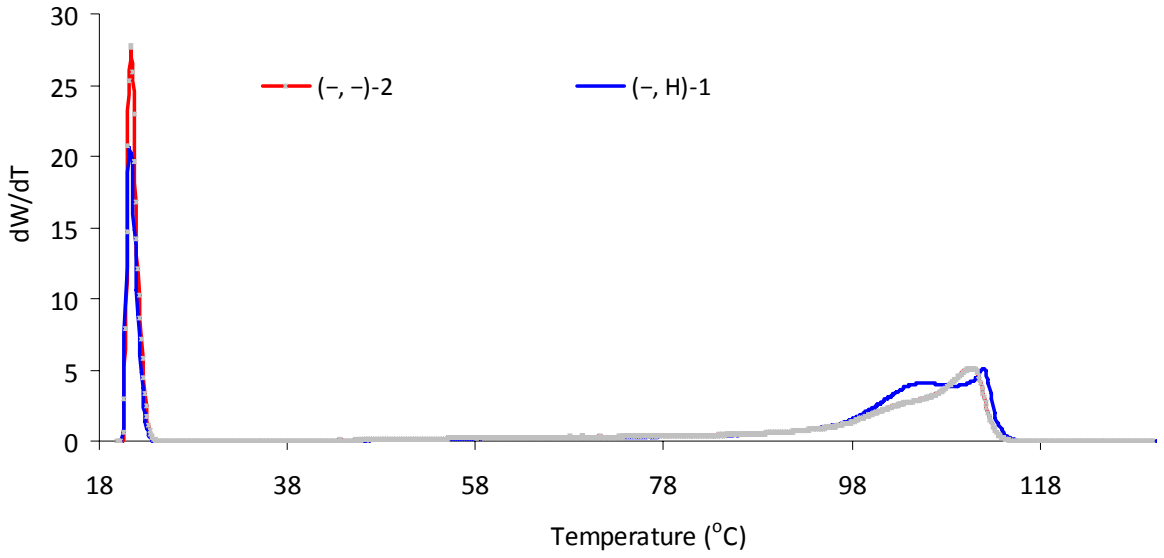

Figure 4-26. Comparison between polypropylene produced at 70°C in the absence of both donor and hydrogen (−, −) and in the presence of hydrogen only (−, H).

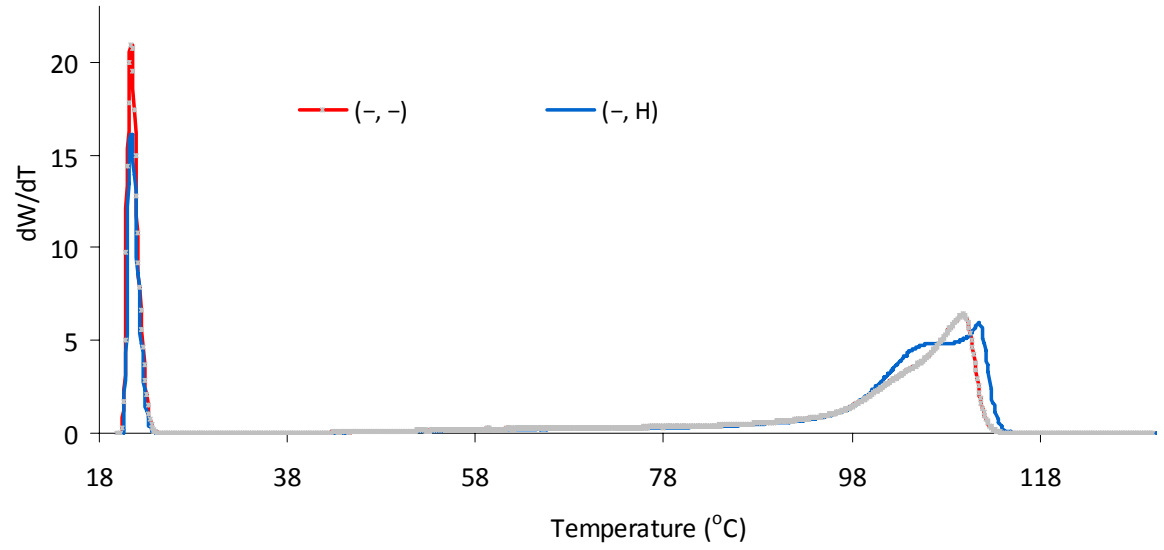

Figure 4-27. Comparison between polypropylene produced at 60°C in the absence of both donor and hydrogen (−, −) and in the presence of hydrogen only (−, H).

4.5. CONCLUSIONS

The effect of hydrogen and external donor on the apparent kinetic rate constants for activation, propagation, deactivation, and chain transfer for the polymerization of propylene with a 4th generation Ziegler-Natta catalyst has been quantified and the Arrhenius law used to estimate the activation energies and pre-exponential constants for these polymerization kinetic parameters.

The rate of polymerization in the presence of donor and hydrogen at 60 and 70ºC is higher than those measured in the absence of hydrogen, or donor, or both. The polymerization activation term increases with the addition of hydrogen in the presence or absence of donor, likely due to the freeing up of 2-1 terminated "dormant" sites.

If external donor is not added to the catalyst, the deactivation term was the highest of all cases, presumably because the aspecific sites deactivate faster than the specific sites. The addition of hydrogen increases the polymerization rate in the presence and absence of external electron donor. Freeing up the dormant sites after 2-1 insertions could be responsible for such rate enhancement. The external donor increases the population of specific sites at the expense of aspecific sites, which are more regioirregular. However, specific sites may also suffer 2-1 insertions, which could be responsible for the slow down in the rate of polymerization curves for Group (D, −) as compared to Groups (D, H).

The number average molecular weight decreases when the polymerization temperature is raised from 60 to 70°C in the absence of external donor, but increases when external donor is added to the reactor. This is could be due to the stabilization of the active sites when complexed with electron donor, making them less susceptible to chain transfer reactions, perhaps by blocking the transition state that leads to β−hydride elimination or transfer to monomer. This donor active sites complexation is stronger at 70°C.

Moreover, hydrogen, external donor, and polymerization temperature effects on polypropylene microstructure were investigated using GPC, ^{13}C NMR, and CEF. In addition to its usual effect as a chain transfer agent, hydrogen was found to increase the *mmmm* pentad fraction of polypropylene made either in the presence or absence of external donor for polymer produced at 60°C. Similar trends were anticipated by our group based on a mathematical model developed to describe the effect of hydrogen and electron donors during propylene polymerization with coordination catalysts. Interestingly, for polypropylene produced at 70°C, the addition of hydrogen led to slightly lower stereoselectivity and crystallizability. Even though a definite explanation for this phenomenon is not clear, the results presented in this chapter show that the combination of GPC, ^{13}C NMR and CEF is a powerful approach to characterize the microstructure of polypropylenes made with multiple-site catalysts.

Chapter 5

EFFECT OF VARYING HYDROGEN, EXTERNAL DONOR, AND POLYMERIZATION TEMPERATURE ON THE KINETICS OF PROPYLENE POLYMERIZATION WITH A 4TH GENERATION ZIEGLER-NATTA CATALYST

5.1. INTRODUCTION

Propylene polymerization in the presence and absence of hydrogen and/or an external electron donor was investigated in Chapter 4. However, the crystallinity and *mmmm* pentad results presented in Chapter 4 for polypropylene samples made at 70°C were not in agreement with those for the other samples in the same set of experiments. For instance, the *mmmm* pentad fraction of samples made at 60°C increased when hydrogen was added to the reactor; on the other hand, the *mmmm* pentad fraction of samples made at 70°C did not change much when hydrogen was used during the polymerization, but the area under the intermediate crystallinity fraction measured by CEF increased. In order to better understand this behavior, three polymerization runs were conducted at 70°C for 10, 30, and 60 minutes to find out if there was a change in CEF profiles as a function of polymerization time. Preparative fractionation (PREP) was also used to separate the intermediate crystallinity shoulder from the high crystallinity peak and both were analyzed by ^{13}C NMR. In addition, hydrogen and donor concentration ranges were expanded in this chapter to produce the polypropylene samples at 70°C with a wider variety of microstructures.

This chapter also investigates the effect of changing hydrogen and donor concentrations on polymerization kinetics and polymer microstructure following experimental Design B (Table 5-1) at polymerization temperatures of 55 and 65°C, extending the polymerization condition

range explored in Chapter 4. Similar identification terminology followed in Chapter 4 is followed here. Therefore, the four polymer sample groups at each polymerization temperature listed in Table 5-1 are classified according to the doubling or halving of hydrogen or donor concentrations. For instance, (0.5D, 2H) means half of the donor and double of the hydrogen concentrations based on a center point of P_{H_2} = 16 psi and Do/Ti = 1.4 mol/mol.

Table 5-1. Experimental conditions for Design B.

Experiment number	Factors		
	Do/Ti (mol/mol)	P_{H_2} (psi)	*T* (°C)
1	2.8	32.0	65
2	2.8	32.0	55
3	2.8	8.0	65
4	2.8	8.0	55
5	0.70	32.0	65
6	0.70	32.0	55
7	0.70	8.0	65
8	0.70	8.0	55
9	1.4	16.0	60
10	1.4	16.0	60

All polymerization and polymer characterization procedures have been previously described in Section 3.2.

5.2. CASE STUDY: EFFECT OF HYDROGEN AND EXTERNAL ELECTRON DONOR ON THE MICROSTRUCTURE OF POLYPROPYLENE PRODUCED AT 70°C

5.2.1. Results and Discussion

In order to verify whether the *mmmm* pentad fraction varied with polymerization time, three polymerization runs were conducted for 10, 30, and 60 minutes and the *mmmm* pentads of the produced polymer determined by ^{13}C NMR. Figure 5-1 shows that the *mmmm* pentad does not change with polymerization time. Moreover, the CEF profiles for the polypropylene produced at the three polymerization times (Figure 5-2) are also very similar. Therefore, it seems that the tacticity of these samples do not depend on polymerization time.

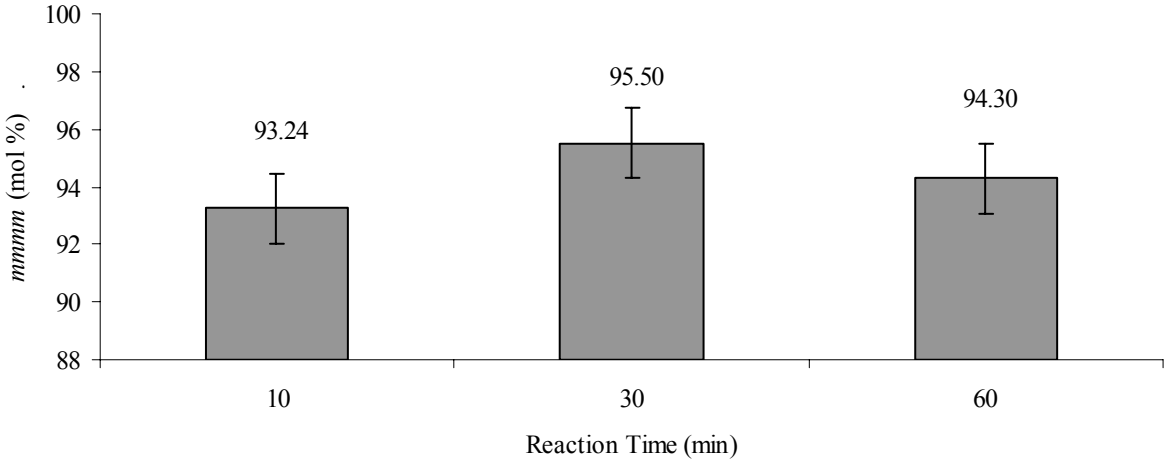

Figure 5-1. Change in *mmmm* pentad for polypropylene produced with donor only (D, −) at 70°C for 10, 30, and 60 minutes (see Table A- 2 in the Appendix for the complete ^{13}C NMR assignments).

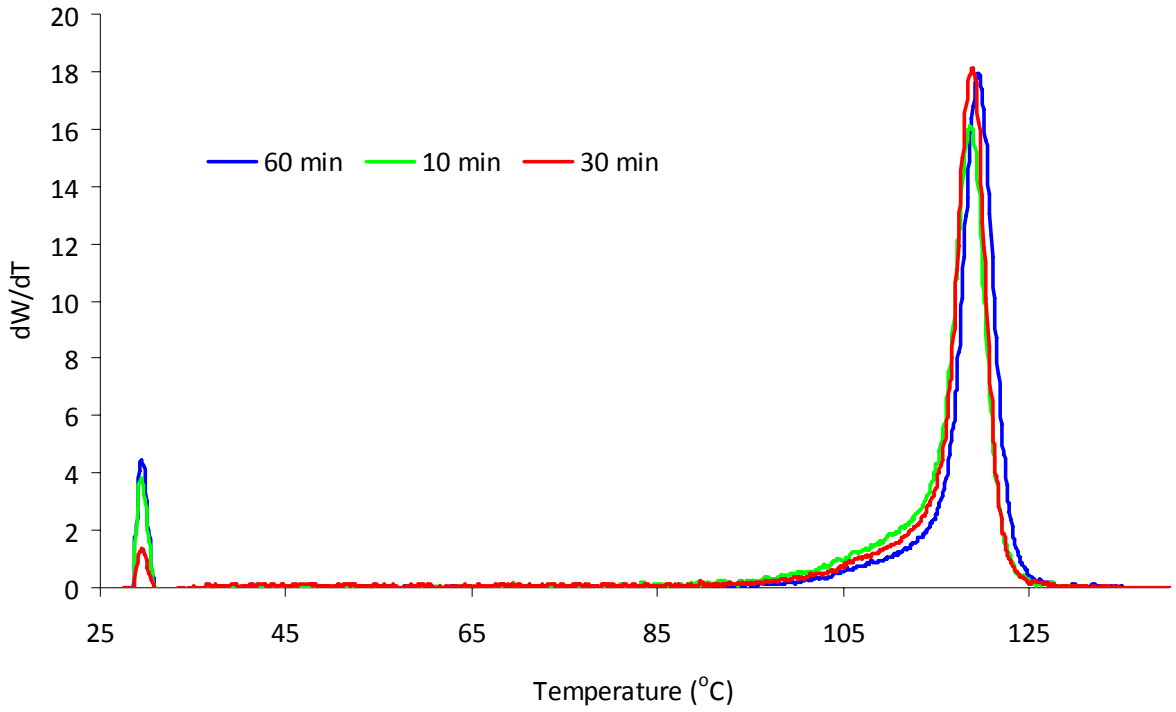

Figure 5-2. CEF profiles for polypropylene produced with donor only Group (D, −) at 70°C for 10, 30, and 60 minutes.

In Chapter 4, the CEF profile for samples made in the presence of donor and hydrogen showed a more prominent intermediate crystallinity shoulder than those made without hydrogen (Figure 4-25). Preparative fractionation (PREP) was used to separate the intermediate crystallinity fraction shoulder observed with Group (D, H).

TREF analysis of the sample was performed to determine the temperature cut point for PREP fractionation. TREF and CEF profiles for the sample are similar, as shown in Figure 5-3. Based on the TREF profile, a temperature of 110°C was selected to fractionate part of the intermediate crystallinity material from the parent resin. A sample of 1.6 grams was fractionated into three cuts, from room temperature to 80°C, from 80 to 110°C, and from 110 to 140°C. The last two fractions (F2 and F3) were filtered and dried, while the first fraction (F1) was discarded because it was too small to be further analyzed. The two fractions accounted for 93.8 wt% of the total resin, as shown in Table 5-2. The CEF analysis for the two fractions is shown in Figure

5-4, indicating that PREP could remove a portion of the intermediate crystallinity fraction from the parent resin. The ^{13}C NMR analysis for fractions F2 and F3, shown in Table 5-2, showed that their *mmmm* pentad contents were 90.6 and 98.1 %, respectively, confirming that the polymer responsible for the intermediate crystallinity shoulder had lower tacticity than that in the main CEF/TREF peak. Therefore, the increase in the area under the intermediate crystallinity shoulder noticed in Chapter 4 with the addition of hydrogen (D, H) at 70°C is due to a decrease in tacticity when compared with polymer made without hydrogen (D, −).

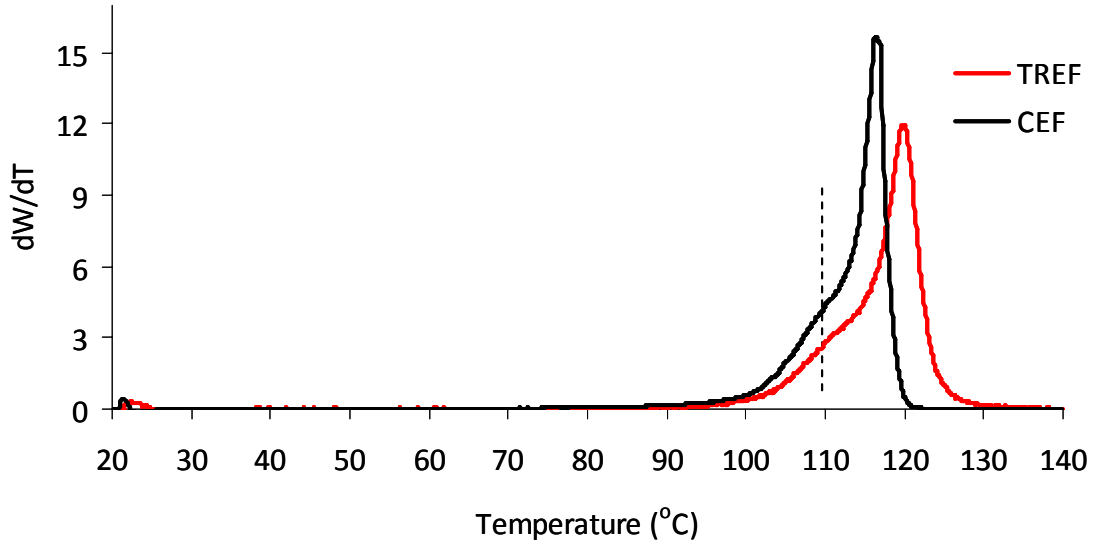

Figure 5-3. CEF and TREF curves for run (D, H)-1 at 70°C.

Table 5-2. ^{13}C NMR data for the fractions obtained using PREP for run (D, H)-1 at 70°C.

	Fraction Range	
	F2	F3
	80 − 110°C	110 − 140°C
Weight Fraction*	9.5	84.2
mmmm (mol %)	90.6	98.1

* 6.2 wt.% is the lost polymer and amorphous fraction (F1).

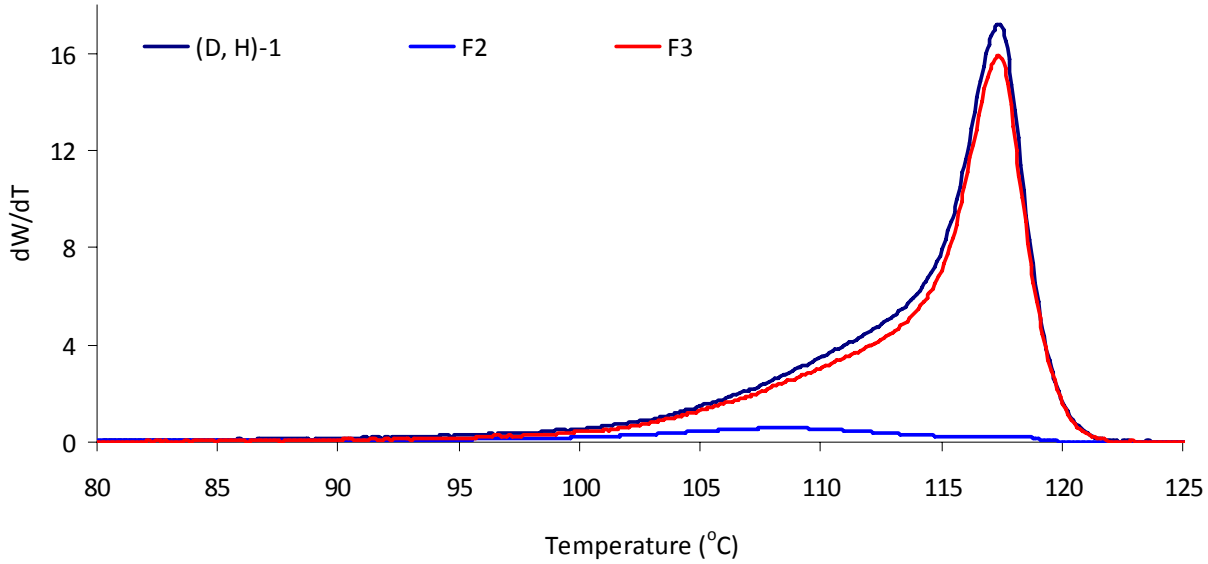

Figure 5-4. CEF profiles for run (D, H)-1 at 70°C and fractions F2 (80 to 110°C) and F3 (110 to 140°C).

Propylene was polymerized over the wider range of hydrogen and donor concentrations shown in Table 5-3 to help clarify the effect of these variables on polypropylene tacticity. All polymerizations were performed with Al/Ti = 900 ± 50 (mol/mol) and at a temperature of 70 ± 0.3°C.

The *mmmm* pentad content increased as the concentration of donor and hydrogen increased, as shown in Figure 5-5. However, the effect of hydrogen concentration on the *mmmm*

pentad is stronger at low donor concentrations. It may be proposed that hydrogen affects the tacticity of chains made on aspecific sites, perhaps by chain transfer reactions after a 2-1 insertion. Since the fraction of aspecific sites decreases with increasing donor concentration, the hydrogen effect becomes less apparent at higher donor concentrations.

Interestingly, a similar trend is predicted when using our previously developed Monte Carlo model for propylene polymerization (see Section 2.4). Figure 5-6 shows the Monte Carlo simulations for a single-site catalyst that undergoes site transformation (aspecific-stereospecific) by donor complexation assuming similar polymerization kinetic for both states. The predicted behavior is the same as the one seen experimentally in Figure 5-5.

Table 5-3. Donor and hydrogen concentrations used in polymerization experiments and corresponding *mmmm* pentad (complete pentad assignments are given in Table A-4 in the Appendix).

Run	*Do*/*Ti* (mol/mol)	P_{H_2} (psi)	*mmmm* (%)
(0.1D, H)	0.15	16	92.5
(0.25D, 0.5H)	0.37	8	93.2
(0.25D, H)	0.37	16	94.3
(0.25D, 2H)	0.37	32	95.1
(0.5D, 0.5H)	0.75	8	95.5
(0.5D, H)	0.75	16	96.3
(0.5D, 2H)	0.75	32	96.3
(D, 0.5H)	1.4	8	96.2
(D, H)	1.4	16	96.9
(D, 2H)	1.4	32	97.4
(D, 4H)	1.4	56	97.3
(2D, 0.5H)	2.8	8	96.5
(2D, H)	2.8	16	97.2
(2D, 2H)	2.8	32	97.5

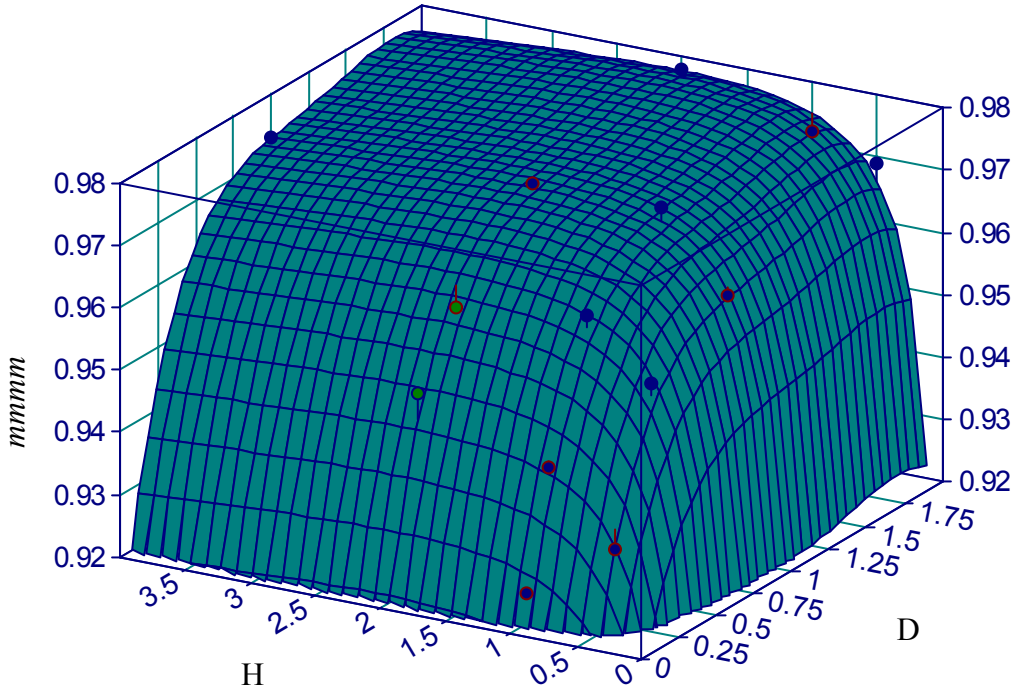

Figure 5-5. Change in *mmmm* pentad fraction as a function of donor and hydrogen concentrations for several polymerization runs at 70°C and Ti/Al=800 mol/mol; the reference donor/Ti ratio is 1.4 mol/mol and the reference hydrogen pressure is 16 psi [i.e. point (D, H) = (1, 1) is the reference data point]

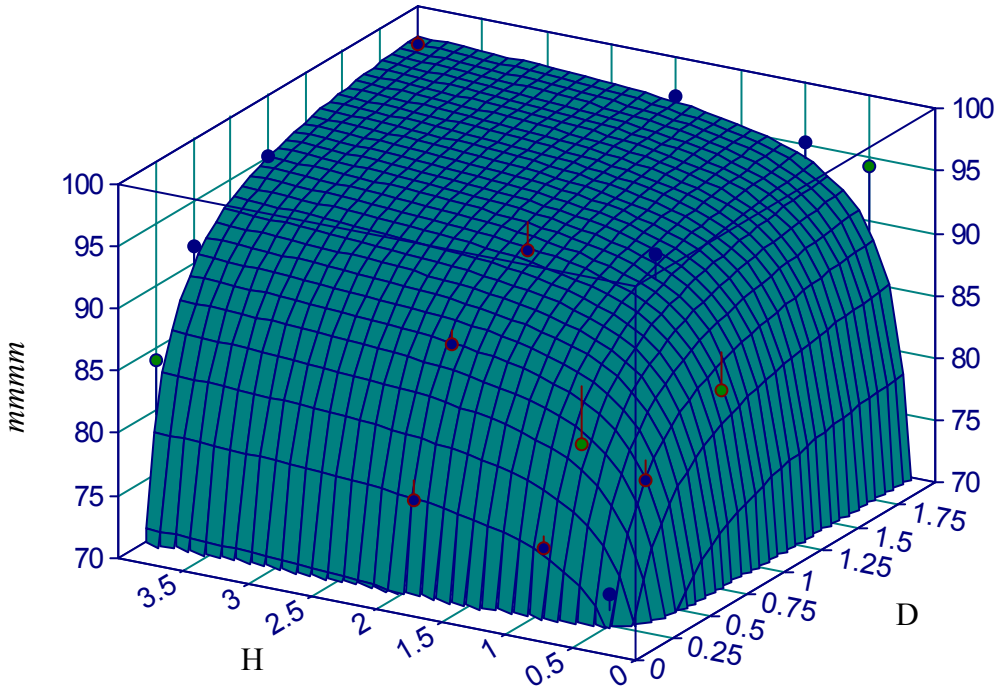

Figure 5-6. Simulated change in *mmmm* pentad fraction as a function of donor and hydrogen concentrations for several Monte Carlo simulations (900,000 sequences) using reference simulation conditions (Alshaiban and Soares, 2011), $R_p^I/R_t^I = R_p^{II}/R_t^{II} = 1364$; $k_{Do}^+ = 150$ L/mol·s, $k_{Do}^- = 0.01$ s^{-1}, reference [D]=0.0007 mol/L and [H_2]=0.004 mol/L [i.e. point (D, H) = (1, 1) is the reference data point]

5.3. POLYMERIZATION EXPERIMENTS: DESIGN B

5.3.1. Polymerization Kinetics

Table 5-4 summarizes the polymerization conditions in Design B. We adopted the terminology (2D, 0.5H) to represent doubling the donor concentration and halving the hydrogen

concentration with respect to reference condition (D, H) where Do/Ti = 1.4 mol/mol and P_{H_2} = 16 psi.

Figure 5-7 and Figure 5-8 show polymerization rates at 55 and 65°C. A clear increase in the overall polymerization rate is noticed when hydrogen concentration is doubled.

Table 5-4. Summary of experimental conditions and catalyst productivities in Design B.

Pol. Temp.	Run	*Al/Ti*	*Do/Ti*	C_o (1)	P_{H_2}	P_{C_3} (2)	Productivity
ºC		mol/mol	mol/mol	mol/L x 10^{-5}	Psi	psi	g-PP/ (g-cat· min)
55	(0.5D, 0.5H)	820	0.61	4.3	9	104	11.1
55	(0.5D, 2H)	839	0.63	3.8	32	76	14.1
55	(2D, 0.5H)	843	2.55	4.2	8	76	10.6
55	(2D, 2H)	780	2.58	4.5	32	104	14.8
65	(0.5D, 0.5H)	838	0.63	4.2	9	80	6.9
65	(0.5D, 2H)	839	0.63	4.2	31	104	12.1
65	(2D, 0.5H)	864	2.60	4.0	8	80	8.0
65	(2D, 2H)	838	2.55	4.2	31	104	11.3
60	(D, H)	852	1.4	4.1	17	86	17.7
60	(D, H)	831	1.4	4.3	15	85	16.8

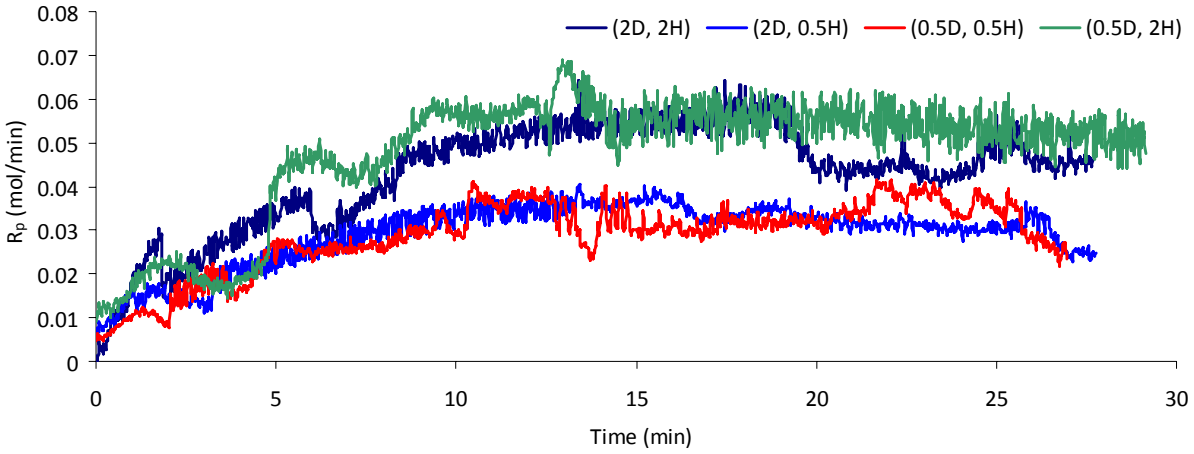

Figure 5-7. Polymerization rates for runs in Design B at 55°C.

A noticeable improvement in the catalyst activation rate was observed at 65°C, as shown in Figure 5-8, and a similar hydrogen rate enhancement effect was observed.

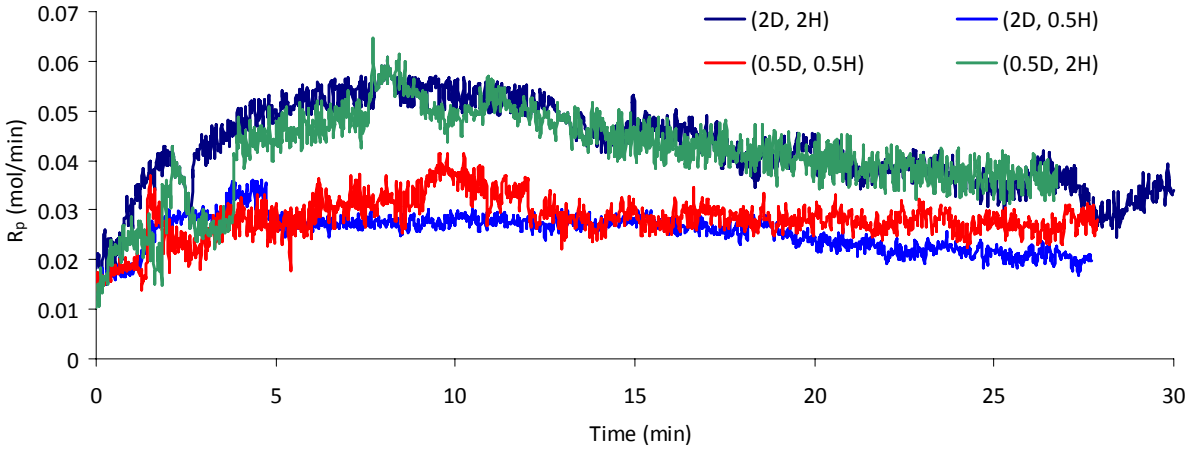

Figure 5-8. Polymerization rates for runs in Design B at 65°C.

Appendix B shows the individual fit solutions, but the estimated activation energies were not adequate because of the experimental noise. Therefore, a procedure similar to the one

described in Section 4.3.1 was followed to estimate the activation energies and pre-exponential constants for catalyst activation, propagation, and deactivation. Figure 5-9 to Figure 5-12 show the model fit for polymerization rates at 55 and 65°C for (0.5D, 0.5H), (0.5D, 2H), (2D, 0.5H), and (2D, 2H).

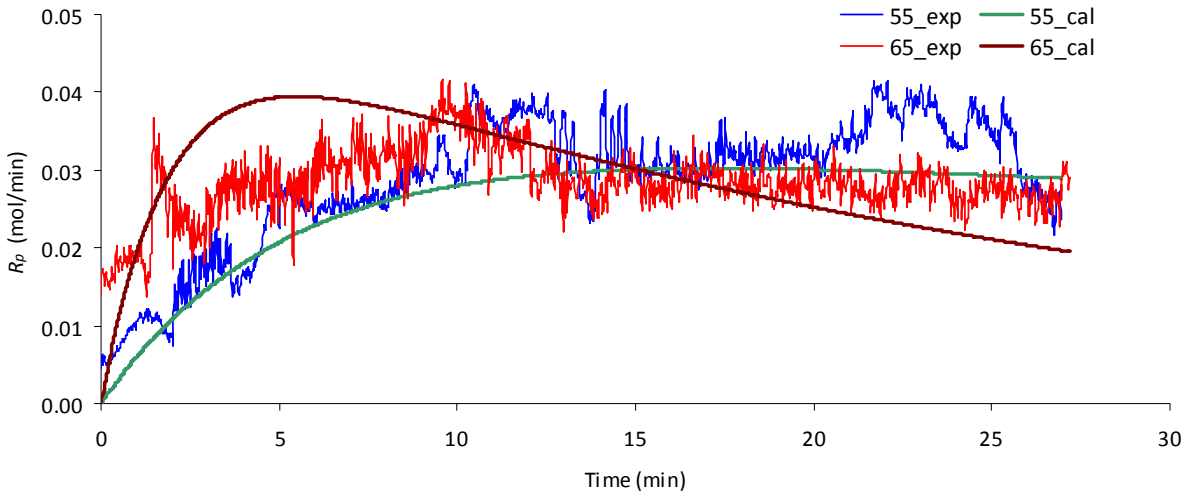

Figure 5-9. Experimental and modeled propylene uptake curves for runs (0.5D, 0.5H) at 55 and 65°C.

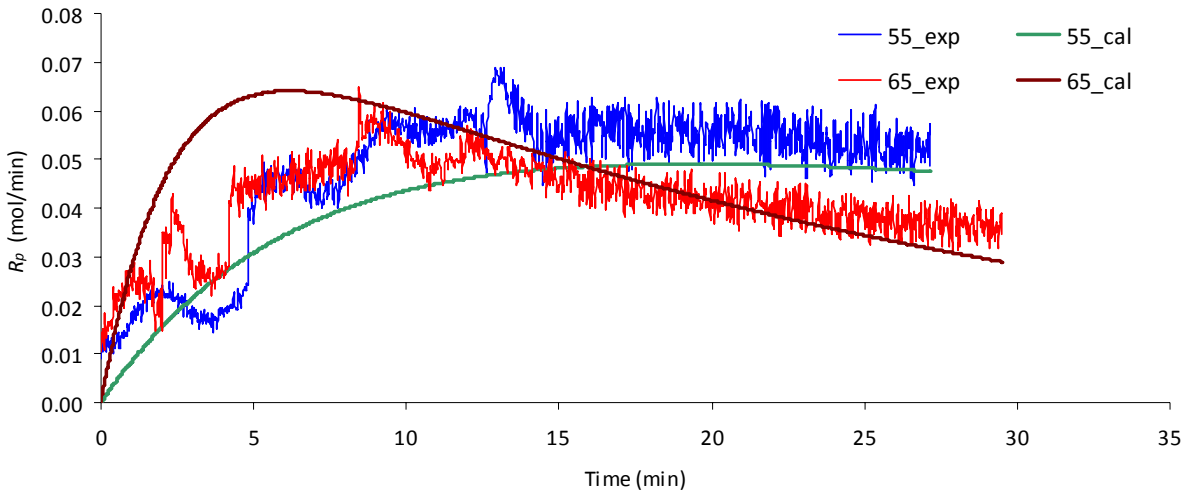

Figure 5-10. Experimental and modeled propylene uptake curves for runs (0.5D, 2H) at 55 and 65°C.

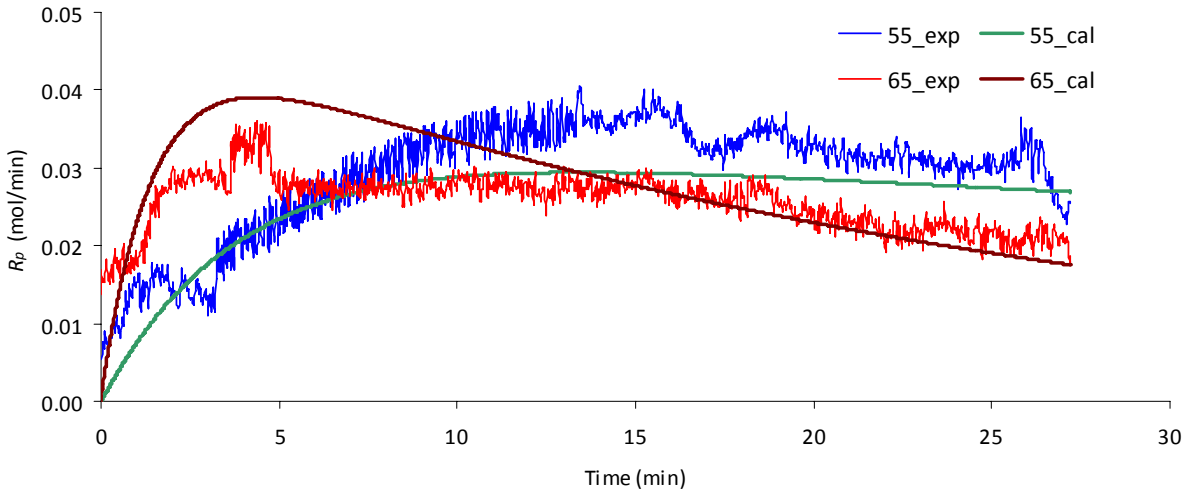

Figure 5-11. Experimental and modeled propylene uptake curves for runs (2D, 0.5H) at 55 and 65°C.

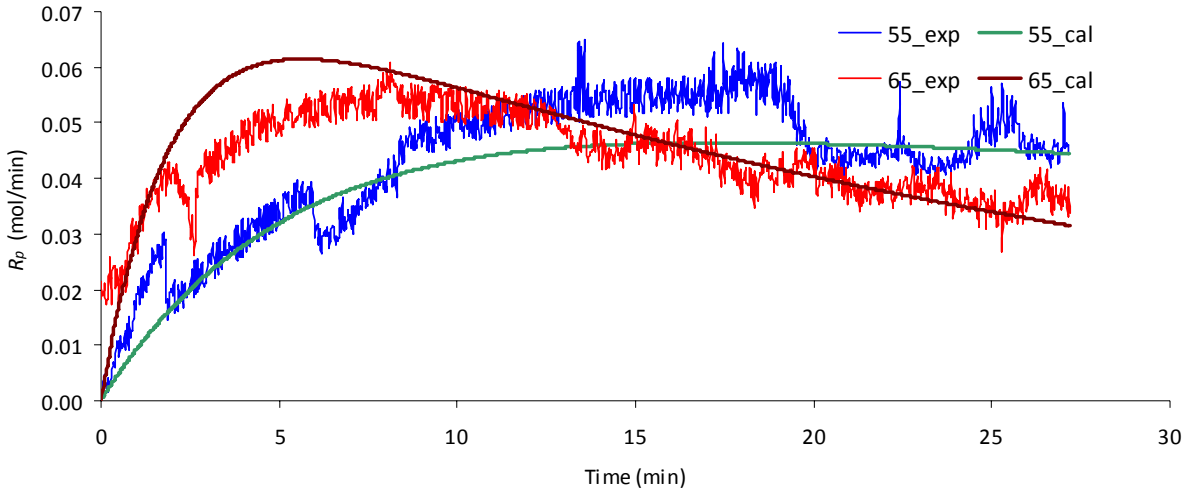

Figure 5-12. Experimental and modeled propylene uptake curves for runs (2D, 2H) at 55 and 65°C.

The estimated activation energies and pre-exponential factors are summarized in Table 5-5. The average activation energy for catalyst activation for the four experimental sets was 22.4 kcal/mol ± 0.3 kcal/mol, which is very close to 21.8 kcal/mol ± 0.4 kcal/mol estimated for Group (H, D) in Design A (see Section 4.3.2). Similarly, the average activation energy for propagation was 8.3 kcal/mol ± 0.1 kcal/mol (compare with 8.1 kcal/mol ± 0.01 kcal/mol for Group (H, D) in Design A), and the average activation energy for catalyst deactivation was 31.4 kcal/mol ± 0.02 kcal/mol (compare with 32.5 kcal/mol ± 0.3 kcal/mol for Group (D, H) in Design A). Therefore, changing polymerization temperature, donor and hydrogen concentration does not seem to affect the apparent activation energies of the three main polymerization kinetic steps, which seems to confirm that these variables affect the aspecific/stereospecific site ratio without influencing too much their polymerization mechanism.

The pre-exponential factor for activation (A_A) was the highest for (0.5D, 0.5H) and the lowest for (2D, 2H) as shown in Figure 5-13; A_A increases by decreasing both donor and hydrogen concentrations. Therefore, the frequency of catalyst site activation decreases with an increase in donor and hydrogen concentrations. Contrarily, the propagation pre-exponential

constant (A_p), was the highest for (2D, 2H), as expected since increasing donor concentration favors the formation of the more active stereospecific sites and hydrogen enhances the polymerization rate by terminating 2-1 dormant sites. The deactivation pre-exponential constants (A_d) were nearly the same for all runs in Design B.

Table 5-5. Activation energies (E_j) and pre-exponential constants (A_j) for site activation (E_A, A_A), propagation (E_p, A_p), and deactivation (E_d, A_d).

	Group				
Energy (kcal/mol)	(0.5D,0.5H)	(0.5D, 2H)	(2D, 0.5H)	(2D, 2H)	(D, H)
E_A	22.8	22.5	22.2	22.2	21.8
E_p	8.1	8.3	8.3	8.4	8.1
E_d	31.5	31.4	31.4	31.4	32.5
Pre-exponential constant					
A_A (min^{-1})	3.0×10^{14}	1.5×10^{14}	1.5×10^{14}	1.0×10^{14}	2.1×10^{14}
A_p ($L \cdot mol^{-1} \cdot min^{-1}$)	7.0×10^{8}	1.7×10^{9}	1.0×10^{9}	1.8×10^{9}	9.0×10^{8}
A_d (min^{-1})	8.0×10^{18}	8.0×10^{18}	8.0×10^{18}	7.0×10^{18}	1.1×10^{19}

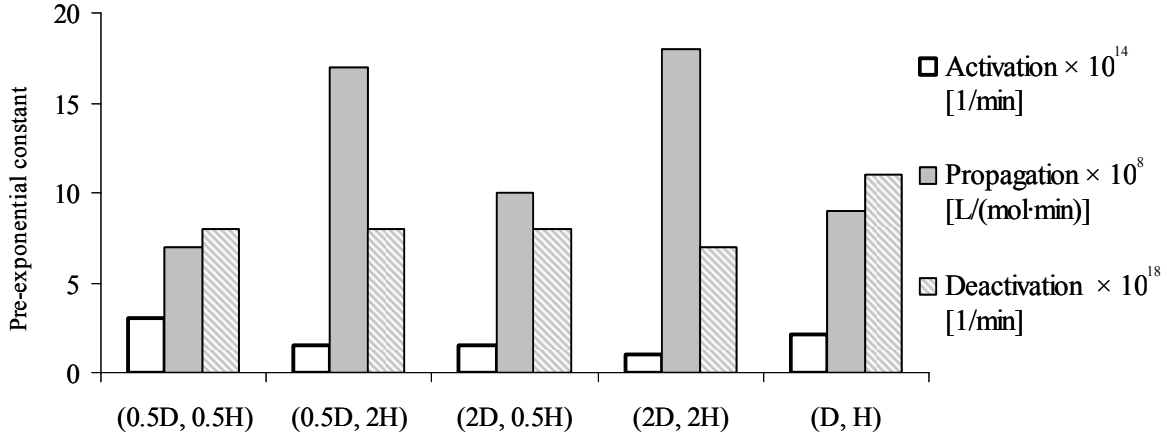

Figure 5-13. Estimated pre-exponential constants for activation, propagation, and deactivation at different donor and hydrogen concentrations.

Using the model parameters shown in Table 5-5, the reaction rate constants for the four sets of experiments at 55 and 65°C were calculated and compared to each other in Figure 5-14, to Figure 5-16. Figure 5-14 shows that the K_A values seem to be similar except for (2D, 0.5H). The higher K_A values for (2D, 0.5H) in both temperatures may be due to the slightly higher *Al/Ti* ratios for these runs, as shown in Table 5-4. The propagation rate constant clearly increased when doubling hydrogen concentration, as shown in Figure 5-15. Finally, Figure 5-16 shows that all k_d values are similar at a given temperature level. However, k_d increases sharply by raising the polymerization temperature.

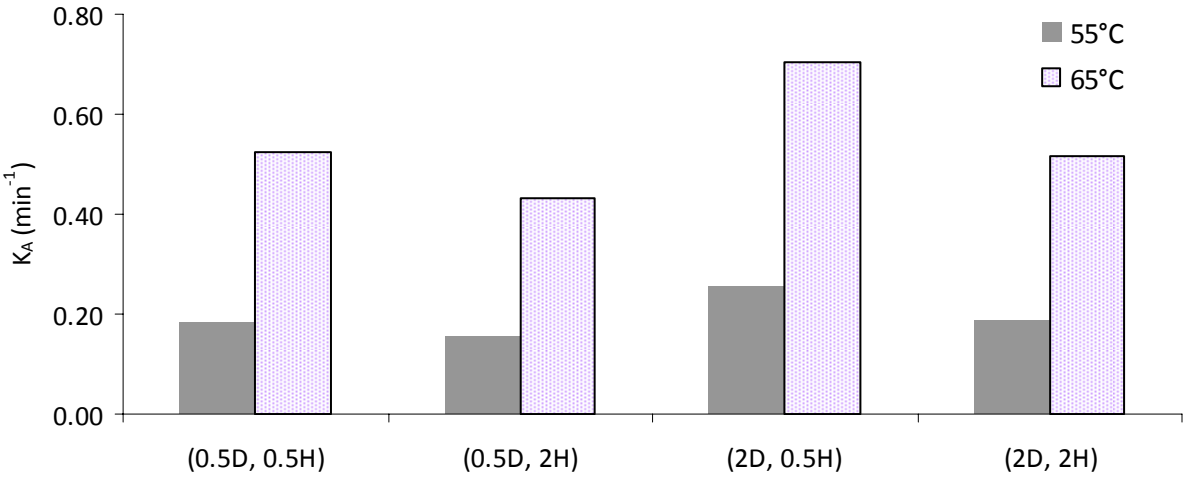

Figure 5-14. Activation rate constants (K_A) for polymerization Design B.

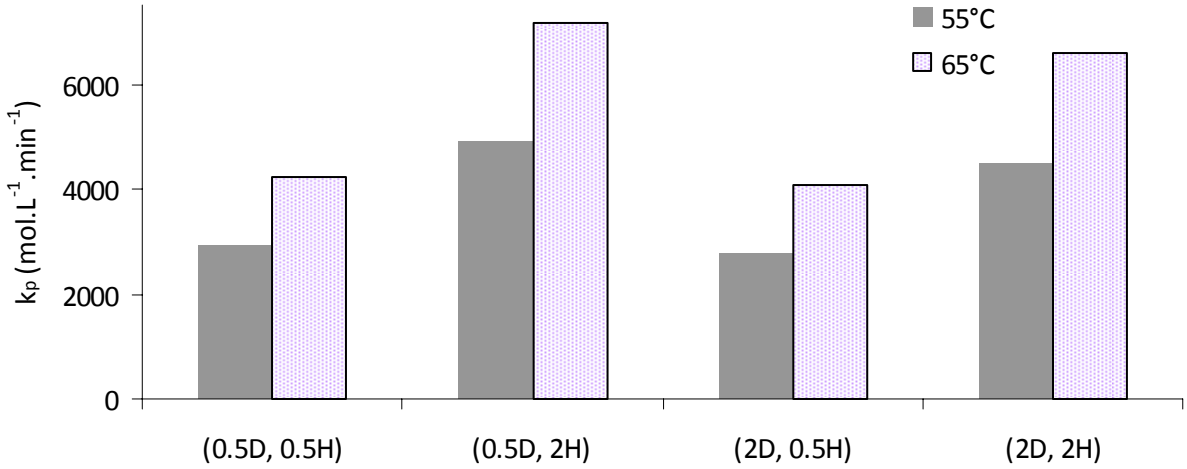

Figure 5-15. Propagation rate constants (k_p) for polymerization Design B.

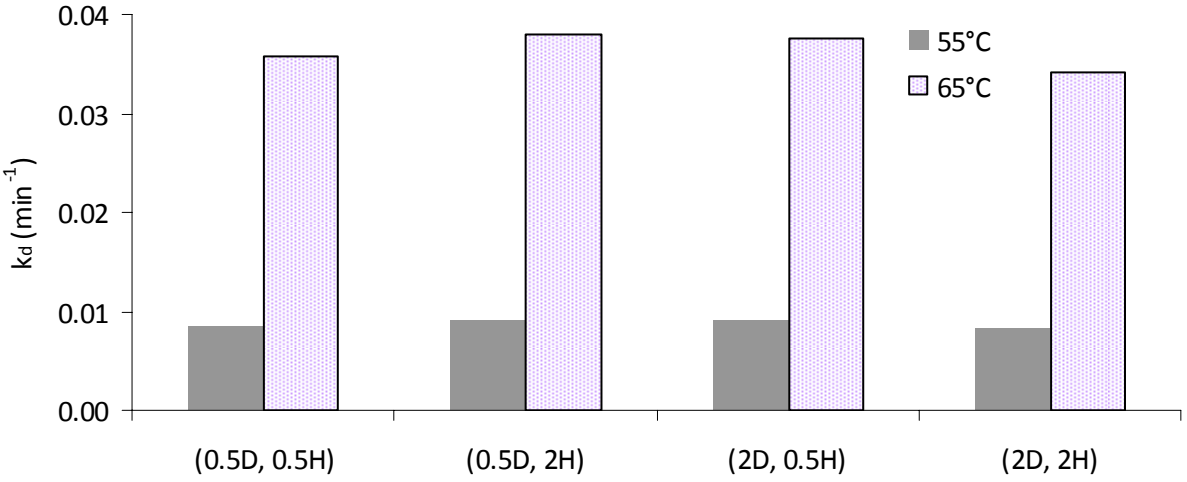

Figure 5-16. Deactivation rate constants (k_d) for polymerization Design B.

5.3.2. Polymer Characterization

The polymer samples described in the previous section were characterized for molecular weight, tacticity, and crystallinity. Table 5-6 and Table 5-7 summarize the number and weight average molecular weights, polydispersities, and MWD deconvolution results. Five site types were needed to describe the MWD of the polymer produced at 55 and 65°C under all polymerization conditions.

Figure 5-17 shows how the M_n for the whole polymer depends on the different polymerization conditions. Increasing donor concentration at the same hydrogen level led to a small increase in M_n. Figure 5-18 shows that the polydispersity does not depend strongly on hydrogen or donor concentration within the studied concentration and polymerization temperature ranges. This is also noticeable when inspecting how the M_n of chains made on different active site type depends on donor concentration. Figure 5-19 and Figure 5-20 show

that doubling donor concentration at the two hydrogen levels had no significant effect on M_n per site type for polymer made at 55 and 65°C.

Table 5-6. Estimated weight fraction (w_i) and number average molecular weight (M_n) for each site type for polymer made in all four groups at 55ºC.

		n					M_n	M_w	*PDI*
Group	Parameter	1	2	3	4	5	($g \cdot mol^{-1}$)	($g \cdot mol^{-1}$)	
(0.5D, 0.5H)	w_i	0.0623	0.1841	0.3494	0.2924	0.1119			
	M_n ($g \cdot mol^{-1}$)	3.9×10^3	13.7×10^3	37.5×10^3	91.7×10^3	23.3×10^4	26×10^3	14×10^4	5.3
(0.5D, 2H)	w_i	0.0707	0.2095	0.3883	0.2453	0.0862			
	M_n ($g \cdot mol^{-1}$)	2.7×10^3	11×10^3	34×10^3	92.3×10^3	24.8×10^4	20×10^3	13×10^4	6.2
(2D, 0.5H)	w_i	0.0491	0.1656	0.3556	0.3043	0.1255			
	M_n ($g \cdot mol^{-1}$)	3.6×10^3	14.2×10^3	40×10^3	10.3×10^4	26.7×10^4	29×10^3	16×10^4	5.6
(2D, 2H)	w_i	0.0533	0.1709	0.3444	0.3037	0.1276			
	M_n ($g \cdot mol^{-1}$)	2.7×10^3	10.4×10^3	29.7×10^3	72.7×10^3	19.6×10^4	24×10^3	14×10^4	5.9

Table 5-7. Estimated weight fraction (w_i) and number average molecular weight (M_n) for each site type for polymer made in all four groups at 65ºC.

		n					M_n	M_w	*PDI*
Group	Parameter	1	2	3	4	5	($g \cdot mol^{-1}$)	($g \cdot mol^{-1}$)	
(0.5D, 0.5H)	w_i	0.0493	0.1558	0.3816	0.3022	0.1111			
	M_n ($g \cdot mol^{-1}$)	3.7×10^3	13.8×10^3	39×10^3	10.3×10^4	27.3×10^4	28×10^3	16×10^4	5.7
(0.5D, 2H)	w_i	0.0672	0.1917	0.3790	0.2682	0.0939			
	M_n ($g \cdot mol^{-1}$)	2.9×10^3	11×10^3	30.9×10^3	77.9×10^3	20.8×10^4	19×10^3	11×10^4	5.6
(2D, 0.5H)	w_i	0.0308	0.1402	0.3813	0.3213	0.1264			
	M_n ($g \cdot mol^{-1}$)	3.0×10^3	12.2×10^3	35.8×10^3	91.7×10^3	24.7×10^4	30×10^3	15×10^4	5.2
(2D, 2H)	w_i	0.0620	0.2128	0.4010	0.2473	0.0769			
	M_n ($g \cdot mol^{-1}$)	3.3×10^3	13.6×10^3	35.4×10^3	86.3×10^3	23.3×10^4	22×10^3	14×10^4	5.1

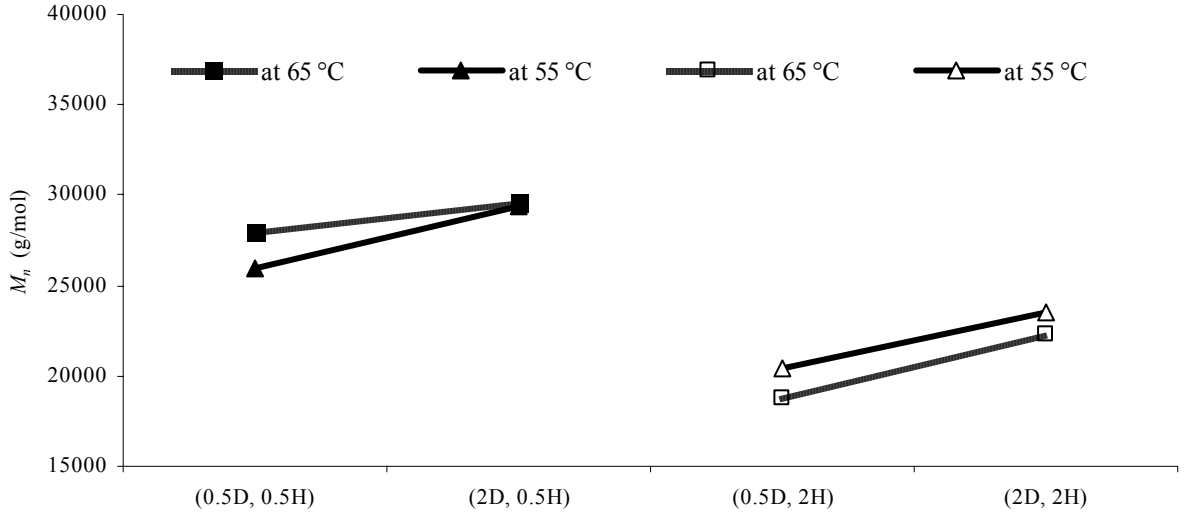

Figure 5-17. Effect of doubling donor concentration on number average molecular weight.

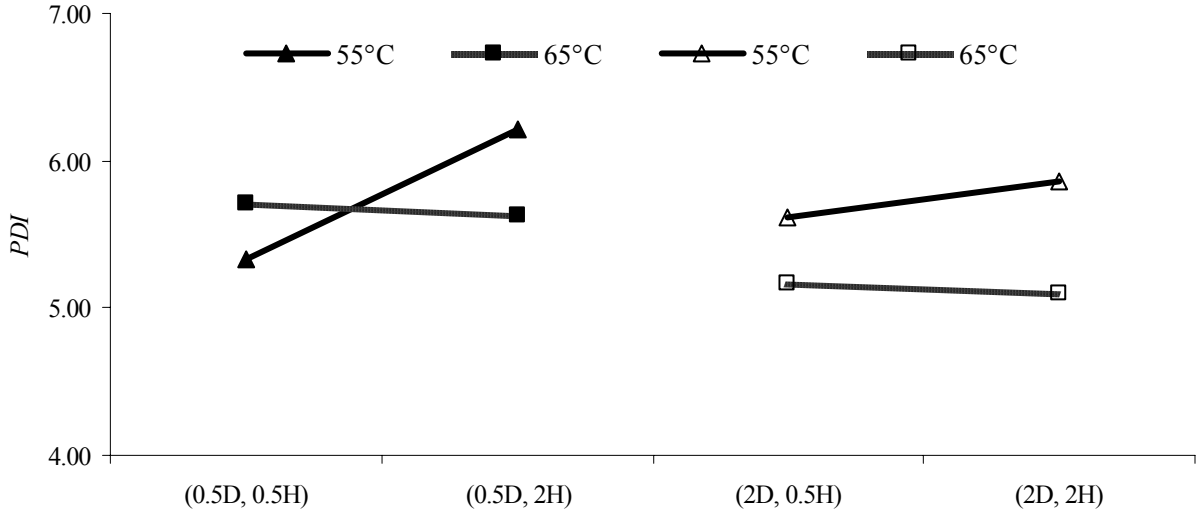

Figure 5-18. Effect of doubling hydrogen concentration on polydispersity.

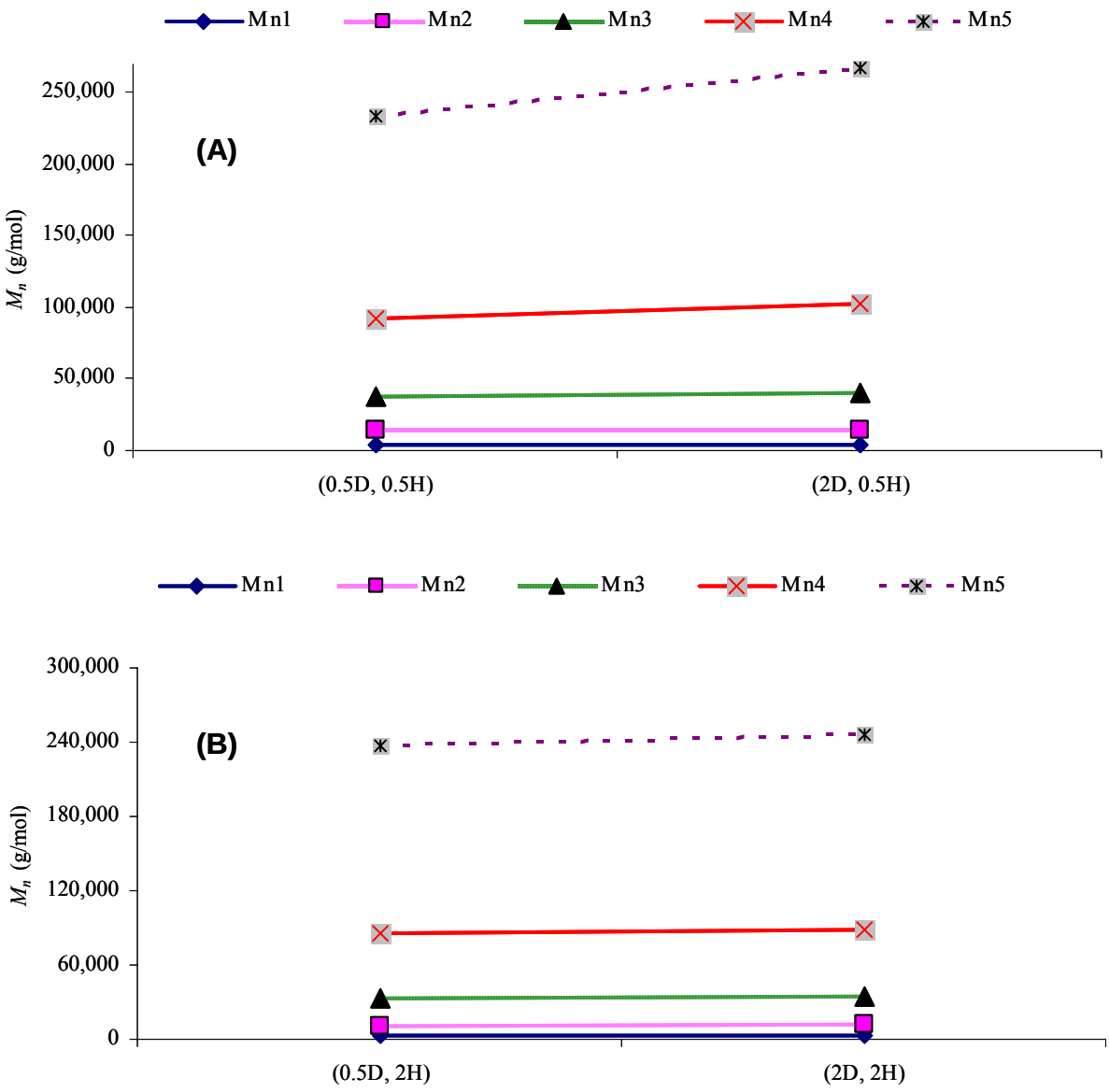

Figure 5-19. Change in the number average molecular weight of chains made on different site types at 55°C when the donor concentration is doubled at: (A) 0.5H and (B) 2H.

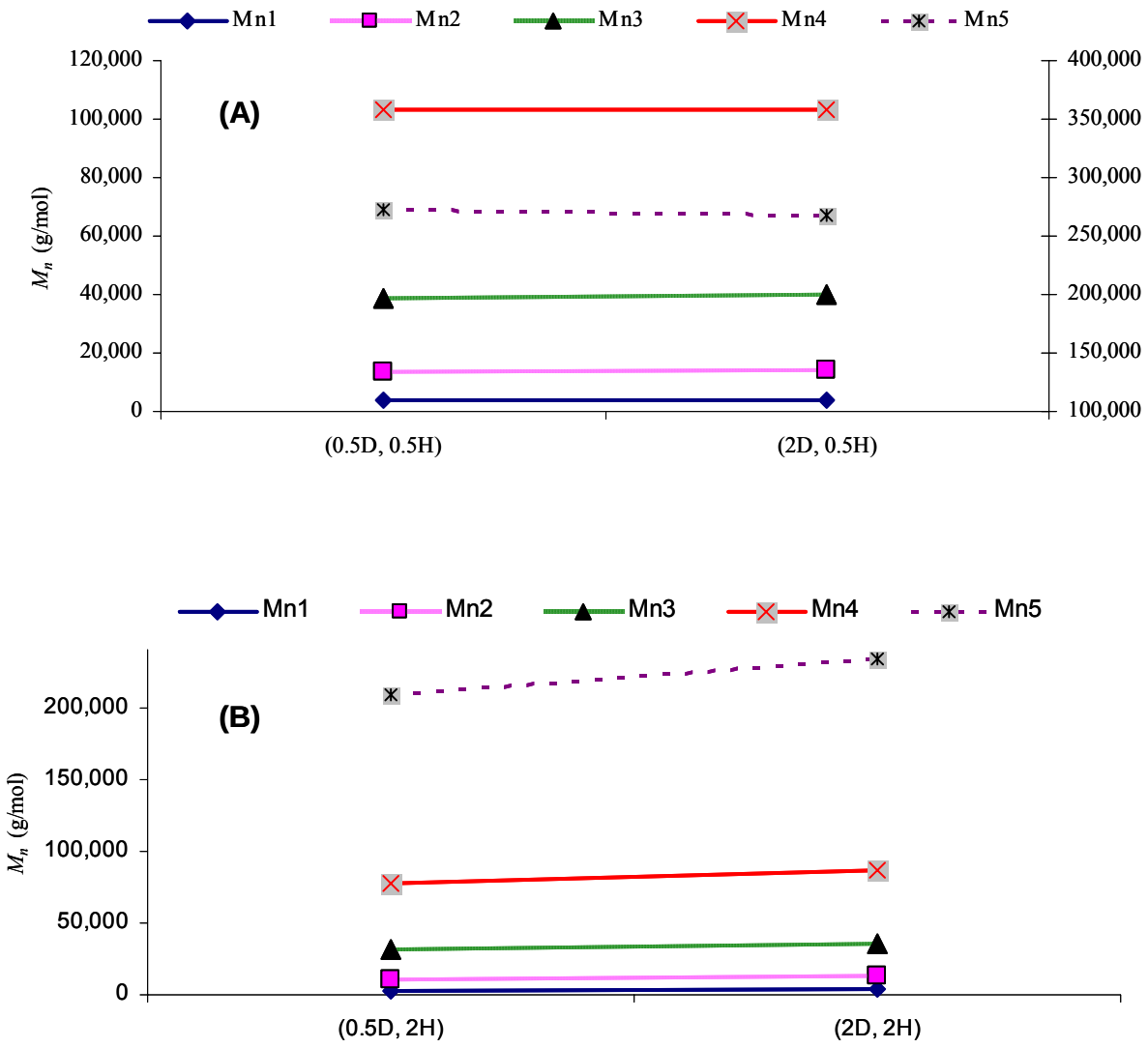

Figure 5-20. Change in the number average molecular weight of chains made on different site types at 65°C when the donor concentration is doubled at: (A) 0.5H and (B) 2H.

On the other hand, increasing hydrogen and donor concentration had a strong impact on the *mmmm* pentad fraction of the produced polymer, as shown in Figure 5-21. It is interesting to notice the increase in tacticity when hydrogen concentration increases, a trend predicted by simulation and illustrated in Figure 4-20. Figure 5-21 also shows that the *mmmm* pentad content of polymer produced according to Design B was not affected by the polymerization

temperature. However, an appreciable difference is apparent on the *mmmm* pentad between (0.5D, 0.5H) at both 55 and 65°C and the one obtained in Section 4.4.2 for (D, −). The *mmmm* pentad for (0. 5D, 0.5H) was 89.5 and 88.9% at 55 and 65°C, respectively, and was 95.5% at 70°C for (D, −).

The CEF of all polypropylene resins made in Design B were similar, as illustrated in Figure 5-22 and Figure 5-23.

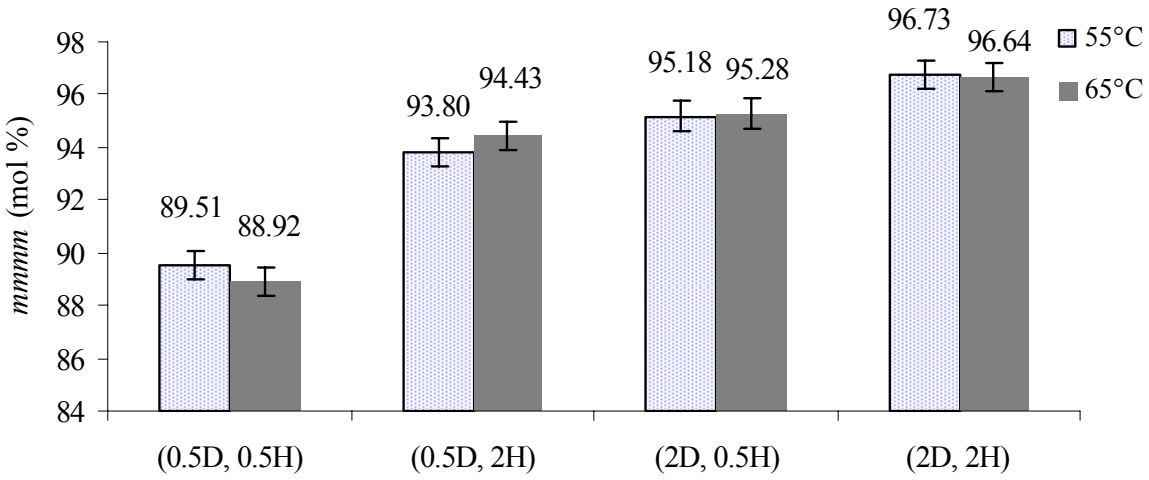

Figure 5-21. Polypropylene *mmmm* pentad % for Design B samples (for full assignment please refer to the Appendix, Table A- 4, and Table A- 5).

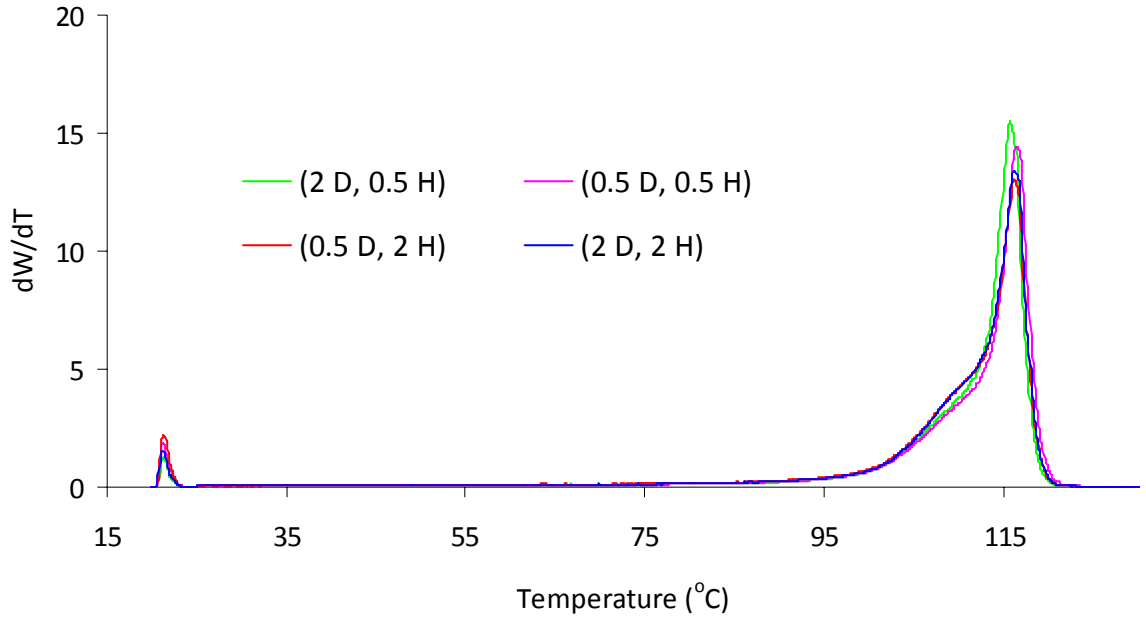

Figure 5-22. CEF profiles for polypropylene samples produced according to Design B at polymerization temperature of 55°C.

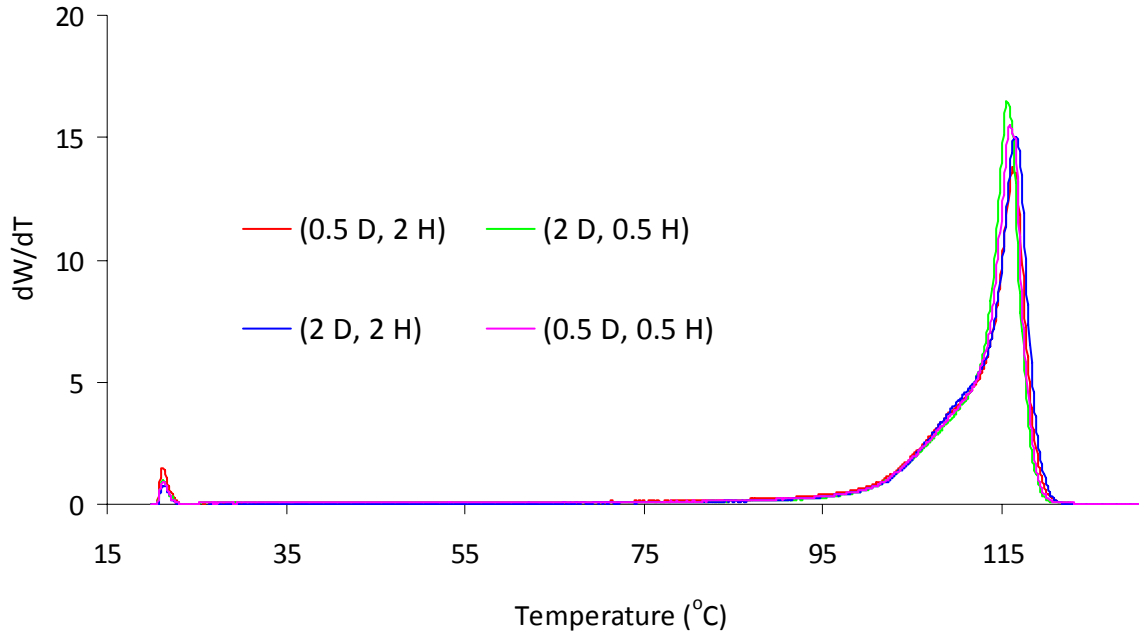

Figure 5-23. CEF profiles for polypropylene samples produced according to Design B at polymerization temperature of 65°C.

5.4. CONCLUSIONS

In this chapter, the effect of varying donor and hydrogen concentrations on polypropylene microstructure and propylene polymerization kinetics were investigated. The *mmmm* pentad fraction of samples made at 70ºC did not drift with polymerization time and the CEF curves were also similar. The increase in the intermediate crystalline fraction discussed in Chapter 4 (CEF shoulder) when adding hydrogen in the presence of donor was found to be due to the presence of lower tacticity polypropylene chains.

Moreover, the effects of varying hydrogen and donor concentration on *mmmm* pentad fraction were experimentally checked using a wider range of concentrations. Hydrogen showed a clear positive effect on the *mmmm* pentad fraction at low donor concentrations, which could

be due to an increase in stereoselectivity of the aspecific sites by hydrogen. By increasing the donor concentration, more aspecific sites are expected to be transformed to stereospecific sites and the hydrogen effect becomes less apparent. It might be tentatively proposed that at 70°C, hydrogen disrupts the complexation of donor molecules to the less stereo and/or regioregular sites, leading to the formation of polymer with lower tacticity, but more experiments are needed to test this hypothesis. It might be also proposed that, in the presence of donor and absence of hydrogen and specifically at polymerization temperature of 70°C, the aspecific sites are significantly less active. The addition of hydrogen, in this case, will reactivate these sites which will produce polymer with less stereoselectivity, but also more experiments are needed to test this hypothesis.

It is important to highlight the good qualitative agreement between our Monte Carlo model and the experimental observations. Monte Carlo simulations showed a similar effect for hydrogen and donor concentrations on the *mmmm* pentad fractions.

In the second section of this chapter, propylene polymerization kinetics and polypropylene microstructural studies according to Design B were conducted at two levels of donor and hydrogen concentration, and at 55 and 65°C. Polymerization rates at double hydrogen concentration were the highest rates in Design B. The estimated activation energies for activation, propagation and deactivation were very close to the values reported in Chapter 4 for the set of experiments in Design A.

Contrarily to hydrogen, increasing donor concentration causes the molecular weight averages to also increase. Moreover, hydrogen was found to increase *mmmm* pentad content of the polymer at both 55 and 65°C. However, no significant difference in the CEF profiles of the produced polymer was found, likely because these differences were too minor to be reflected on CEF profiles.

Chapter 6

PROPYLENE POLYMERIZATION WITH A MIXTURE OF EXTERNAL ELECTRON DONORS USING A 4TH GENERATION ZIEGLER-NATTA CATALYST: POLYMERIZATION KINETIC AND MICROSTRUCTURAL STUDY

6.1. INTRODUCTION

As described in Section 2.3.2, the use of donor mixtures with improved polymerization activity and stereoselectivity while maintaining polymerization self extinguishing characteristics is an interesting area of research (Chen and Nemzek, 2006; Campbell and Chen, 2008; Chen, 2008).

Chen and Nemzek (2006) used a normally dominating donor that led to high catalyst activity and good polypropylene properties, and a normally dominated donor that had little influence on the polypropylene properties. For instance, they illustrated the use of combinations of silane dominating donors, such as DCPDMS, DIBDMS, DCHDMS, or NPTMS, with carboxylic acid ester dominated donor (PEEB) to improve catalyst activity while maintaining the advantage of polymerization self-extinguishing properties.

The 4th generation catalyst used in this thesis achieves its best productivity with silane external donors; therefore, screening experiments with different silane dominating donors (D, P, and N) were conducted to select one that had the highest activity and produced polymer with highest crystallinity. This "optimal" donor was mixed with PEEB, the dominated donor, at different molar ratios. The molar ratio of the silane donor to PEEB was constrained by a maximum drop in polymerization activity of 10%, while maintaining the same polymer properties.

6.2. POLYMERIZATION EXPERIMENTS

All the polymerization experiments were conducted in the 300 mL stainless steel semi-batch stirred reactor described in Section 3.2. Table 6-1 summarizes the polymerization conditions for all experiments. Polymer Char CEF was used for the crystallinity analysis, and ^{13}C NMR was used to determine the pentad distribution, as explained in Section 3.2.

Table 6-1. Summary of experimental conditions and catalyst productivities using different donors and the mixture of D and PEEB donors.

Donor	Run #	*Al*/*Ti*	*Do*/*Ti*	C_o [(1)]	P_{H_2}	P_{C_3} [(2)]	Productivity
		mol/mol	mol/mol	mol/L x 10^{-5}	psi	psi	g-PP/ (g-cat· min)
D	186	862	1.3	4.1	16	86	12.4
P	176	839	1.3	4.2	16	86	6.5
N	178	838	1.3	4.2	16	86	4.8
PEEB	190	823	1.3	4.3	16	85	4.6
(D, PEEB)							
(100, 0)	212	823	1.3	4.2	0	74	11.1
(0, 100)	213	823	1.2	4.3	0	74	4.5
(90, 10)	214	837	1.3	4.2	0	74	5.0
(95, 5)	215	872	1.3	4.0	0	74	14.3
(98, 2)	216	857	1.3	4.1	0	74	13.7

(1) The weight percent of titanium in the catalyst added to the reactor was 1.7 wt% Ti for all runs [see Section 4.3.1 Equation (4.15)].

(2) Propylene pressure was varied to maintain the same monomer concentration in the hexane solvent for all runs at 2.1 mol/L as described in Section 3.3.2.

6.3. RESULTS AND DISCUSSION

Three external electron donors were compared for activity and stereoselectivity: D, N, and P donors were used to polymerize propylene at 70°C, Do/Ti = 1.4 mol/mol, Al/Ti = 900 mol/mol, P_{H_2} = 16 psi, and P_{C_3} = 86 psi. Figure 6-1 shows the rate of polymerization with D, N, and P and PEEB donors. D donor showed the highest rate of polymerization among all of the other donors. Moreover, D and P donors produced polypropylene with the highest crystallizability profiles, as measured by the CEF curves shown in Figure 6-2. Therefore, D donor was selected to be the dominating donor to be mixed with PEEB.

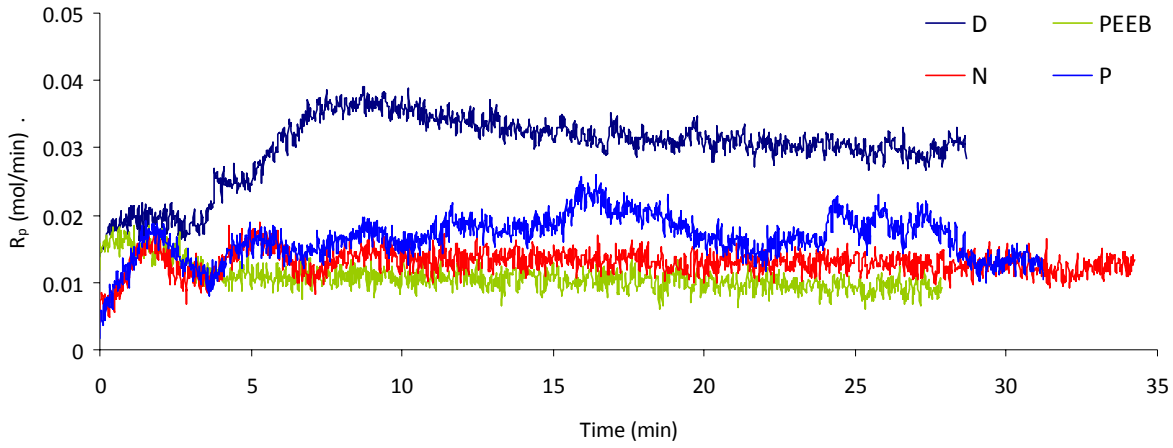

Figure 6-1. Rates of polymerization using different donors (D, N, P and PEEB donors)

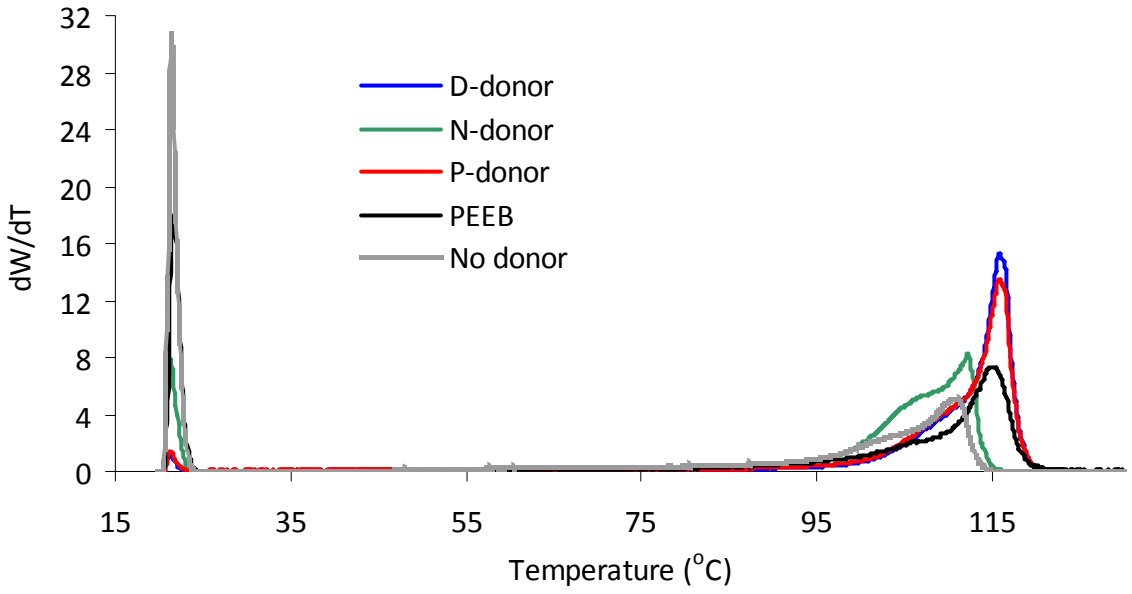

Figure 6-2. CEF profiles for polypropylene produced with different donors (D, N, P, PEEB donors) and without donor.

D donor and PEEB were mixed in different proportions and tested for polymerization activity and polymer crystallinity. Figure 6-3 shows the rate of polymerization with different D-donor/ PEEB molar percent ratios. The rate of polymerization with PEEB only (0, 100) and with (D-donor, PEEB) of (90, 10) had the lowest rates among all tested ratios, even though the crystallinity and *mmmm* content of the polymer produced at (90, 10) was as high as the polypropylene produced with pure D-donor (100, 0), as shown in Figure 6-4 and Figure 6-5. The CEF profiles show that an improvement on crystallizability was noticed when using pure PEEB compared with runs done without any donor (0, 0). However, mixtures with different D donor/PEEB ratios produced polymer with about the same CEF profiles. On the other hand, the *mmmm* pentad content was 78.5 % when PEEB was used alone, and was around 95.4% when the percentage of D donor varied from 100% to 90%. Interestingly, the catalyst activation rate increased when PEEB was mixed with D-donor at 95 and 98 D donor mol % (Figure 6-3). This is an attractive result since the polymerization activity increased without harming the

crystallinity and *mmmm* content of the polymer. From a commercial prospective, this finding may have some relevant economic implications, since the most costly component in propylene polymerization processes is the catalyst.

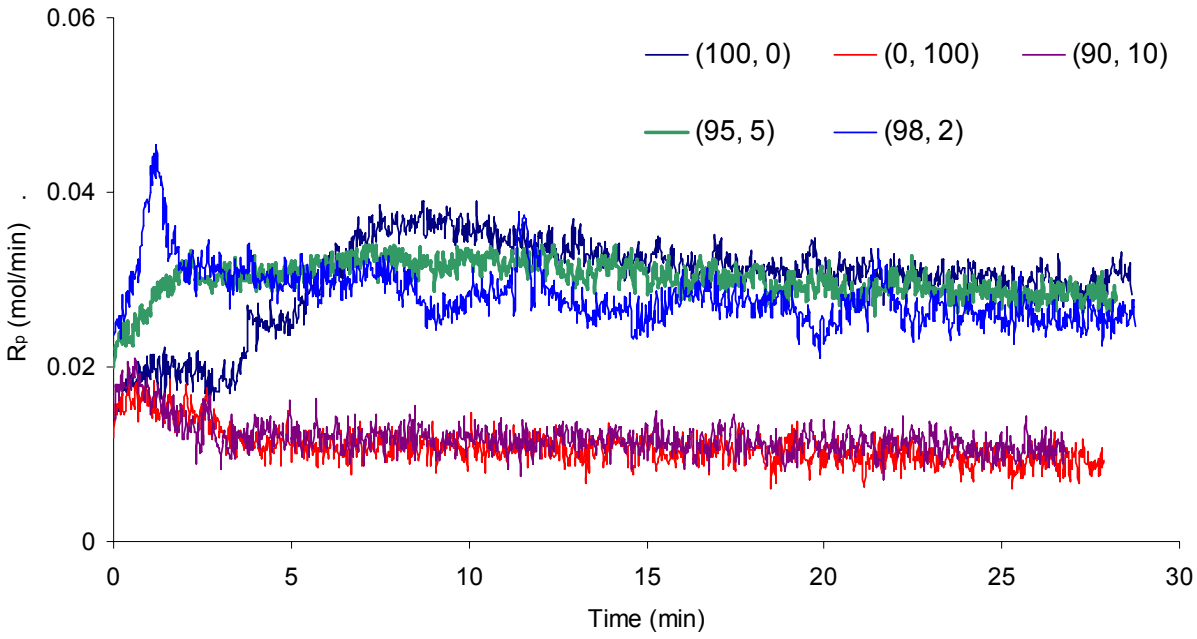

Figure 6-3. Rate of polymerization with mixture of two donors (D-donor, PEEB) (in mol %) at polymerization temperature of 70°C.

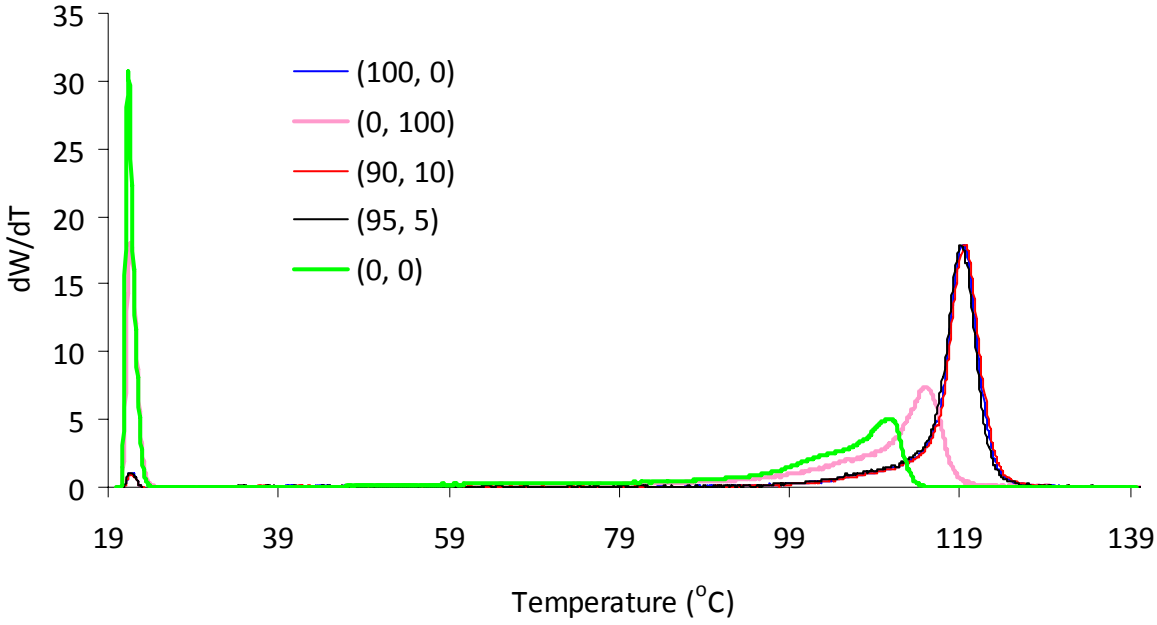

Figure 6-4. CEF profiles for polypropylene produced with mixture of two donors (D-donor, PEEB) (in mol %) at 70°C.

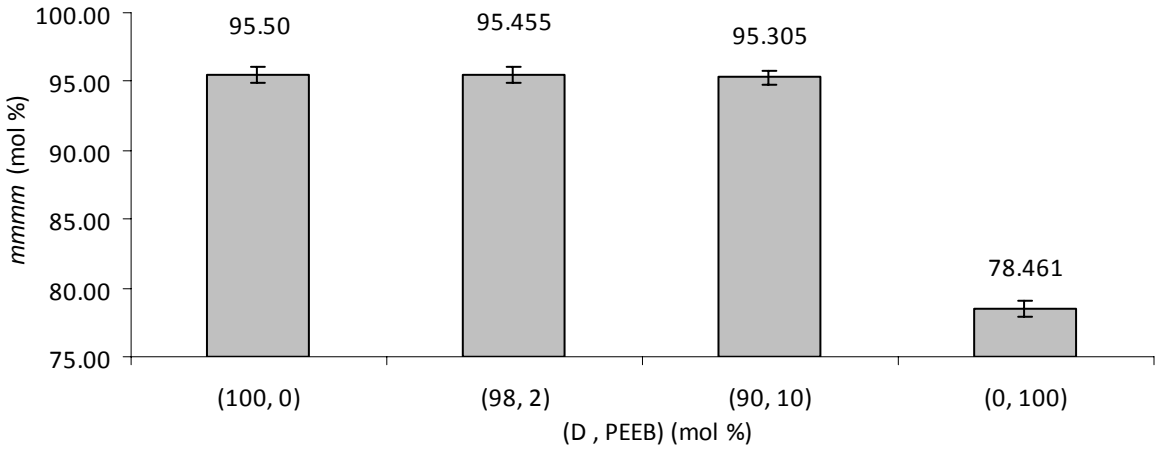

Figure 6-5. *mmmm* pentad for polypropylene produced with mixture of two donors (D-donor, PEEB) (in mol %) at 70°C.

Polymerization self extinguishing is performed by stopping all the reactant feeds including cocatalyst, to the reactor while continuously feeding PEEB or its mixture with a dominating donor. Figure 6-6 shows the individual rate of polymerization with pure D donor (100, 0), and pure PEEB (0, 100). In addition to these runs, a polymerization run was started using D donor only (1.4 mol/mol Do/Ti) and after 20 minutes of polymerization the PEEB donor was fed to the reactor (1.4 mol/mol Do/Ti) causing a drop on the polymerization rate as indicated by (100, 100, sim) in Figure 6-6. It is interesting to notice the match between the individual rates and the simultaneous rate of polymerization. The rate of polymerization data between the time interval of 21 and 30 minutes was the period of PEEB donor addition and setting back the propylene pressure.

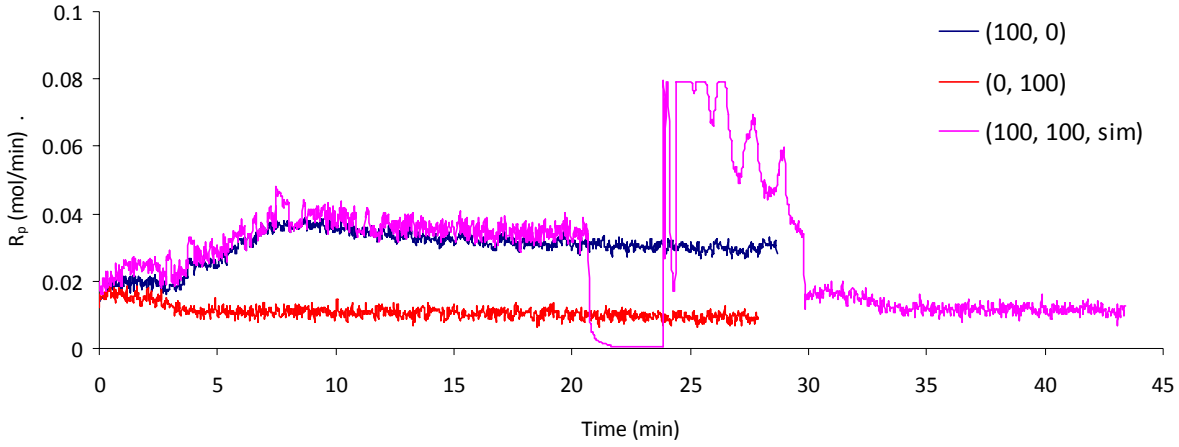

Figure 6-6. Individual and simultaneous propylene uptake rates using D donor (100,0), PEEB donor (0, 100), and D donor followed by PEEB donor (100, 100, sim) after 20 minutes of reaction time at a polymerization temperature of 70°C

6.4. CONCLUSIONS

In this short chapter, P and D donors showed better stereoselectivity compared with N and PEEB donors when used with the 4th generation Ziegler Natta catalyst investigated in this

thesis. In addition, D donor showed the best activity among P, N, and PEEB donors. The D/PEEB 90/10 (mol/mol) donor mixture showed a good stereoselectivity but low activity, but when the ratio was increased to 95/5 and 98/2, very good activity and stereoselectivity was achieved.

Interestingly, PEEB in small amounts (2-5 mol%) has a positive effect on the activation term of the polymerization rate when added to D donor. An associated positive production cost reduction for the D/PEEB mixture at these ratios can be anticipated.

Chapter 7

CONCLUSIONS AND RECOMMENDATIONS

The effect of adding hydrogen and/or external donor (Design A) on the apparent kinetic rate constants for activation, propagation, deactivation, and chain transfer for the polymerization of propylene with a 4^{th} generation Ziegler-Natta catalyst was quantified. The estimated activation energies for each step were found to be nearly independent of the presence or absence of hydrogen and/or donor and comparable to some values for different catalyst systems reported in the literature.

The apparent reaction rate constants for activation, propagation and deactivation were calculated based on the estimated activation energies and pre-exponential constants. These estimated kinetic parameters can be incorporated within process simulators used by commercial plants for better prediction of polymer properties and to optimize process conditions and optimal grade transition time.

The propylene polymerization rate was the highest when both donor and hydrogen were added to the reactor. The apparent catalyst activation rate increased with the addition of hydrogen, in the presence or absence of donor. The deactivation rate was highest in the absence of donor, indicating that aspecific sites deactivate faster than specific sites.

The number average molecular weight decreased when the polymerization temperature was increased from 60 to 70°C in the absence of external donor. However, the addition of electron donor increased the molecular weight and this increase was more pronounced at 70°C and on the active site types that makes longer chains, probably due to the stabilization effect of donor on the active sites. In this case electron donor makes these sites less likely to undergo

chain transfer reactions, perhaps by blocking the transition state that leads to β−hydride elimination or transfer to monomer.

Interestingly, the polypropylene *mmmm* pentad fraction increased upon hydrogen addition for most cases, a trend that had been anticipated with a Monte Carlo mathematical model developed to describe the effect of hydrogen and electron donor on polypropylene tacticity. A different behavior was observed at 70°C, when the addition of hydrogen in the presence of external donor decreased catalyst stereoselectivity and polymer crystallizability slightly.

At a polymerization temperature of 70°C, the hydrogen concentration showed a positive effect on *mmmm* pentad content at low donor concentrations, which could be due to an increase in stereoselectivity of the aspecific sites by hydrogen. By increasing the donor concentration, more aspecific sites were transformed into stereospecific sites, where hydrogen was no longer effective. The Monte Carlo simulation results showed a similar behavior for the hydrogen and donor concentrations to the *mmmm* pentad.

Moreover, propylene polymerizations at varying hydrogen and donor concentrations were conducted at two levels of donor and hydrogen at 55 and 65°C (Design B). Polymerization rates at double hydrogen concentration were the highest rates in Design B, confirming the rate enhancement effect by hydrogen. The estimated activation energies for activation, propagation and deactivation were very close to the values reported for Design A, indicating that varying hydrogen and donor concentration does not seem to affect the basic polymerization mechanism. Polypropylene molecular weight increased with donor concentration. In addition to donor, hydrogen was also found to increase *mmmm* pentad fraction of polymer made at 55 and 65°C.

Finally, different external donors were compared for their activities and stereoselectivities. P and D donors had better stereoselectivities than N and PEEB donors. The D donor had the best activity of all donors tested in this investigation. The D/PEEB at 90/10 (mol/mol) showed good stereoselectivity but a very poor activity, but when the ratio was increased to 95/5 and 98/2, good activity and stereoselectivity were obtained. One of the

interesting finding in this study is the positive effect on the activation term of the polymerization rate when a small amount of carboxylic acid ester (PEEB) is added to the silane external donor (D donor). An associated positive cost impact with this achievement is certainly expected.

It might be suggested to test this type of commercial catalyst at polymerization temperatures higher than 70ºC and find out whether the addition of hydrogen in the presence of donor will lead to low stereoregularity.

This type of commercial catalyst could be also tested using another silane electron donors with C_5 and C_6 cyclic groups such as cyclohexyl-methyl-dimethoxysilane (CHMDMS) or C-donor, and report the trend of molecular weight and microstructure of the produced polymer with respect of the polymerization temperature, presence and absence of the hydrogen and donor, and varying the concentration of hydrogen and donor. It would be also interesting to compare the activation energies and their pre-exponential constants with this work.

APPENDIX A: ^{13}C NMR Spectra

Table A- 1. Normalized pentad assignments for the hierarchal design of experiments for runs (D, H)-1 and (D, H)-2 of Group (D, H) of polymer made at 70ºC.

Run	Analysis	*mmmm*	*mmmr*	*rmmr*	*mmrr*	*mmrm + rmrr*	*rmrm*	*rrrr*	*rrrm*	*mrrm*
(D, H)-1	A1	94.29	2.56	0.37	0.21	0.75	0	0.75	0	1.07
	A2	94.33	2.53	0.39	0.18	0.77	0	0.70	0	1.10
	A3	96.32	0.84	0.89	0	1.88	0.07	0	0	0
	A4	94.92	2.41	0	0.18	1.21	0.91	0	0	0.37
(D, H)-2	A5	94.18	2.39	0.84	0.14	0.78	0	0.52	0.05	1,09
	A6	94.89	1.92	0	0.39	1.39	0.25	0.19	0.03	0.94
	A7	94.60	1.75	1.01	0.23	1.03	0	0.14	0.11	1.12
	A8	93.67	2.39	1.97	0.42	0.35	0	0.14	0.54	0.53

Table A- 2. Normalized pentad assignments for runs of 10, 30, and 60 minutes of reaction time.

Reaction Time (min)	Run#	*mmmm*	*mmmr*	*rmmr*	*mmrr*	*mmrm + rmrr*	*rmrm*	*rrrr*	*rrrm*	*mrrm*
10	201	93.24	3.01	0.09	1.45	0.69	0	0.7	0.37	0.45
30	158	95.50	2.20	0	1.3	0.19	0	0.50	0	0.31
60	200	94.30	2.47	0.87	1.08	0.65	0	0.48	0	0.15

Table A- 3. Normalized pentad assignments for runs of case study (Chapter 5, Section 5.2) at polymerization temperature of 70°C.

Run	*mmmm*	*mmmr*	*rmmr*	*mmrr*	*mmrm + rmrr*	*rmrm*	*rrrr*	*rrrm*	*mrrm*
(0.1D, H)	92.5	3.0	0.5	1.7	1.0	0	0.5	0.5	0.5
(0.25D, 0.5H)	93.2	3.4	0	0.8	2.2	0	0.2	0.2	0.2
(0.25D, H)	94.3	2.6	0.5	1.1	0.7	0	0.4	0.2	0.2
(0.25D, 2H)	95.1	2.4	0	0.8	0.4	0	0.2	0.2	0.9
(0.5D, 0.5H)	95.5	2.2	0.5	0.8	0.5	0	0.2	0.1	0.1
(0.5D, H)	96.3	1.9	0.3	0.6	0.3	0	0.2	0.2	0.2
(0.5D, 2H)	96.3	2.0	0.1	0.7	0.4	0	0.1	0.2	0.2
(D, 0.5H)	96.2	2.4	0	0.6	0.4	0	0.1	0.1	0.2
(D, H)	95.6	4.0	0	1.1	0.7	0	0	0.2	0.2
(D, 2H)	97.4	1.6	0	0.5	0.3	0	0	0.1	0.1
(D, 4H)	97.3	1.6	0	0.5	0.3	0	0	0.2	0.1
(2D, 0.5H)	95.2	2.9	0	0.8	0.6	0	0.2	0.2	0.1
(2D, H)	97.2	1.7	0.1	0.4	0.3	0	0	0.1	0.1
(2D, 2H)	96.7	1.9	0	0.5	0.5	0	0.1	0.2	0.1

Table A- 4. Normalized pentad assignments for runs of Design B at 55ºC.

Run	*mmmm*	*mmmr*	*rmmr*	*mmrr*	*mmrm + rmrr*	*rmrm*	*rrrr*	*rrrm*	*mrrm*
(0.5D, 0.5H)	89.51	3.38	1.18	1.19	1.21	1.83	0	0	1.71
(0.5D, 2H)	93.80	2.94	0.11	0.84	1.51	0.09	0	0.09	0.61
(2D, 0.5H)	95.18	1.65	0	0.97	1.09	0.36	0.29	0	0.46
(2D, 2H)	96.73	0.44	0.20	1.16	0	0.82	0	0.61	0.06

Table A- 5. Normalized pentad assignments for runs of Design B at 65ºC.

Run	*mmmm*	*mmmr*	*rmmr*	*mmrr*	*mmrm + rmrr*	*rmrm*	*rrrr*	*rrrm*	*mrrm*
(0.5D, 0.5H)	88.92	3.49	0	3.26	0	0	0.16	0.94	3.23
(0.5D, 2H)	94.43	2.71	0.83	0.19	0	0	0	0.25	1.58
(2D, 0.5H)	95.28	3.07	0	0.68	0.72	0	0	0.14	0.12
(2D, 2H)	96.64	2.14	0	0.64	0.35	0	0	0.12	0.1

APPENDIX B: Individual Verses Simultaneous Solutions for the Polymerization Rates of Design A and B

This appendix compares the values obtained for the activation energies of activation, propagation, and deactivation when they were estimated individually or simultaneously with the other polymerizations at different polymerization temperatures. The simultaneous solution was used to overcome the noise or variation on polymerization rate that led to lower values on the reaction rate constant (i.e. reaction rate constant of activation at 70°C of Design-A when compared to 60°C). However, the use of Arrhenius law (simultaneous solution) still shows good estimates for most of the cases as discussed in Chapter 4. Table B- 1 summarizes the individual estimated activation energies of polymerization experiments for Design A. From this table, the E_A is 21.52 kcal/mol with a 95% confidence interval of ± 1.23 kcal/mol. However, the E_p is 8.33 kcal/mol with a 95% confidence interval of ± 0.24 kcal/mol, and the E_d is 31.95 kcal/mol with a 95% confidence interval of ± 0.57 kcal/mol.

The individual solutions fitted better the monomer uptake curves than the simultaneous solutions. For instance, Figure B- **1** shows the experimental and predicted rates of polymerization for run (0.5D, 0.5H) of Design B using the simultaneous solution approach, while Figure B- **2** shows the same results obtained using the individual solution method. The predicted rates of polymerization were closer to the experimental values when using individual solutions. Similarly, the polymerization rates for the other three groups, (0.5D, 2H), (2D, 0.5H), and (2D, 2H), are better using individual solutions, as shown in Figure B- **3** to Figure B- **8**, and as seen by their lower chi-squared values in Table B- 2 and Table B- 3. However, individual solution predicts, in some cases, negative values for apparent activation energies, which has no physical meaning, likely due to experimental uncertainties due to catalyst injection in the reactor at the beginning of the polymerization. Therefore, the simultaneous solution method that enforces the Arrhenius law may lead to a less "optimal" fit, but it ensures that the model is theoretically sound. More experiments covering a wider range of temperatures, are recommended to solve this model limitation.

Table B- 1. Activation energies of activation (E_A), propagation (E_p), and deactivation (E_d) estimated individually for each experiment of Design A and the overall confidence region.

Experiment	E_A (kcal/mol)	E_p (kcal/mol)	E_d (kcal/mol)
(D, −)	84.74	8.58	9.07
(−, −)	49.68	8.22	13.12
(D, H)	29.81	8.21	24.54
(−, H)	57.33	7.99	23.00
Average	55.39	8.25	17.43
Standard Deviation	22.75	0.24	7.53
95 % Confidence	22.29	0.24	7.38

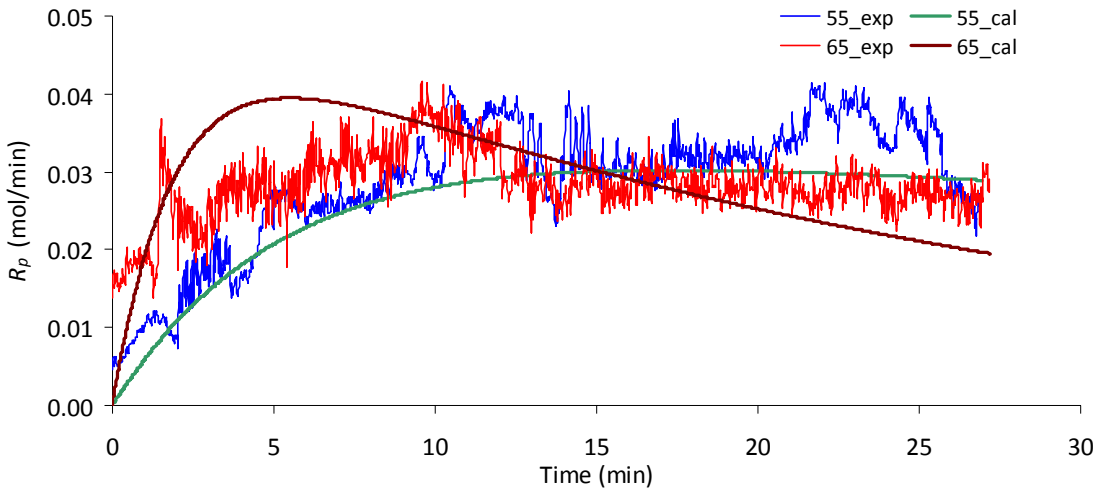

Figure B- 1. Experimental and predicted rate of polymerizations for (0.5D, 0.5H) at 55 and 65°C obtained using simultaneous solution.

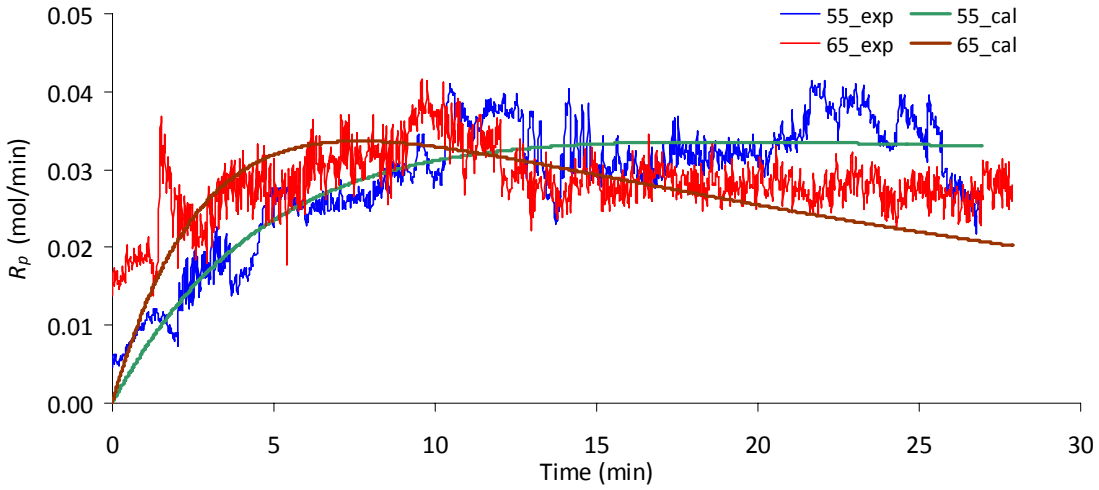

Figure B- 2. Experimental and predicted rate of polymerizations for (0.5D, 0.5H) at 55 and 65°C obtained using individual solution.

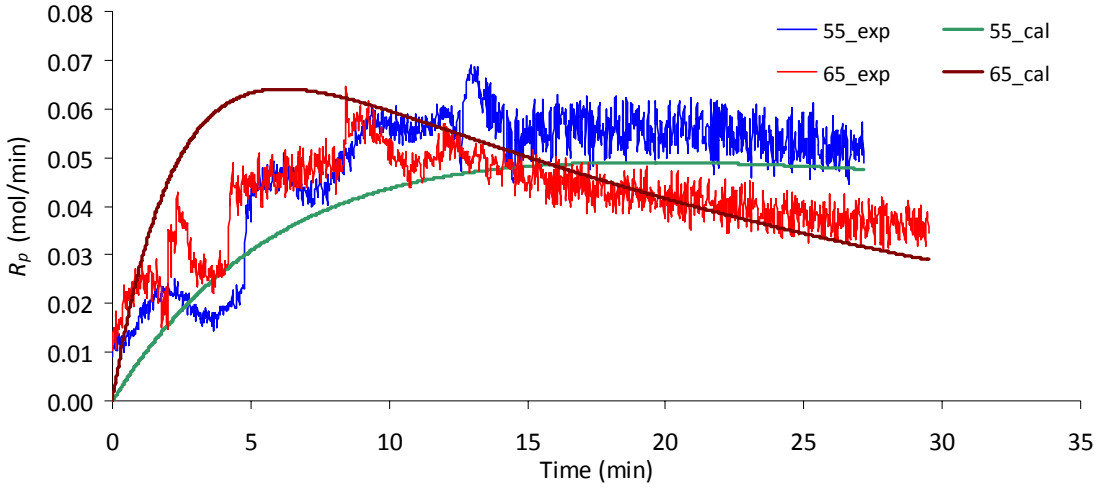

Figure B- 3. Experimental and predicted rate of polymerizations for (0.5D, 2H) at 55 and 65°C obtained using simultaneous solution.

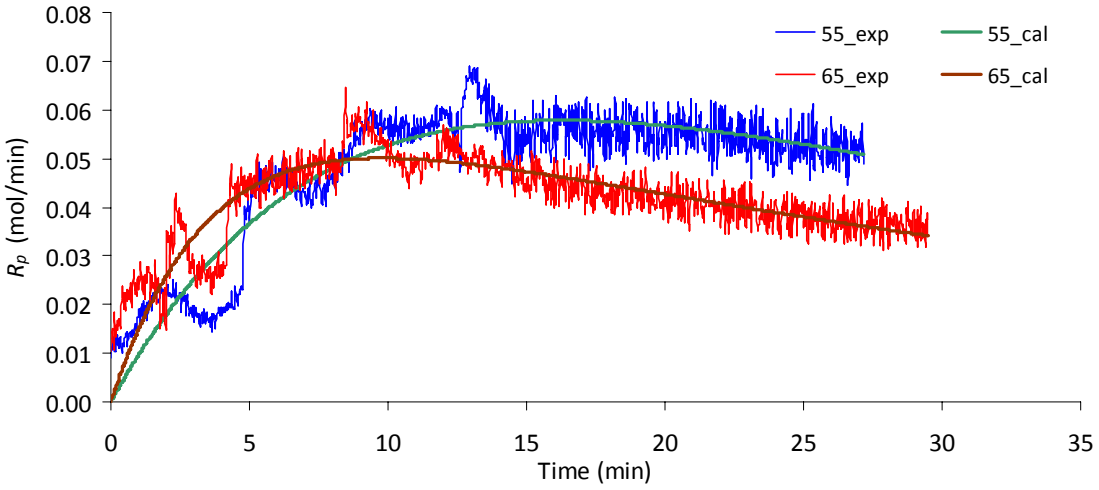

Figure B- 4. Experimental and predicted rate of polymerizations for (0.5D, 2H) at 55 and 65°C obtained using individual solution.

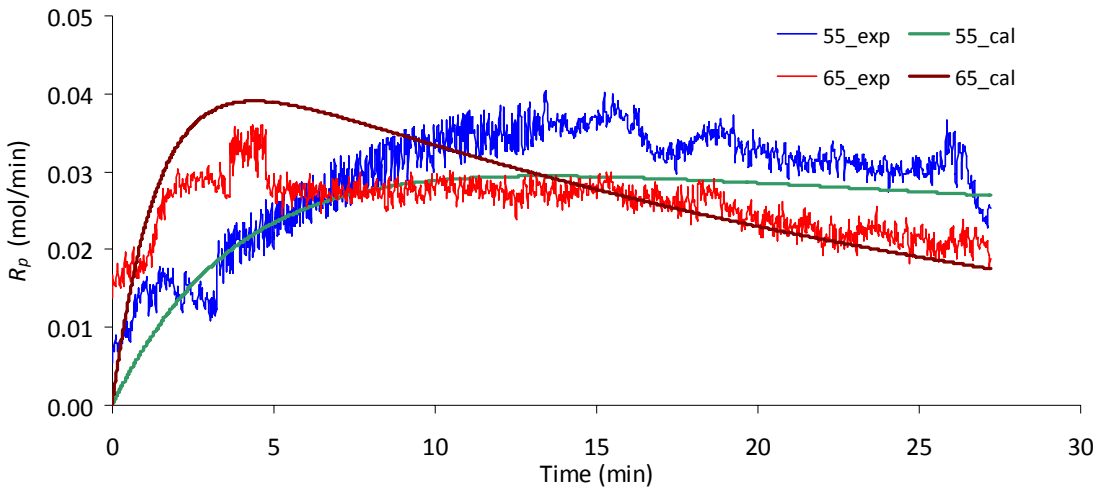

Figure B- 5. Experimental and predicted rate of polymerizations for (2D, 0.5H) at 55 and 65°C obtained using simultaneous solution.

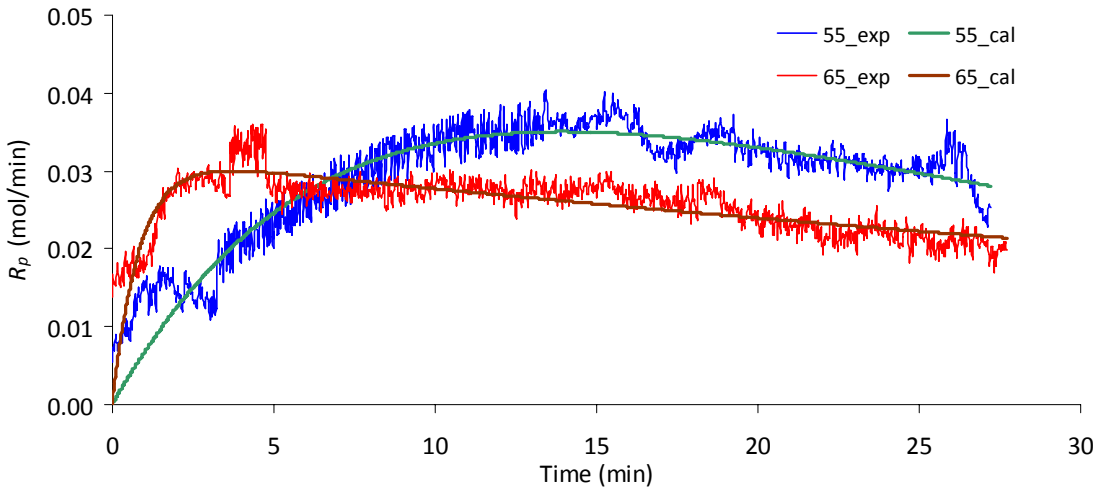

Figure B- 6. Experimental and predicted rate of polymerizations for (2D, 0.5H) at 55 and 65°C obtained using individual solution.

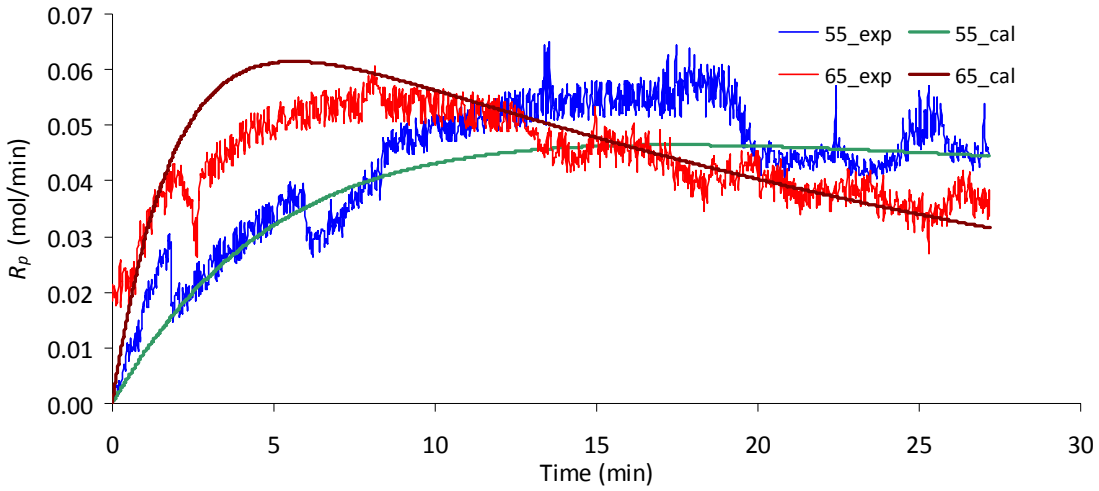

Figure B- 7. Experimental and predicted rate of polymerizations for (2D, 2H) at 55 and 65°C obtained using simultaneous solution.

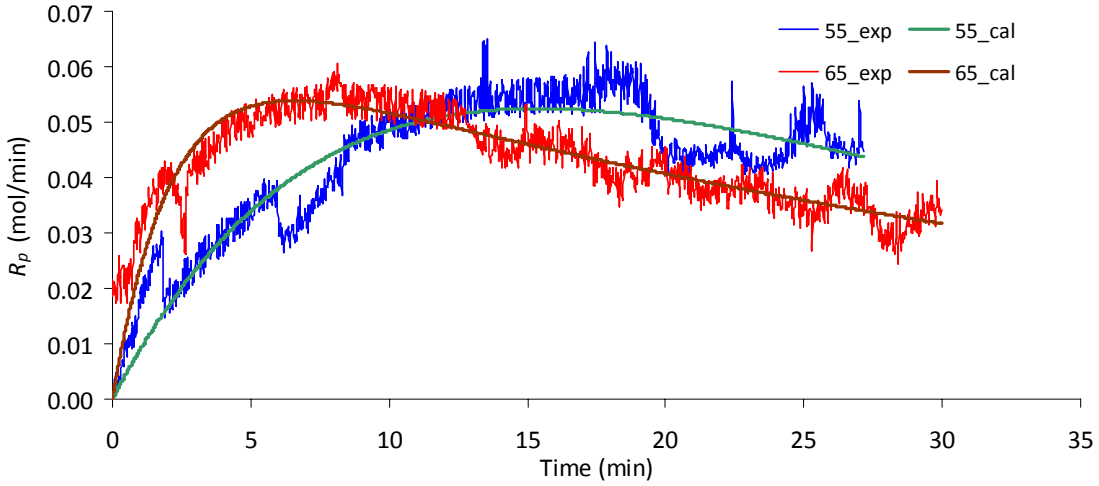

Figure B- 8. Experimental and predicted rate of polymerizations for (2D, 2H) at 65 and 65°C obtained using individual solution.

Table B- 2. Summary of the estimated kinetic parameters of Design B and their corresponding chi-squares using simultaneous solution.

	0.5D, 0.5H		0.5D, 2H		2D, 0.5H		2D, 2H	
T (°C)	55	65	55	65	55	65	55	65
A_{A0}	3.00×10^{14}		1.50×10^{14}		1.50×10^{14}		1.00×10^{14}	
E_A	22.82		22.49		22.16		22.09	
A_{p0}	7.00×10^{8}		1.70×10^{9}		1.00×10^{9}		1.80×10^{9}	
E_p	8.07		8.31		8.34		8.41	
A_{d0}	8.00×10^{18}		8.00×10^{18}		8.00×10^{18}		7.00×10^{18}	
E_d	31.47		31.43		31.44		31.41	
χ^2	1.57	3.87	3.76	2.72	1.85	1.66	1.41	1.81

Table B- 3. Summary of the estimated kinetic parameters of Design B and their corresponding chi-squares using individual solution.

	0.5D, 0.5H		0.5D, 2H		2D, 0.5H		2D, 2H	
T (°C)	55	65	55	65	55	65	55	65
A_{A0}	3.00×10^{14}		6.01×10^{12}		1.59×10^{32}		3.82×10^{28}	
E_A	22.10		20.64		49.68		44.70	
A_{p0}	7.00×10^{8}		2.43×10^{9}		5.20×10^{8}		1.84×10^{9}	
E_p	8.16		8.47		7.93		8.29	
A_{d0}	8.00×10^{18}		4.41×10^{-6}		2.22×10^{-15}		1.46×10^{-16}	
E_d	31.60		-5.78		-19.82		-22.01	
χ^2	0.96	2.10	2.51	2.51	1.53	0.79	1.01	1.78

REFERENCES

Alberta-Polypropylene Market Study, CMAI , (Sep. **2004**)

Albizzati, E, U. Giannini, G. Morini, M. Galimberti, L. Barino, R. Scordamaglia, *Macromol. Symp*., 89, 73 89 (**1995**)

Alghyamah, A.A., J. B. P. Soares, Macromol. Rapid Commun., 3. 384 (**2009**)

Alshaiban, A. and J. B. P Soares, *Macroml. Symp*, 285, 8 (**2009**)

Alshaiban, A. and J. B. P. Soares, *Macromol. React. Eng.*, 5, 96−116 (**2011**)

Alshaiban, A., University of Waterloo, Waterloo, Ontario, Canada, MSc. thesis (**2008**)

Arlman, E. and P. Cossee, *J. Catal.*, 3, 99 (**1964**)

Barino L., Scordamaglia R., *Macromol. Theory Simul*. 7, 407 (**1998**)

Beigzadeh, D., J. B. P. Soares, T. A. Duever, *J. Appl. Polym. Sci.*, 80, 2200 (**2001**)

Busico V., Cipullo R., Corradini P., De Biasio R., *Macromol. Chem. Phys.*, 196, 491 (**1995**).

Busico V., Cipullo R., Corradini P., *Makromol. Chem. Rapid Commun,* 13, 15 (**1992**).

Busico V., Cipullo R., Monaco G., Talarico G., Chadwick J.C., Segre A.L., Sudmeijer O., *Macromolecules* 32, 4173 (**1999**)

Busico V., Corradini P., De Martino L., Proto A., Savino V., Albizzati E., *Makromol. Chem*. 186, 1279 (**1985**).

Busico, V. and R. Cipullo, *Prog.Polym.Sci.*, 26, 443 (**2001**)

Busico, V., R. Cipullo, G. Monaco, M. Vacatello, A. L. Segre, *Macromol.*, 30, 6251−6263 (**1997**)

Busico, V., R. Cipullo, G. Monaco, M. Vacatello, J. Bella, A. L. Segre, *Macromol.*, 31, 8713−8719 (**1998**)

Busico, V., R. Cipullo, G. Talarico, Proceeding of the International Symposium on Microkinetics and Dynamics of Individual Active Sites in Catalytic Reactions, Kanazawa, Japan, March 6−8, (**2001**)

Busico, V., V. V. A. Castelli, P. Apera, R. Cipullo, A. Segre, G. Talarico, M. Vacatello, *J. Am. Chem. Soc.*, **125**, 5451−5451 (**2003**).

Campbell R. E. and L. Chen, U.S. Patent No. 7,381,779, (**2008**)

Canavos G. C. and I. A. Koutrouvelis, "An Introduction to the Design & Analysis of Experiments", Prentice Hall, pp. 139–260 (**2009**)

Canu P. and W. H. Ray, *Computers in Chemical Engineering*, 15, 549–564 (**1991**)

Cerruti L., *HYLE*, 5, issue 1, 3 (**1999**)

Chadwick J.C. *Macroml. Symp.*, 173, 21−35 (**2001**)

Chadwick J.C., Heere J.J.R., Sudmeijer O., *Macroml. Chem. Phys.*, 201, 1846 (**2000**)

Chadwick J.C., Meedema A., Sudeijer O., *Macromol. Chem. Phys.* 195, 167 (**1994**)

Chadwick J.C., Morini G., Albizzati E., Balbontin G., Mingozzi A. C., Sudmeijer O., van Kessel G. M. M. *Macroml. Chem. Phys.*, 197, 2501 (**1996**)

Chadwick J.C., Morini G., Balbontin G., Camurati I., Heere J.J.R., Mingozzi I., Testoni F., *Macromol. Chem. Phys.* 202, 1995 (**2001**).

Chadwick J.C., van Kessel G. M. M., A. C., Sudmeijer O. *Macroml. Chem. Phys.*, 196, 1431 (**1995**)

Chakravarti, S., Ray W. H., Zhang S. X., *J. Appl. Polym. Sci.* 81, 1451−1459 (**2001**)

Chakravarti,S. and W. H. Ray, *J. Appl. Polym. Sci.* 81, 2901−2917 (**2001**)

Chang M, Liu X., Nelson P.J., Munzing G.R., Gegan T.A., Kissin V. Y., *J. Catalysis*, 239, 347 (**2006**)

Chen L. and T. Zemzek, U.S. Patent No. 7,141,635, (**2006**)

Chen L., U.S. Patent No. 7,420,021, (**2008**)

Chien, J. C. W., B. Rieger, R. Sugimoto, D. T. Mallin, M. D. Rausch, *Stud. Surf. Sci. Catal.*, **56**, 535−574 (**1990**)

Chien, J. C. W.; Y. Iwamoto, M. D. Rausch, W. Wedler, H. H. Winter, *Macromolecules*, **30**, 3447−3458 (**1997**)

Chien, J. C. W.; Y. Iwamoto,M. D. Rausch, *J. Polym. Sci. A*, **37**, 2439−2445 (**1999**).

Chemical Market Resources Inc. "CMR" report, Vol. 7, issue 4, (February/March **2002**)

Choi, Y., J. B. P. Soares, *Polymer*, **51**, 4713−4725 (**2010**)

Coates, G. W., R. M. Waymouth, *Science*, **267**, 217−219 (**1995**)

Collette J. W., C. W. Tullock, R. N. MacDonald, W. H. Buck, A. C. L. Su, J. R. Harrell, R. Mulhaupt, and B. C. Anderson, *Macromolecules*, 22, 3851−3858 (**1989A**).

Collette, J.W., D. W. Ovenall, W. H. Buck, R. C. Ferguson, *Macromolecules*, 22, 3858−3866 (**1989B**)

Corradini P, Napolitano R., Oliva L., Petraccone V., Pirozzi B., *Makromol Chem Rapid Commun*., 3, 753 (**1982**)

Corradini, P, Napolitano R., Oliva L., Petraccone V., Pirozzi B., *Makromol Chem Rapid Commun*., 3, 753 (**1982**)

Cossee, P. J, *J. Catal.,* 3, 80-89 (**1964**)

Cox W.W. and A.A. Duswalt, *Polym Eng. Sci.*, 7, 307 (**1967**)

Duever, T. A., Trip M. T., Tzoganakis C., *J. Cellular Plastics*, 38, 103−112 (**2002**)

Duranel, L., Spitz R., Soto T., United States Patent 5192732 (**1993**)

Ewen, J. A., *J. Am. Chem. Soc.*, 106, 6355-6364 (**1984**)

Ewen, J. A., R. L. Jones, A. Razavi, J. D. Ferrara, *J. Am. Chem. Soc.*, 110, 6255-6256 (**1988**)

Ewen, J. A.; M. J. Elder, R. L. Jones, L. Haspeslagh, J. L. Atwood, S. G. Bott,; K. Robinson, *Macromol.Symp.*, 48:9, 253–295 (**1991**).

Farina, M., G. Di Silvestro, P. Sozzani, *Macromol.*, 15, 1451−1452 (**1982**)

Flory, P. J., "Pricipels of Polymer Chemistry", Cornell University Press: New York (**1953**)

Forte M. C. and F. M.B. Coutinho, *Eur. Polym. J*., 32, No. 5, 605 (**1996**)

Guastalla G., Giannini U., *Makromol. Chem. Rapid Commun.,* 4, 519 (**1983**)

Harkonen M., Seppala J., Chujo R., Kogure Y., *Polymer,* 36, 1499 (**1995**)

Hauptman, E.; R. M. Waymouth,J. W. Ziller, *J. Am. Chem. Soc.*, 117, 11586-11587 (**1995**).

Hoffman, J.D. and J.J. Weeks, *J. Chem. Phys.*, 42, 4301 (**1965**)

Hutchinson, R. A. and W. H. Ray, *J. Appl. Polym. Sci.* 43, 1271, (**1991)**.

Inoue Y., Nishioka A, Chujo R., *Makromol Chem.,* 168, 163 (**1972**)

Kakugo M., Miyatake T., Naito Y., Mizunuma K., *Macromolecules*, 21, 314 (**1988**)

Kaminsky, W., M. Arndt, , Angew. Chem., *Adv*. *Polym. Sci.*, **127**, 143– 187 (**1997**)

Kaminsky, W., K. Kulper, H.-H. Brintzinger, F. R. Wild, *Angew. Chem.*, *Int. Ed. Engl.*, 24, 507– 508 (**1985**)

Keii T., E. Suzuki, M. Tamura, Y. Doi, *Makromol. Chem.*, 183, 2285–2304 (**1982**)

Keii T.,K. Soga, N. Saiki, *J. Polym. Sci.*, Part C, 16, 1507–1519 (**1967**)

Keii T.,Y. Doi, E. Suzuki, M. Tamura, M. Murata, K. Soga, *Makromol. Chem.*, 185, 1537–1557 (**1984**)

Kim Y.C., Ahn W., Kim C.Y., *Polym. Eng. Sci.*, 7, 309 (**1997**)

Kim, J. D., J. B. P. Soares, G. L. Rempel, *J. Polym. Sci., Part A: Polym. Chem.*, 37, 331. (**1999**)

Kissin, Y. V., *Makromol. Chem.*, *Macromol. Symp.*, 66, 83 (**1993**)

Kissin, Y. V., J. *Molecular Cat. A: Chem.*, 33, 227 (**1995**)

Kissin V. Y., Liu X., Pollick D.J., Brungard N.L., Chang M, *J. Moleculare Catalysis A: Chemical*, 287, 45 (**2008**)

Kissin Y. V. and L. A. Rishina, *Polym. Sci. Ser. A Polym. Phys.*, Vol. 50, No. 11, 1101−1121 (**2008**)

Kissin Y. V., R. Ohnishi, T. Konakazawa, *Macromol. Chem. Phys.*, 205, 284−301 (**2004**)

Kissin, Y. V., Alkene Polymerization Reactions with Transition Metal Catalysts, Elsevier (**2008**)

Lin, S.; E. Hauptman, T. K. Lal, R. M. Waymouth, R. W. Quan, A. B. Ernst, *J. Mol. Catal. A: Chem.*, 136, 23-33 (**1998**).

Maier, C. and T.Calafut, "Polypropylene: the definitive user's guide and databook", William Andrew publishing, (**1998**)

Matos, V., A. G. M. Neto, J. C. Pinto, *J. App. Polym. Sci.*, 79, 2076−2108 (**2001**)

Matos, V., Neto A. G. M., Nele M., Pinto J. C.; *J. Appl. Polym. Sci*. 86, 3226−3245 (**2002**)

McKenna, T. F. and J. B. P. Soares, *Chem. Eng. Sci.* 56, 3931−3949 (**2001**)

McMurry, J. "Organic Chemistry", Cole Publishing Co., Monterey, California (**1984**)

Miller, S. A., J. E. Bercaw, *Abstr. Am. Chem. Soc.,* 217, 151−INOR (**1999**)

Miro N. D. and M. Ohkura, U.S. Patent No. 6,087,459, (**2000**)

Miro N. D., U.S. Patent No. 6,566,294 (**2003**)

Monasse B. and J.M. Haudin, *Colloid Polym. Sci.*, 263, 822 (**1985**)

Monrabal B., *J. Appl. Polym. Sci.*, 52, 491 (**1994**)

Monrabal B., Sancho-Tello J., Mayo N, Romero L., *Macroml. Symp.*, 257, 71 (**2007**)

Monrabal B., U.S. Patent 5,222,390; (**1991**)

Montgomery, D. ,"Design and Analysis of Experiments", John Wiley & Sons Inc, 7th edition (**2009**), pp. 162−504

Moore E.P., "Polypropylene Handbook", Hanser, Munich (**1996**)

Muller, A., W. Hopf, W. Kaminsky, L. Piet, L. Joachim, *Polymer*, 45, 1815–1822 (**2004**)

Natta, G.; Pino P.; Corradini P.; Danusso F.; Mantica E.; Mazzanti G.; Moraglio, G. *J.Am.Chem.Soc.*, 77, 1708-1710.(**1955**)

Nieto J., Oswald T., Blanco F., Soares J. B. P., Monrabal B., *J. Polym. Sci., Part B: Polym. Phys.*, 39, 1616 (**2001**)

Odian, G., "Principles of Polymerization", 4th ed., J. Wiley & Sons (**2004**)

Pater, J. T. M., G. Weickert, W. P. M. van Swaaij, *Chem. Eng. Sci.*, 57, 3461–3477 (**2002**)

Pino, P., P. Cioni, J. Wei, *J. Am. Chem. Soc*., 109, 6189–6191 (**1987**)

Potter, D.P.B, *Chem.Week*, 163, 3-7 (**2001**)

Ray, W. H., *J. Macromol. Sci., Rev. Macromol. Chem.*, C8, 1–56 (**1972**)

Razavi, A., L. Peters, L. Nafpliotis, D. Vereecke, K. Den Daw, *Makromol. Symp.*, 89, 345− (**1995**).

Razavi, A. and J. L. Atwood, *J. Organmet. Chem.,* 497, 105–111 (**1995**)

Reid R. C., Prausnitz J. M., Poling B. E., "The Properties of Gases & Liquids", 4th edition (**1987**)

SABIC, standard operating procedure, R&T-QC-SOP-004 (**2005**)

Shaffer W. K. and H. W. Ray, *J. Appl. Polym. Sci.* 65, 1053 (**1997**)

Sinn, H. and W. Kaminsky, *Adv. Organomet. Chem.*, 18, 99−149 (**1980**)

Soares, J. B. P., A. E. Hamielec, *Polymer*, 36, 2257 (**1995**)

Soares J. B. P. and A. E. Hamielec, *Polym React Eng*, 4, 153–191 (**1996**)

Soares J. B. P., *Macromol. Symp.*, 257, 1(**2007**).

Soares J. B. P., McKenna T., Cheng C., Chapter 2: Coordination polymerization. In Polymer Reaction Engineering, JM Asua (Ed.), Blackwell Publishing (**2007**)

Soares, J. B. P, McMaster University, Hamilton, Ontario, Canada, PhD. thesis (**1994**)

Soares, J. B. P. and A. E. Hamielec, *Polymer,* 36, 11, 2257−2263 (**1995**)

Soares, J. B. P. and A. E. Hamielec, *Polymer,* 37, 20, 4607−4614 (**1996**)

Soares, J. B. P., Kim J. D., Rempel G. L., *Ind. Eng. Chem. Res.*, 36, 1144− 1150 (**1997**)

Soga K., Shiono T., *Prog Polym. Sci.*, 22, 1503 (**1997**)

Spitz, R., J. L. Lacombe, A. Guyot, *J. Polym. Sci., Part A: Polym. Chem.*, 22, 2641– 2660 (**1984**)

Tsutsui, T., N. Kashiwa, A. Mizuno, *Makromol. Chem. Rapid Commun.*, 11, 565– 570 (**1990**)

Wild L., Ryle T. R., Knobeloch D. C., Peat I. R., *J. Polym. Sci. Polym. Phys*, 20, 441(**1982**)

Wong, W., "Flow Injection Polymer Analysis (FIPA) for Quality and Process Control", Viscotek (**2008**)

www.MarketPublisher.com, (Jan. **2010**)

Xu J., Feng L., Yang S., Yang Y., Kong X., *Eur. Polym. J.*, 34, No. 3/4, 431 (**1998**)

Xu J., Yang Y., Feng L., Kong X., Yang S., *J. Appl. Polym. Sci.*, 62, 727 (**1996**)

Xu Z. G.,S. Chakravarti, W. H. Ray, *J. App. Polym. Sci.*, 80, 81–114 (**2001**)

Yoshino, K., A.Ueda, T. Demura, Y. Miyashita, K. Kurahashi, Y. Matsuda, Proceedings of the 7th International Conference on Properties and Applications of Dielectric Materials, P1–16, (**2003**)

Zakharov V. A., *React. Kinet. Catal. Lett.*, 9 : 3, 251–256 (**1978**)

Zambelli A., Locatelli P., Bajo G., Bovey F.A., *Macromol.*, 8, 687 (**1975**)